NASA/TM–1999-208767

The Thin Oil Film Equation

James L. Brown and Jonathan W. Naughton
Ames Research Center, Moffett Field, California

National Aeronautics and
Space Administration

Ames Research Center
Moffett Field, California 94035-1000

March 1999

Available from:

NASA Center for AeroSpace Information
7121 Standard Drive
Hanover, MD 21076-1320
(301) 621-0390

National Technical Information Service
5285 Port Royal Road
Springfield, VA 22161
(703) 487-4650

THE THIN OIL FILM EQUATION

James L. Brown
Jonathan W. Naughton

Ames Research Center

SUMMARY

A thin film of oil on a surface responds primarily to the wall shear stress generated on that surface by a three-dimensional flow. The oil film is also subject to wall pressure gradients, surface tension effects and gravity. The partial differential equation governing the oil film flow is shown to be related to Burgers' equation. Analytical and numerical methods for solving the thin oil film equation are presented. A direct numerical solver is developed where the wall shear stress variation on the surface is known and which solves for the oil film thickness spatial and time variation on the surface. An inverse numerical solver is also developed where the oil film thickness spatial variation over the surface at two discrete times is known and which solves for the wall shear stress variation over the test surface. A One-Time-Level inverse solver is also demonstrated. The inverse numerical solver provides a mathematically rigorous basis for an improved form of a wall shear stress instrument suitable for application to complex three-dimensional flows. To demonstrate the complexity of flows for which these oil film methods are now suitable, extensive examination is accomplished for these analytical and numerical methods as applied to a thin oil film in the vicinity of a three-dimensional saddle of separation.

1. INTRODUCTION

The response of a thin oil film on a surface subjected to a three-dimensional (3D) aerodynamic flow proves to be of interest to the fluid mechanics community for several reasons. First, the study of thin oil films has led to new instrumentation which accurately measures the wall shear stresses generated by 3D flows. Second, extensive use of oil flow visualization on surfaces bounding 3D flows requires that we understand the limitations of these oil flow techniques in the neighborhood of the complex topological features, including singularities, of the limiting surface streamlines. Additionally, the study of thin oil films provides an opportunity to consider the solution of nonlinear partial differential equations with clear practical significance and which require minimal computational and programming resources.

Instrumentation based on thin oil films has undergone sustained development (Tanner, et al.[1-4]; Monson, et al.[5-7]; Mateer, Monson, and Menter[8]) to provide accurate measurement of the wall shear stresses generated on a test surface by aerodynamic flows. Recent improvements (Naughton and Brown[9-11]), particularly for 3D flow applications, in the form of the oil film wall shear stress instrument have been made possible by the application of Computational Fluid Dynamics (CFD) solution techniques to the thin oil film equation. Experimental wall shear stress measurements guide development of turbulence models to further improve CFD solvers. An important barrier to the accurate prediction by Navier-Stokes CFD solvers of complex 3D flows is the accurate modeling of the flowfield turbulent Reynolds stresses. Considerable effort has been expended over the past six decades in turbulence modeling with advances in this difficult area being frustratingly slow. The pace of improvement in turbulence modeling has improved recently, however, partly due to a maturation in the numerical methods of Navier-Stokes solvers, and partly due to enhanced instrumentation. Two instruments most relevant to improvements in turbulence modeling are the laser Doppler velocimeter (LDV) and the laser interferometric skin friction (LISF) instruments. The LISF and related successor skin friction instruments deduce the wall shear stress by analysis of either the thinning rate or the detailed shape of an oil film which is initially spread on a test surface and which then responds to the aerodynamic flow over that test surface. Prior to this study, self-similar 1D solutions for the oil film response were used[1-8] in the analysis for the oil-film based instruments. However, as these oil-film based instruments are now being applied to complex 3D flow situations, a more rigorous treatment of the oil film response is now required and is addressed by this present work.

A further reason to study the thin oil flow equation is the utility of surface oil flow visualization technique (Maltby[12]). Surface oil flow visualization is one of several techniques to discern the limiting streamline flow patterns on the surface. An aid to understanding complex 3D flows is the topological analysis of these limiting streamlines (Tobak and Peake[13]; Chapman and Yates[14]). Visualization, both of numerical solutions and experimental flows, of these surface streamlines and associated singularities provides an overall

topological framework for categorizing and comprehending the complex flow patterns which may arise. For 3D flows, the types of singularity points which may occur on surfaces are the saddle of separation, the saddle of attachment, the node of separation, the node of attachment, the focus of separation, and the focus of attachment. Limiting separation or attachment lines connect these point singularities. A further surface streamline topological rule is that these singularity points appear in combinations such that for a simply connected closed body:

$$N - S = 2$$

where N is the total number of nodal and focal points appearing in the flow and S is the total number of saddle points appearing in the flow. Easily overlooked are the node of attachment at the nose of an aerodynamic body and the node of separation at the tail. Symmetry of the flow can also lead to an undercount since a singular point may then actually appear twice. The flowfield need not be uniquely defined by the surface streamline patterns observed.

The importance of the ability to correctly identify these singularity points and further to predict with a Navier-Stokes solver the location of these singularity points is generally underestimated. In particular, the saddle of separation and the saddle of attachment can be difficult to identify and yet either can appear in some flows at a particular location with significant impact on the flowfield pattern above the surface. To miscalculate a singularity point for a turbulent flow may be the consequence of an improper grid or more importantly an improperly constructed turbulence model.

Squire[15] provided the first theoretical study of the thin oil film equation. Numerical solutions for the 1D thin oil film under a 2D aerodynamic flow were presented. In particular, the behavior of oil flow visualization in the vicinity of 2D separation was addressed. Squire concluded that the thin oil film did not significantly alter the boundary layer and that oil flow visualization would tend to indicate 2D separation slightly upstream of the actual boundary layer separation due to pressure gradient effects. Part of the purpose of this present work is to extend the earlier work of Squire to consider 2D thin oil films under 3D aerodynamic flows.

A third reason for the study of the thin oil film equation lies in its utility in the study of numerical methods. The thin oil film equation is an extension of the familiar Burgers equation often used to test CFD numerical methods. As with Burgers' equation[16], the thin oil film equation is a scalar hyperbolic wave equation which may be solved by numerous solution methods, including finite-difference, finite-volume, characteristic and Lagrangian techniques. These thin oil film solutions can be accomplished in 1D or 2D on a workstation. Additional advantages accrue to the study of the thin oil film equation, however, in that for both the 1D and 2D forms the eigenvalue(s) and hence characteristic direction can be forced to change sign at a particular location in a model problem. Further, in the present article, we will demonstrate an inverse solution numerical method useful for the skin friction instrument. Additionally, the thin oil film equation offers a context to study 1D and 2D

model problems both numerically and experimentally which can provide particular insight when fluid mechanics students are introduced to numerical methods.

Note that the 1D thin oil film problems are associated with 2D aerodynamic flows, while 2D thin oil film problems are associated with 3D aerodynamic flows. Where clarity in this paper requires, we will specifically state, for example, 2D thin oil problem or 2D aerodynamic flow. Also, the two fluids need not be restricted to oil and air, but to clearly distinguish between the flow of the two fluids, we shall use the terms "oil flow" and "aerodynamic flow" throughout the remainder of the paper.

In the present study, both direct and inverse numerical solution techniques for the thin oil film equation are developed. The direct numerical solver considers the case where the wall shear stress field on the surface, $\vec{\tau}_w(x,z)$, is known and the direct solver provides the oil film thickness variation with time over the surface, $h(x,z,t)$. The inverse numerical solver considers the case where the oil film thickness variation at two discrete times, $h(x,z,t_1)$ and $h(x,z,t_2)$, is known and the inverse solver then provides the wall shear stress variation over the surface, $\vec{\tau}_w(x,z)$.

In the sections to follow, the thin oil film equation is first derived. Next, various solutions are demonstrated including exact 1D and 2D self-similar cases. Then numerical procedures for both the direct and inverse solutions are presented. These solvers are then applied to several example practical problems. Programs to solve these example problems are written in the c programming language for use on a Unix workstation and are available from the first author.

2. THE GOVERNING PARTIAL DIFFERENTIAL EQUATION

The Navier-Stokes equations describe the response of a thin film of viscous liquid, typically oil, which is initially spread on a surface and which then experiences a 3D flow of a second fluid, typically air, over that surface. Simplifications to the Navier-Stokes equations for such an oil film flow are possible which still result in an accurate description of the oil flow while considerably reducing the difficulty of the solution method. The thin oil film equation derived below is essentially the continuity equation integrated across the thickness of the thin oil film, with additional information incorporated from simplifications of the x- and z-momentum equations. The derivation of the thin oil film equation is quite straightforward but is described below to establish the restrictions on the equation and to clarify the numerical procedures used to solve the equation.

Consider a thin film of viscous liquid, such as a silicone oil, initially placed on a test surface as shown in figure 1. Typically, the thickness of oil is a few microns in thickness which varies with location and time. This test surface, and thus the oil film, is then subjected to a 3D aerodynamic flow over the test surface. The 3D aerodynamic flow generates on the test surface a wall shear stress vector, $\vec{\tau} = (\tau_x(x,z), \tau_z(x,z))$, acting tangential to the surface, and a wall normal stress or pressure, $P(x,z)$, acting normal to the surface. The oil film will flow in response to these wall stresses and to the gravitational body force acting on the oil. Additionally, the oil film will experience surface tension effects related to the curvature of the oil film surface. For the purposes of this derivation we assume the 3D aerodynamic flow is steady with time.

The thickness of the film, $h(x,z,t)$, will vary with position on the surface and with time. To derive the differential equation governing the oil film behavior, consider the control volume of figure 1. The control volume encloses the full height of the oil film, h, and is of finite length, Δx, and width, Δz, aligned with the x and z axes, respectively. Thus, the oil mass in the control volume at any time is given by $m_{cv} = \rho_o h \Delta x \Delta z$. A change in film thickness, h, and, thus, mass in the control volume occurs during a time interval, Δt, due to the differences in mass flux normal to the four sides of the control volume through which oil may flow:

$$\Delta m_{cv}/\Delta t + \Delta_x F + \Delta_z G = 0$$

where

$$m_{cv} = \rho_o h \Delta x \Delta z$$

$$F = \int\int \rho_o u dA = \int_0^h \rho_o u dy \Delta z = \rho_o U_c h \Delta z$$

$$G = \int\int \rho_o w dA = \int_0^h \rho_o w dy \Delta x = \rho_o W_c h \Delta x$$

Taking limits of Δx, Δz and $\Delta t \Rightarrow 0$, we obtain:

$$\partial h/\partial t + \partial U_c h/\partial x + \partial W_c h/\partial z = 0$$

where we have defined:

$$U_c h \equiv \int_0^h u dy, \text{ and } W_c h \equiv \int_0^h w dy$$

The fluxes, F and G, can be evaluated by means of a low-Reynolds number simplification of the x- and z-momentum equations. The film Reynolds number may be evaluated as a ratio of inertial effects to viscous effects:

$$Re_f = (\rho_o U_c^2/L)/(\mu_o U_c/h^2) = (\rho_o U_c h/\mu_o)(h/L)$$

To estimate the film Reynolds number we make use of Tanner's 1D self-similar solution result, $U_c = \tau h/2\mu_o$, along with estimates for $h = 10^{-6}m$, $L = 10^{-2}m$, $\tau = 20N/m^2$, $\rho_o = 1000Kg/m^3$, and $\nu_o = 100$ centiStokes to obtain:

$$Re_f \approx \tau h^3/2\rho_o \nu_o^2 L = 10^{-8}$$

As a consequence of the low Reynolds number, we ignore the inertial terms in the x-momentum equations, giving within the oil film:

$$0 = \partial \tau_{x,o}/\partial y - \partial P_o/\partial x + \rho_o g_x$$

For the purposes of clarity in this derivation, we introduce the subscript, o, to signify the shear stress and pressure within the oil film, and the subscript, a, to signify the aerodynamic wall shear stress and wall pressure which are applied as boundary conditions to the oil film at the air/film interface located at $y = h$.

Integrating, from the air/film interface inward, for the shear stress variation through the film layer:

$$\int_h^y \frac{\partial \tau_{x,o}}{\partial y} dy = \tau_{x,o} - \tau_{x,a} = (\frac{\partial P_o}{\partial x} - \rho_o g_x)(y - h)$$

Note, the y-momentum equation implies that the pressure, $P_o(x, z)$, may be assumed constant across the oil film thickness.

Integrating again, but from the wall out into the film, gives:

$$\int_0^y \tau_{x,o} dy = \int_0^y \mu_o \frac{\partial u}{\partial y} dy = \mu_o u = \tau_{x,a} y + (\frac{\partial P_o}{\partial x} - \rho_o g_x)(y^2/2 - hy)$$

Or, considering both the x and z components of velocity within the oil film:

$$u = (\tau_{x,a} y + (\frac{\partial P_o}{\partial x} - \rho_o g_x)(y^2/2 - hy))/\mu_o \tag{2.1a}$$

$$w = (\tau_{z,a} y + (\frac{\partial P_o}{\partial z} - \rho_o g_z)(y^2/2 - hy))/\mu_o \tag{2.1b}$$

Integrating yet again finally gives us an expression for the mean convective velocity:

$$U_c h = \int_0^h u dy = \tau_{x,a} h^2/2\mu_o - (\frac{\partial P_o}{\partial x} - \rho_o g_x)(h^3/3\mu_o)$$

Similarly, from the z-momentum equation:

$$W_c h = \int_0^h w dy = \tau_{z,a} h^2/2\mu_o - (\frac{\partial P_o}{\partial z} - \rho_o g_z)(h^3/3\mu_o)$$

To account for surface tension effects, note that the pressure, P_o, within the film will be altered from the aerodynamic wall pressure, P_a, due to the curvature ($1/R_x$ and $1/R_z$) of the oil film surface, hence:

$$P_o = P_a + \sigma(1/R_x + 1/R_z) \approx P_a - \sigma(h_{xx} + h_{zz})$$

Summarizing, the differential equation governing the response of a thin film of oil to a 3D aerodynamic flow is:

$$\frac{\partial h}{\partial t} + \frac{\partial U_c h}{\partial x} + \frac{\partial W_c h}{\partial z} = 0 \tag{2.2a}$$

$$U_c = \frac{\tau_x h}{2\mu_o} - (\frac{\partial P}{\partial x} - \frac{\partial \sigma(h_{xx} + h_{zz})}{\partial x} - \rho_o g_x)(h^2/3\mu_o) \tag{2.2b}$$

$$W_c = \frac{\tau_z h}{2\mu_o} - (\frac{\partial P}{\partial z} - \frac{\partial \sigma(h_{xx} + h_{zz})}{\partial z} - \rho_o g_z)(h^2/3\mu_o) \tag{2.2c}$$

Equation 2.2, with slight rearrangement, was first given by Squire[15], and we refer to this equation as "Squire's Form" of the thin oil film equation. Tanner[1] gave a different form which we refer to as "Tanner's Form" of the thin oil film equation. In Appendix A, the equivalence of the two forms of the thin oil film equation is demonstrated through a metric transformation.

The issue of boundary conditions will be treated in the solution subsections below. Note, we have dropped the subscript, a, on τ_x, τ_z and P in the equation above and for the rest of the paper since this subscript was introduced for clarity to distinguish between the values within the oil film and the values imposed from the aerodynamic flow. Henceforth, the aerodynamic wall shear stress and wall pressure meanings for these terms are assumed.

In the absence of the surface tension term, which for many problems is negligible, the thin oil film equation is first-order hyperbolic or wave-like with the characteristic direction of information propagation being indicated by the mean convective velocity vector, (U_c,W_c). With inclusion of the surface tension term, the equation becomes elliptic.

Further observe that the τ terms are multiplied by h^2 whereas the remaining terms are multiplied by h^3. Thus, for h very small, the τ terms typically dominate except near singularities, where the shear stress approaches zero.

For the case where the pressure, gravity and surface tension terms are negligible compared to the shear stress term, the thin oil film equation becomes:

$$\frac{\partial h}{\partial t} + \frac{\partial \tau_x h^2/2\mu_o}{\partial x} + \frac{\partial \tau_z h^2/2\mu_o}{\partial z} = 0 \tag{2.3}$$

In a coordinate independent form, the above equation becomes:

$$\frac{\partial h}{\partial t} + \nabla \cdot (\frac{h^2}{2\mu_o}\vec{\tau}) = 0 \tag{2.4}$$

3. ANALYTICAL SOLUTIONS

Analytical solutions for the thin oil film equation are considered in this section. These analytical solutions are for relatively simple test case conditions, but do include both 1D and 2D thin oil film problems for 2D and 3D aerodynamic flows, respectively. These analytical solutions can be instructive as to general thin oil film behavior as well as being useful in their own right. More general cases, whether for 1D or 2D oil films, require numerical solution procedures. Even for numerical procedures, the analytical solutions aid in formulating boundary conditions. Furthermore, the analytical solutions considered in this section then provide known test cases to assess the validity and accuracy of the more general numerical solution procedures.

We start by establishing a self-similar form of the 2D oil film equation. Then, we further reduce this equation to an ordinary differential equation for the 1D self-similar thin oil film problem, and establish several self-similar relationships. Analytical 1D solutions are then established. We then return to the 2D self-similar form, and, for special forms of the wall shear stress under a 3D aerodynamic flow, establish 2D analytical solutions.

Consider the thin oil film equation where the pressure gradient, gravity and surface tension terms are negligible:

$$\frac{\partial h}{\partial t} + \frac{\partial}{\partial x}\left(\frac{\tau_x h^2}{2\mu_o}\right) + \frac{\partial}{\partial z}\left(\frac{\tau_z h^2}{2\mu_o}\right) = 0 \tag{3.1}$$

We consider solutions which are self-similar in time of the form:

$$h(x, z, t) = H(x, z)/t \tag{3.2}$$

Thus, $\partial h/\partial t = -H/t^2$, giving the 2D self-similar form of the thin oil film equation:

$$-H + \frac{\partial}{\partial x}\left(\frac{\tau_x H^2}{2\mu_o}\right) + \frac{\partial}{\partial z}\left(\frac{\tau_z H^2}{2\mu_o}\right) = 0 \tag{3.3}$$

In coordinate independent form, the above equation becomes:

$$-H + \nabla \cdot \left(\frac{H^2}{2\mu_o}\vec{\tau}\right) = 0 \tag{3.4}$$

The self-similar solution, $H(x, z)$, describes the asymptotic shape of the thin oil film at large time.

3.1 1D ANALYTICAL SOLUTIONS

For a 1D thin oil film, the self-similar partial differential equation reduces to an ordinary differential equation:

$$H - \frac{d}{dx}(\frac{\tau H^2}{2\mu_o}) = 0 \tag{3.5}$$

One 1D self-similar relation (Tanner and Blows[1]) can be established by integrating the above equation from the leading edge where $H = 0$ at $x = x_0$:

$$\tau(x) = \frac{2\mu_o}{H^2}\int_{x_0}^{x} H\ dx = \frac{2\mu_o}{h^2 t}\int_{x_0}^{x} h\ dx \tag{3.6}$$

Another self-similar relation is found by defining $\zeta \equiv (\tau/\mu_o)^{1/2}H$ and substituting in equation 3.5 giving:

$$\zeta(\mu_o/\tau)^{1/2} - \frac{d}{dx}(\zeta^2/2) = 0$$

or, rearranging

$$(\mu_o/\tau)^{1/2} = d\zeta/dx$$

Integrating, with $\zeta = 0$ at $x = x_0$, and rearranging gives the 1D self-similar relation (also, Tanner and Blows[1]):

$$H = ht = (\mu_o/\tau)^{1/2}\int_{x0}^{x}(\mu_o/\tau)^{1/2}dx \tag{3.7}$$

The relation given by equation 3.7 may be solved for H(x) given known $\tau(x)$ by numerical methods or, where suitable, in closed analytical form. Likewise, the relation given by equation 3.6 may be solved for $\tau(x)$ given known H(x). The studies of Tanner and of Squire provide several such 1D solutions.

The simplest 1D self-similar thin oil film solution is for the case of constant wall shear stress, $\tau(x)$, where:

$$H\tau = ht\tau = \mu_o(x - x_0) \tag{3.8}$$

Axisymmetric Analytical Solutions

For flows over axisymmetric bodies, the governing equation for a thin oil film becomes:

$$\frac{\partial h}{\partial t} + (\frac{1}{r})\frac{\partial}{\partial s}(\frac{r\tau h^2}{2\mu_o}) = 0 \tag{3.9}$$

and the time self-similar form becomes:

$$H - (\frac{1}{r})\frac{d}{ds}(\frac{r\tau H^2}{2\mu_o}) = 0 \tag{3.10}$$

Rearranging and integrating from s_0, where $h = 0$, to s:

$$\tau = (\frac{2\mu_o}{rH^2})\int_{s_0}^{s} rH\ ds = (\frac{2\mu_o}{rh^2t})\int_{s_0}^{s} rh\ ds \tag{3.11}$$

Alternatively, substituting $\zeta^2 \equiv r\tau H^2/\mu_o$ into equation 3.10:

$$H = ht = (\frac{\mu_o}{r\tau})^{1/2}\int_{s_0}^{s}(\frac{\mu_o r}{\tau})^{1/2}\ ds \tag{3.12}$$

As one example of a closed form axisymmetric thin oil film solution, consider the case where the aerodynamic flow consists of the region about an axisymmetric stagnation point or node of attachment formed by placing a circular plate normal to the flow. For this case, $r = s$. A laminar solution for this axisymmetric stagnation point has been given by Homann[17], and is reported in both White[18] and Churchill[19]. The wall shear stress on the plate varies linearly as:

$$\tau = \beta r,\ \beta > 0 \tag{3.13}$$

Assume the "leading edge" of the axisymmetric oil film is located some small distance, r_0, from the stagnation point. Integrating equation 3.12 with the known wall shear stress, equation 3.13, gives the oil film shape:

$$H = ht = (\mu_o/\beta)(1 - r_0/r),\ r > r_0 \tag{3.14}$$

For distances far from the stagnation point the oil will tend toward a uniform thickness, which varies inversely with time. For locations close to the stagnation point, pressure gradient effects become important which then require a non-similar numerical solution. For an axisymmetric node of separation, we may also assume that the local shear stress varies according to $\tau = \beta r$, except $\beta < 0$. The oil film leading edge is applied at $r = r_0$, and the flow of oil is inward toward the node of separation. The solution then is:

$$H = ht = (\mu_o/|\beta|)(r_0/r - 1),\ r < r_0 \tag{3.15}$$

For the axisymmetric node of separation, the singularity at $r = 0$ is avoided due to both surface tension and pressure gradient effects not included in this time self-similar solution.

3.2 2D ANALYTICAL SOLUTIONS

Closed form analytical solutions may also be found for a number of interesting cases of a 2D thin oil film responding to a 3D aerodynamic flow. The flow of a 2D thin oil film in the immediate vicinity of 3D surface streamline topological singularities, such as nodes and saddles, leads to closed form solutions. Additional 2D thin oil film test cases suitable for testing numerical 2D thin oil film solvers involve axisymmetry and are also treated in this section. These closed form solutions serve as suitable test cases for the more general numerical 2D thin oil solvers, both direct and inverse, discussed in following sections. In this subsection, we develop several of these closed form analytical solutions.

Analytical Solutions for Saddles and Nodes

A linearized form of the flow field about surface streamline singularities in 3D aerodynamic flows was developed by Perry and Fairlie[20]. In this section, we make use of relations based on their work to provide appropriate surface shear and wall pressure fields which may be generated by the flowfield so as to study the response of a thin oil film about such surface streamline singularity points. Through a suitable coordinate rotation and stretching[20], a "canonical" form of the surface singularities may be obtained. Thus, in this section, although we consider saddles located on a plane of symmetry, the results are more general. The papers of Perry and Fairlie[20] and of Hung, Sung, and Chen[21] should be referred to for a more extensive development of the shear field and pressure field in the vicinity about a singularity or critical point in 3D aerodynamic flows.

Consider the case of a surface streamline singularity, either a saddle or a node, located on a surface along a plane of symmetry. Figures 2a and 2b show the defining streamlines about a saddle of attachment and a saddle of separation, respectively. The streamlines depicted are either constrained to the surface or form in a symmetry plane for the aerodynamic flow above the saddle. Note for the saddle of separation, a streamline originates from the singularity point and departs into the flow upward from the surface. For a saddle of attachment this streamline will have flow toward the surface. Figures 3a and 3b further depict the surface streamlines about a saddle of attachment and a saddle of separation, respectively. Figures 3c and 3d depict the surface streamlines about a node of attachment and a node of separation, respectively. For convenience, we place the origin of the coordinate system at the location of the surface streamline singularity, $(x, z) = (0, 0)$, with the plane of symmetry occurring along $z = 0$. At the surface singularity point, both the x- and z-component of the wall shear stress go to zero, $((\tau_x, \tau_z) = (0, 0)$ at $(x, z) = (0, 0))$.

For some region locally about this singularity point, the wall shear stress varies according to:

$$\begin{aligned} \tau_x &= ax \\ \tau_z &= bz \end{aligned} \tag{3.16}$$

The relative values of a and b determine the characteristics of the singularity. The saddles and nodes of separation and attachment may thus be distinguished by the values of a and b:

$$\begin{aligned} &a < 0,\ b < 0,\ a+b < 0 : \text{node of separation} \\ &a < 0,\ b > 0,\ a+b < 0 : \text{saddle of separation} \\ &a < 0,\ b > 0,\ a+b > 0 : \text{saddle of attachment} \\ &a > 0,\ b > 0,\ a+b > 0 : \text{node of attachment} \end{aligned} \tag{3.17}$$

The pressure field on the surface may also be found, following the analysis of Perry and Fairlie[20]:

$$\begin{aligned} \frac{\partial P}{\partial x} &= -(3a+b)/\tan\theta \\ \frac{\partial P}{\partial z} &= 0 \end{aligned} \tag{3.18}$$

where θ is the departure angle of that limiting streamline which emanates from the singularity point and which departs the surface into the flow above as depicted in figure 2b. As an aside, equation 3.18 implies that for a given value of $\partial\tau_x/\partial x = a < 0$, a lower pressure gradient will be associated with a saddle of attachment than the pressure gradient associated with a saddle of separation. This may be of practical importance where a laminar flow generates a saddle of attachment for a given geometry, while a turbulent flow generates a saddle of separation for the same flow geometry.

For the two types of saddles and for the node of separation, we have $a < 0$. The oil leading edge is applied as a straight edge at, for example, $x_0 < 0$, and the oil flows toward the saddle point or node. The solution domain for the thin oil film is then $x_0 < x < 0$. For the node of attachment, flow is away from the node, and we may chose the solution domain as $x < x_0 < 0$. For the node of attachment, the leading edge of the oil film can also be chosen to be at the node point ($x_0 = 0$). Note that the special case of either the axisymmetric node of separation or of attachment as treated in the previous section differs in that $a \equiv b$ and the oil leading edge is applied not as a straight line but at the circle defined by $r = r_0$.

We first derive the shape of the surface streamlines, since along any given surface streamline:

$$\frac{dz}{dx} = \frac{\tau_z}{\tau_x} = \frac{bz}{ax}$$

If we assume the streamline passes through the arbitrary point, (x_s, z_s), we may integrate the above streamline relation to obtain:

$$\frac{z}{z_s} = (\frac{x}{x_s})^{b/a} = (\frac{x_s}{x})^{b/-a} \tag{3.19}$$

Curves demonstrating the above streamline equation for several values of a/b are shown in figures 3a-3d for the saddles and nodes of attachment and separation.

To proceed toward a closed form solution for the thickness distribution for an oil film near a surface streamline singularity point, first consider the saddle of separation. The streamline flow along the surface in the plane of symmetry is toward the saddle, and thus:

$$a < 0, \text{ and } b > 0$$

Consider that the wall shear stress effects predominate over the pressure gradient and surface tension effects, except very close to $x = 0$. To more properly examine the inclusion of these effects, we will later resort to numerical solvers. With the assumption of negligible pressure and surface tension, the 2D thin oil film equation takes the form of equation 3.1, which we repeat here:

$$\frac{\partial h}{\partial t} + \frac{\partial}{\partial x}(\frac{\tau_x h^2}{2\mu_o}) + \frac{\partial}{\partial z}(\frac{\tau_z h^2}{2\mu_o}) = 0$$

First, apply the known shear field of $\tau_x = ax$, and $\tau_z = bz$, and expand:

$$\frac{\partial h}{\partial t} + a\frac{\partial}{\partial x}(\frac{xh^2}{2\mu_o}) + \tau_z\frac{\partial}{\partial z}(\frac{h^2}{2\mu_o}) + b(\frac{h^2}{2\mu_o}) = 0$$

Note that if the oil thickness, h, initially varies at most in x then there is no driving force for h to subsequently acquire a variation in the z-direction. Thus, $\partial h/\partial z = 0$ not only initially, but for all time. A variation in x must occur due to the leading edge. Thus, $h = h(x,t)$, which leads to:

$$\frac{\partial h}{\partial t} + a\frac{\partial}{\partial x}(\frac{xh^2}{2\mu_o}) + b(\frac{h^2}{2\mu_o}) = 0$$

Now, applying the self-similarity relation ($h(x,t) = H(x)/t$) and rearranging ($b \neq 0$ avoids the trivial 1D case):

$$dH/(\mu_o - (a+b)H/2) = dx/(ax) \tag{3.20}$$

Excluding the special case where $a + b = 0$, we integrate from x_0, where $h = 0$, to x:

$$H = (\frac{2\mu_o}{a+b})[1 - (\frac{x}{x_0})^{\frac{(a+b)}{-2a}}], \text{ for } 0 < x < x_0 \tag{3.21}$$

This solution, also see Tanner[4], covers the interesting case of thin oil film response in the vicinity of the surface singularities known as saddles of separation and saddles of

attachment and is also valid for the node of separation, when such singularities are located on a plane of symmetry. We will in later sections of this paper also obtain numerical solutions and discuss in greater depth.

A node of attachment($a+b>0,\ a>0,\ b>0$) has a different domain of solution and thus different limits of integration for equation 3.20, resulting in:

$$H = (\frac{2\mu_o}{a+b})[1 - (\frac{x_0}{x})^{\frac{(a+b)}{2a}}],\ \text{for}\ 0 < x_0 < x \tag{3.22}$$

Oddly, for a node of attachment with the "leading edge" located at $x_0 = 0$, the only allowable self-similar solution is:

$$H = 2\mu_o/(a+b),\ \text{for all}\ x$$

The behavior of the oil film at the location of the saddle differs considerably for the two types of saddles:

$$\text{saddle of separation}(a+b<0,\ a<0,\ b>0):\ H \to \infty,\ \text{as}\ x \to 0$$
$$\text{saddle of attachment}(a+b>0,\ a<0,\ b>0):\ H = 2\mu_o/(a+b),\ \text{for}\ x = 0$$

Also,

$$\text{node of separation}(a+b<0,\ a<0,\ b<0):\ H \to \infty,\ \text{as}\ x \to 0$$

For the special case where $a+b=0$, note that for oil to flow from the oil film leading edge at $x = x_0$ to the singularity at $x = 0$, we must have $a < 0$. For this special case, integration of the ODE above from x_0 toward $x = 0$ yields:

$$ht = H = (-\mu_o/a)\ln x_0/x,\ \text{for}\ x < x_0,\ a < 0,\ \text{and}\ a+b=0 \tag{3.23}$$

Examination of the form of these solutions, equations 3.21 and 3.23, suggests that a suitable plot of H vs $\log_{10} x$ should prove useful in determining the ratio of the wall shear stress slopes b/a and thereby, for example, allow determining whether a saddle is a saddle of attachment or saddle of separation.

Analytical 2D Thin Oil Film Relations

For somewhat more general 2D thin oil film cases we can establish useful relations. Consider equation 3.1, where we further assume that τ_x is a function of x only, and $\tau_z = bz + f(x)$:

$$\frac{\partial h}{\partial t} + \frac{\partial}{\partial x}(\frac{\tau_x h^2}{2\mu_o}) + \tau_z \frac{\partial}{\partial z}(\frac{h^2}{2\mu_o}) + b(\frac{h^2}{2\mu_o}) = 0 \tag{3.24}$$

Note that $h = h(x,t)$ is a possible solution. If the initial h is only a function of x, $(h_0 = h_0(x))$, then initially $\partial(h^2)/\partial z = 0$ and, consequentially, there is no driving force for h to subsequently acquire a variation in the z-direction. Thus, we may seek solutions for h where h is only a function of time and x.

Applying the self-similarity relation where $h = H/t$, noting $\partial/\partial z = 0$, and rearranging:

$$\frac{d}{dx}(\frac{\tau_x H^2}{2\mu_o}) = H - (\frac{bH^2}{2\mu_o}) \tag{3.25}$$

Integrating from x_0, where $h = 0$, to x:

$$\tau_x = (\frac{2\mu_o}{H^2}) \int_{x_0}^{x} H[1 - (\frac{bH}{2\mu_o})]\, dx \tag{3.26}$$

4. NUMERICAL SOLUTIONS

Numerical procedures are required to solve for the general time-dependent response of a thin oil film on a surface subjected to an aerodynamic flow. In the previous section, we discussed special cases where time self-similar solutions of analytical form were possible. However, the inclusion of initial conditions, pressure gradient, gravity, centrifugal, or surface tension effects, lead to a time-dependent oil film response which needs not be self-similar in time. Also, the geometry of the oil film or the aerodynamic flow will not typically lend itself to a known analytical solution. Fortunately, CFD methods are readily available for application to the numerical solution of the general thin oil film problem. In this section, we describe those methods which we have found most suitable.

Two primary numerical approaches were developed in the present studies. The first approach we refer to as a direct solver, where the oil film thickness, $h(x, z, t)$, is solved for knowing the aerodynamic wall shear stress and wall pressure, and where gravity, centrifugal and/or surface tension effects are included. The second approach we refer to as an inverse solver, where the wall shear stress, $\vec{\tau}(x, z)$, is deduced knowing the response of the oil film thickness at several times, $h(x, z, t_1)$ and $h(x, z, t_2)$, and the surface flow direction, $\gamma(x, z)$, as well as known wall pressure, and where the gravity, centrifugal and/or surface tension effects are included. The inverse solver, in particular, provides a rigorous foundation for the oil film method of experimental measurement of wall shear stress.

The numerical method described is chosen for its simplicity for use with both the direct and inverse solvers. For the direct solver, the h solution is advanced in time, with repeated sweeps through the grid. For the inverse solver, the τ solution is simply marched once in space through the grid. The dominant physical phenomenon described by the thin oil film equation is hyperbolic, having a known characteristic direction. The characteristic direction may be thought of as the direction in which information propagates. Each point in the thin oil film is only under the immediate influence of its upwind neighboring points. Thus, the dominant hyperbolic nature of the thin oil film equation allows the direct solver to advance the solution in time by means of a point-by-point implicit solution. Each point is advanced in time once those neighbor points which are upwind are advanced in time. Each time-advance sweep through the grid proceeds from the boundary points inward to the interior points.

For the direct solver, addition of the surface tension term introduces an elliptic feature, which allows information to propagate in all directions. However, the influence of the surface tension effects on a thin oil film will occur over only a quite limited region. The oil film is thin (typically a few microns) and is assumed to cover an extended region of the test surface. For surface tension to be significant, the curvature of the film surface must be significant. For the film to remain thin, this curvature cannot cover a large region. A variety of elliptic solution methods may be applied to implement the surface tension terms. Particularly in two directions, implicit methods unnecessarily complicate the solver. Due to the large time scale associated with the surface tension terms, however, the simplest

approach is to incorporate the surface tension explicitly and limit the time step. The time scale for surface tension, ($\Delta t_\sigma \approx \mu_o L_\sigma^4/\sigma h^3$), is typically quite large (days rather than seconds), particularly when compared to the time scale required for accurate solution of the shear stress terms. Thus, explicit treatment of the complete surface tension terms in an otherwise implicit point-wise direct solver should prove sufficient and quite practical for most shear-driven applications. An example of a line-implicit treatment of the surface tension term (for one predominant direction only) is included in the application section.

For the inverse solver, in contrast, the thin oil film equation remains hyperbolic, even with the inclusion of the surface tension terms, which then are known source terms.

In the following subsections, we first describe the numerical procedures we use for an interior node of the direct solver. A Box-Implicit numerical method is described. The associated numerical boundary conditions are then described. An alternative Finite-Volume Upwind-Implicit numerical method is also presented. In the final subsection, the inverse solver numerical methods are described.

4.1 DIRECT NUMERICAL SOLUTIONS

To simplify the derivation of the numerical method, we first neglect the pressure gradient, gravity, centrifugal and surface tension effects and then add these effects later in the section. Considering only the viscous terms in the oil flow, the partial differential equation for an interior point of a thin oil film is given by a simplified version of equation 2.2:

$$\frac{\partial h}{\partial t} + \frac{\partial}{\partial x}(U_c h) + \frac{\partial}{\partial z}(W_c h) = 0 \tag{4.1a}$$

$$U_c = \frac{\tau_x h}{2\mu_o} \tag{4.1b}$$

$$W_c = \frac{\tau_z h}{2\mu_o} \tag{4.1c}$$

The above partial differential equation is hyperbolic and at any point considered the equation represents a specialized form of the continuity equation which depicts the convection of the conserved variable h (related to the oil mass at a point) at a velocity U_c in the x-direction and at a velocity W_c in the z-direction. Any numerical method to be successful for application with this equation should be conservative and time-accurate, with consideration given to the direction of the convective velocity.

First integrate the partial differential equation at an arbitrary point with respect to time, between the two times, t_1 and t_2, giving:

$$(h_2 - h_1) + \frac{\partial}{\partial x}\left(\frac{\tau_x}{2\mu_o}\int_{t_1}^{t_2} h^2 dt\right) + \frac{\partial}{\partial z}\left(\frac{\tau_z}{2\mu_o}\int_{t_1}^{t_2} h^2 dt\right) = 0 \tag{4.2}$$

Note, the wall shear stress components, $\tau_x(x,z)$ and $\tau_z(x,z)$, are assumed to be known from the aerodynamic flow and are steady in time. We also assume the oil viscosity is steady in time. We have seen in the prior section on analytical solutions that the oil film thickness tends to vary inversely with time according to $h \approx t^{-1}$. Because of this inverse time relation over much of the oil film, greater practical accuracy can be obtained by evaluating the integral with the numerical quadrature given by:

$$\int_{t_1}^{t_2} h^2 dt = h_1 h_2 (t_2 - t_1) \tag{4.3}$$

The above quadrature is exact for $h \approx t^{-1}$ while only formally first-order accurate. Use of a formally second-order accurate quadrature, such as $(h_1 + h_2)^2(t_2 - t_1)/4$, actually results in a reduction in time accuracy for many practical cases where the $h \approx t^{-1}$ time-similarity is approached. As a consequence of the time-integration, equation 4.2 becomes:

$$(h_2 - h_1) + \frac{\partial}{\partial x}(\frac{\tau_x}{2\mu_o} h_1 h_2 \Delta t) + \frac{\partial}{\partial z}(\frac{\tau_z}{2\mu_o} h_1 h_2 \Delta t) \tag{4.4}$$

Box-Implicit Direct Solver: Interior Node

We now require spatial-discretization of the oil film into a 2D array of nodes, ($i = 1, i\max$, and $j = 1, j\max$), with even spacing, Δx and Δz in x and z, respectively. Thus, $x_{i,j} = i\Delta x$ and $z_{i,j} = j\Delta z$. More complex gridding treatments can be accommodated but are not treated here.

To develop the Box-Implicit numerical procedure, consider the solution molecule shown in figure 4. It is assumed that we know the solution at the time level t_1 and that we desire to advance the solution at node (i,j) to the new time level, t_2. We assume the convective velocities are $U_c > 0$ and $W_c > 0$. Thus, to solve for $h_{2,i,j} = h(x_{i,j}, z_{i,j}, t_2)$ we require the solution at nodes $(i-1,j)$, $(i,j-1)$, and $(i-1,j-1)$ to have already been advanced to the new time level, t_2. To achieve second-order accurate approximations to the spatial derivatives, $\partial/\partial x$ and $\partial/\partial z$, we evaluate at the midpoint of the control volume, $i - 1/2, j - 1/2$:

$$\left.\frac{\partial(\tau_x h_1 h_2/\mu_o)}{\partial x}\right|_{i-1/2,j-1/2} = [(\tau_x h_1 h_2/\mu_o)_{i,j} - (\tau_x h_1 h_2/\mu_o)_{i-1,j} + (\tau_x h_1 h_2/\mu_o)_{i,j-1} - (\tau_x h_1 h_2/\mu_o)_{i-1,j-1}]/(2\Delta x)$$

and

$$\frac{\partial(\tau_z h_1 h_2/\mu_o)}{\partial z}_{i-1/2,j-1/2} = [(\tau_z h_1 h_2/\mu_o)_{i,j} - (\tau_z h_1 h_2/\mu_o)_{i,j-1} + (\tau_z h_1 h_2/\mu_o)_{i-1,j} - (\tau_z h_1 h_2/\mu_o)_{i-1,j-1}]/(2\Delta z)$$

where $\Delta x = (x_{i,j} - x_{i-1,j})$ and $\Delta z = (z_{i,j} - z_{i,j-1})$. Substituting into equation 4.4 and gathering terms:

$$\begin{aligned} h_{2,i,j} + \Delta t(h_1 h_2/\mu_o)_{i,j}(\frac{\tau_x}{\Delta x} + \frac{\tau_z}{\Delta z})_{i,j} = \\ [h_{1,i,j} + (h_1 - h_2)_{i-1,j-1} + (h_1 - h_2)_{i-1,j} + (h_1 - h_2)_{i,j-1}] \\ + [(\tau_x h_1 h_2/\mu_o)_{i-1,j-1} + (\tau_x h_1 h_2/\mu_o)_{i-1,j} - (\tau_x h_1 h_2/\mu_o)_{i,j-1}](\Delta t/\Delta x) \\ + [(\tau_z h_1 h_2/\mu_o)_{i-1,j-1} + (\tau_z h_1 h_2/\mu_o)_{i,j-1} - (\tau_z h_1 h_2/\mu_o)_{i-1,j}](\Delta t/\Delta z) \end{aligned} \tag{4.5}$$

Now solving for $h_{2,i,j}$, the oil film thickness at the new time level:

$$\begin{aligned} h_{2,i,j} = \{ & [h_{1,i,j} + (h_1 - h_2)_{i-1,j-1} + (h_1 - h_2)_{i-1,j} + (h_1 - h_2)_{i,j-1}] \\ & + [(\tau_x h_1 h_2/\mu_o)_{i-1,j-1} + (\tau_x h_1 h_2/\mu_o)_{i-1,j} - (\tau_x h_1 h_2/\mu_o)_{i,j-1}](\Delta t/\Delta x) \\ & + [(\tau_z h_1 h_2/\mu_o)_{i-1,j-1} + (\tau_z h_1 h_2/\mu_o)_{i,j-1} - (\tau_z h_1 h_2/\mu_o)_{i-1,j}](\Delta t/\Delta z)\} \\ & /[1 + \Delta t(h_1/\mu_o)_{i,j}(\frac{\tau_x}{\Delta x} + \frac{\tau_z}{\Delta z})_{i,j}] \end{aligned} \tag{4.6}$$

Equation 4.6 is the 2D Box-Implicit algebraic equation which allows us to numerically solve the 2D thin oil film equation, equation 4.1, at an interior node. The Box-Implicit node equation, as derived here, is second-order accurate in space, with "quasi"-higher-order treatment of the time variation. The equation is conservative of the oil mass. The Box method is known to be unconditionally stable. The related boundary condition treatment required to solve a problem is dealt with in the next subsection.

The interior node equation, equation 4.6, clearly can be solved a single node at a time, with each interior node being solved sequentially.

The form of the Box-Implicit interior node equation, as given by equation 4.6, is incomplete in that it does not include additional effects, for example, pressure gradient effects. If the oil film is sufficiently thin, these additional effects are of minimal significance. However, a more complete form of the interior node equation is:

$$\begin{aligned} h^{[k]}_{2,i,j} = \{ & [h_{1,i,j} + (h_1 - h_2)_{i-1,j-1} + (h_1 - h_2)_{i-1,j} + (h_1 - h_2)_{i,j-1}] \\ & + [(T_x - \Pi_x)_{i-1,j-1} + (T_x - \Pi_x)_{i-1,j} - (T_x - \Pi_x)_{i,j-1}](\Delta t/\Delta x) \\ & + [(T_z - \Pi_z)_{i-1,j-1} + (T_z - \Pi_z)_{i,j-1} - (T_z - \Pi_z)_{i-1,j}](\Delta t/\Delta z)\} \\ & /[1 + \Delta t(\frac{\widetilde{T}_x - \widetilde{\Pi}^{[k]}_x}{\Delta x} + \frac{\widetilde{T}_z - \widetilde{\Pi}^{[k]}_z}{\Delta z})_{i,j}] \end{aligned} \tag{4.7}$$

where

$$
\begin{aligned}
T_x &\equiv \tau_x h_1 h_2/\mu_o = \tau\cos(\gamma) h_1 h_2/\mu_o \\
T_z &\equiv \tau_z h_1 h_2/\mu_o = \tau\sin(\gamma) h_1 h_2/\mu_o \\
\Pi_x &\equiv (\partial P/\partial x - \rho_o g_x) h_1 h_2 (h_1 + h_2)/3\mu_o \\
\Pi_z &\equiv (\partial P/\partial z - \rho_o g_z) h_1 h_2 (h_1 + h_2)/3\mu_o \\
\widetilde{T}_x &\equiv \tau_x h_1/\mu_o = \tau\cos(\gamma) h_1/\mu_o \\
\widetilde{T}_z &\equiv \tau_z h_1/\mu_o = \tau\sin(\gamma) h_1/\mu_o \\
\widetilde{\Pi}_x^{[k]} &\equiv (\partial P/\partial x - \rho_o g_x) h_1 (h_1 + h_2^{[k-1]})/3\mu_o \\
\widetilde{\Pi}_z^{[k]} &\equiv (\partial P/\partial z - \rho_o g_z) h_1 (h_1 + h_2^{[k-1]})/3\mu_o \\
h_{2,i,j}^{[0]} &= h_{1,i,j} \\
k &= 1, ..., k\max = \text{node iteration level}
\end{aligned}
\tag{4.8}
$$

To derive equation 4.7, we have made use of the numerical quadrature given by:

$$
\int_{t_1}^{t_2} h^3 dt = (\frac{h_1 + h_2}{2}) h_1 h_2 (t_2 - t_1) \tag{4.9}
$$

As with equation 4.3, equation 4.9 is first-order accurate in time, but is a quasi-higher-order time variation treatment since the numerical quadrature is exact for the practical case of $h \approx t^{-1}$.

Due to the presence of h_2 in the $\widetilde{\Pi}_x$ and $\widetilde{\Pi}_z$ terms, iteration at each node ($k = 1, k\max$) is required to advance the solution to the new time level. Also, the (i, j, etc.) subscripts are absorbed inside the parentheses as required to allow evaluation of each term of equation 4.7 at the proper locations.

An important property of the interior node equation (either equation 4.6 or 4.7) is that the 1D self-similar problem solution for constant τ (eq. 3.8, $h\tau t = \mu_o x$) exactly satisfies either of these algebraic relations. This property of consistency of the interior node algebraic equations with the 1D self-similar problem considerably enhances the accuracy of the solution method for most practical problems encountered.

Surface Tension Terms

Equation 4.7, as shown, does not include surface tension effects, and, thus, the hyperbolic nature of the partial differential equation is exploited by requiring only a node-by-node solution procedure. The inclusion of surface tension incorporates an elliptic feature and the solution molecule at node (i, j) should then include, for the additional surface tension terms, information from the nodes between $(i-2, j)$ and $(i+2, j)$ and between $(i, j-2)$ and $(i, j+2)$.

The simplest surface tension thin oil film approach is to recognize that the time scale which characterizes surface tension is typically much greater than the time scale which characterizes a thin oil film acting under shear stress. Thus, the surface tension adjustment to the wall pressure at each node will be essentially constant during the integration time step, Δt. A sufficient treatment of surface tension for most thin oil film calculations would be an explicit approach where the adjustment to pressure is made at the known time level, t_1, prior to each time step:

$$P = P_{air} + P_\sigma, \text{ where } P_\sigma \equiv -\sigma[(h_1)_{xx} + (h_1)_{zz}] \tag{4.10}$$

An example of an implicit elliptical surface tension treatment is given in the application section for problems where surface tension acts only in the x direction. However, we normally would take the above rather simplistic explicit approach due to the predominance of the viscous terms over surface tension for the thin films which we likely will have an interest in solving. This is done in order to maintain the simple to code node-by-node solution procedure.

Numerical Boundary Conditions

The solution at the interior nodes must be started with an initial condition, where an initial value of oil film thickness $h(x, z, t_0)$ is assigned, and then the solution is advanced to the next time level starting at boundary nodes. Thus, numerical treatments of the initial and boundary conditions are required. The types of boundary conditions required include a leading edge case, a corner leading edge case, a plane of symmetry case, a general surface streamline case and a boundary wall (no-flow) case. An important consideration for 2D oil film problems is that the boundary condition treatment will depend on whether the characteristics point into or out of the oil film domain at any particular location on the boundary.

Leading Edge Boundary Condition

The leading edge of an oil film is the contact line separating the region of the test surface covered by the oil film from the region of the test surface exposed directly to the aerodynamic flow. The wall shear stress at the leading edge will cause oil to flow from the leading edge into the region covered by the oil. A leading edge may be used as a boundary condition since the oil film height at the leading edge is known ($h = 0$), and the direction of the wall shear stress, τ_x and τ_z, suggests that the convective velocities, U_c and W_c, within the oil film immediately adjacent to the leading edge allow solution at the interior nodes. In contrast, at a trailing edge, the wall shear stress will have a direction pointing out of the oil film region. The advancement of the oil film trailing edge over a fresh surface can be a difficult subject, involving finger instabilities, and is not treated in this present work. Therefore, the trailing edge is not a suitable boundary condition for a thin oil film solver.

Over an extended period of time for which air flow occurs past a thin oil film, the leading edge of the thin oil film will eventually move in the direction of the aerodynamic flow, uncovering the test surface. However, here we consider the use of oil films in aerodynamics testing, and for moderate run times the oil film leading edge may be considered to be stationary.

Further, a complete consideration of the fluid mechanics occurring at the leading edge of a thin oil film will include surface tension effects. At the leading edge, a contact line occurs which is defined by the juncture of the solid-air, solid-oil, oil-air interfaces as depicted in figure 5. Discussion of surface tension effects at the leading edge will be deferred to the applications section (Section 5). However, the amount of oil mass present in the control volume associated with the boundary nodes is quite small and for many practical cases, the simplified treatment of the leading edge presented here proves sufficient.

The simplest leading edge treatment is to align the grid so that either the $i = 0$ or $j = 0$ boundary nodes line up precisely along the actual oil film leading edge. The oil film thickness for these boundary nodes is then simply held at $h = 0$, and the solution actually

starts at the next row of interior nodes, $i = 1$ or $j = 1$, using a variant of the interior node equation 4.6:

$$h_{2,1,j} = [h_{1,1,j} + (h_1 - h_2)_{1,j-1} + (h_1 h_2 \Delta t/\mu_o)_{1,j-1}(\frac{2}{3}\frac{\tau_z}{\Delta z} - \frac{\tau_x}{\Delta x})_{1,j-1}] \\ /[1 + (h_1 \Delta t/\mu_o)_{1,j}(\frac{\tau_x}{\Delta x} + \frac{2}{3}\frac{\tau_z}{\Delta z})_{1,j}],\ j = 2, .., j\max \tag{4.11}$$

Equation 4.11 is the boundary condition equation for the $i = 1$ row of interior node points for a leading edge at $i = 0$. Derivation of equation 4.11 is based on a control volume analysis which makes use of the mass flux in the z-direction integrated over the face between $(1, j)$ and $(0, j)$:

$$\int_{t_1}^{t_2}\int_0^{\Delta x} \tau_z h_1 h_2/\mu_o dx dt = (\tau_z h_1 h_2/\mu_o)_{1,j}\Delta t \Delta x/3 \tag{4.12}$$

Note that at the leading edge the oil film thickness varies as $h \approx x/t$ between nodes at $i = 0$ and $i = 1$. A similar node equation is easily derived for the case of a leading edge at $j = 0$.

The intersection of two leading edges, with the $i = 0$ row of boundary node points forming one leading edge and the $j = 0$ row of boundary node points forming the other leading edge, creates the natural place, $(i = 1, j = 1)$, to start the process of solving for interior nodes. Again, a control volume analysis for this corner node with $h_{0,1} = h_{1,0} = h_{0,0} = 0$, and assuming a linear variation of oil film thickness toward the node at $(1, 1)$ leads to the corner leading edge node equation:

$$h_{2,1,1} = h_{1,1,1}/[1 + \Delta t(h_1/\mu_o)_{1,1}(\frac{\tau_x}{\Delta x} + \frac{\tau_z}{\Delta z})_{1,1}] \tag{4.13}$$

Plane of Symmetry Boundary Condition

A plane of symmetry for the aerodynamic flow may serve as a boundary condition for the thin oil film equation. Consideration of the plane of symmetry (aligned with the x-axis) leads to the following relations:

a. $\partial h/\partial z = 0$, but $h \not\equiv 0$.

b. $\gamma = 0$, but $\partial\gamma/\partial z \not\equiv 0$, which implies $\tau_z = 0$, but $\partial\tau_z/\partial z \not\equiv 0$.

c. $\rho_o g_z = 0$, but $\partial\rho_o g_z/\partial z \not\equiv 0$.

d. $\partial P/\partial z = 0$, but $P \not\equiv 0$, and $\partial^2 P/\partial z^2 \not\equiv 0$.

The surface streamline angle, $\tan(\gamma) = \tau_z/\tau_x$, may be derived from the known shear field.

We assume the row of boundary nodes, $(i = 1, i\max$, and $j = 0)$, is aligned along the line of symmetry formed in the thin oil film. The numerical form of the symmetry boundary conditions is based on equation A.3, repeated here as:

$$\frac{\partial h}{\partial t} + \frac{\partial \tau h^2/2\mu_o}{\partial x} + (\tau h^2/2\mu_o)\frac{\partial \gamma}{\partial z} = 0$$

Evaluating at $(i-1/2, 0)$ using the same numerical techniques leading to the interior node equation 4.6 results in:

$$\begin{aligned} h_{2,i,0} =& [h_{1,i,0} + (h_1 - h_2)_{i-1,0} + \Delta t(\tau_x h_1 h_2/\mu_o)_{i-1,0}(\frac{1}{\Delta x} - \frac{1}{2}\frac{\partial \gamma}{\partial z})_{i-1,0}] \\ & /[1 + \Delta t(\tau_x h_1/\mu_o)_{i,0}(\frac{1}{\Delta x} + \frac{1}{2}\frac{\partial \gamma}{\partial z})_{i,0}] \end{aligned} \tag{4.14}$$

Equation 4.14 applies in the absence of pressure and/or gravitational effects. For the more general case where pressure and/or gravitational effects are included, we start with the complete form of the plane of symmetry equation:

$$\frac{\partial h}{\partial t} + \frac{\partial}{\partial x}(\frac{\tau_x h^2}{2\mu_o}) + (\frac{\tau_x h^2}{2\mu_o})\frac{\partial \gamma}{\partial z} - \frac{\partial}{\partial x}[(\frac{\partial P}{\partial x} - \rho_o g_x)\frac{h^3}{3\mu_o}] - (\frac{h^3}{3\mu_o})(\frac{\partial^2 P}{\partial z^2} - \frac{\partial \rho_o g_z}{\partial z}) = 0 \tag{4.15}$$

An equation similar to the interior node equation 4.7, but for the boundary nodes located on the plane of symmetry can now be derived from equation 4.15:

$$\begin{aligned} h_{2,i,0}^{[k]} =& [h_{1,i,0} + (h_1 - h_2)_{i-1,0} + \Delta t(\frac{T_x - \Pi_x}{\Delta x} - \frac{1}{2}T_x\frac{\partial \gamma}{\partial z} - \Pi_n)_{i-1,0}] \\ & /[1 + \Delta t(\frac{\widetilde{T}_x - \widetilde{\Pi}_x^{[k]}}{\Delta x} + \frac{1}{2}\widetilde{T}_x\frac{\partial \gamma}{\partial z} + \widetilde{\Pi}_n^{[k]})_{i,0}] \end{aligned} \tag{4.16}$$

where

$$\begin{aligned} T_x \equiv& \tau_x h_1 h_2/\mu_o = \tau\cos(\gamma)h_1 h_2/\mu_o \\ \Pi_x \equiv& (\partial P/\partial x - \rho_o g_x)[h_1 h_2(h_1 + h_2)/3\mu_o] \\ \Pi_n \equiv& (\partial^2 P/\partial z^2 - \partial \rho_o g_z/\partial z)[h_1 h_2(h_1 + h_2)/6\mu_o] \\ \widetilde{T}_x \equiv& \tau_x h_1/\mu_o = \tau\cos(\gamma)h_1/\mu_o \\ \widetilde{\Pi}_x^{[k]} \equiv& (\partial P/\partial x - \rho_o g_x)[h_1(h_1 + h_2^{[k-1]})/3\mu_o] \\ \widetilde{\Pi}_n^{[k]} \equiv& (\partial^2 P/\partial z^2 - \partial \rho_o g_z/\partial z)[h_1(h_1 + h_2^{[k-1]})/6\mu_o] \\ h_{2,i,j}^{[0]} =& h_{1,i,j} \\ k =& 1, ..., k\max = \text{node iteration level} \end{aligned} \tag{4.17}$$

The $\partial \rho_o g_z / \partial z$ term may appear if the plane of symmetry of the body cuts vertically through the body. The addition of the pressure and gravity terms requires an iteration at each node as was done for the interior node equation 4.7. Further, as with the interior node equation 4.7, if surface tension terms are to be included, we adjust the pressure using equation 4.10 in a global iteration scheme.

Wall or No-Flow Boundary Condition

A wall boundary condition may be used if the thin oil film is bounded on one side by a solid wall. The development is similar to the plane of symmetry boundary condition in that there is no oil flow through the boundary. Indeed, in the absence of pressure gradient or gravity effects, the plane of symmetry equations, equations A.3 and 4.14, may be used for a solid wall boundary.

If the effects of pressure gradients, gravity, and/or surface tension are to be included, however, the $\partial P / \partial z$ and $\partial h / \partial z$ gradients need not be zero for the wall boundary conditions. As a consequence, a preferable form of the applicable governing differential equation for the thin oil film along a wall boundary is:

$$\begin{aligned} \frac{\partial h}{\partial t} + \frac{\partial}{\partial x}\left(\frac{\tau_x h^2}{2\mu_o}\right) + \left(\frac{\tau_x h^2}{2\mu_o}\right)\frac{\partial \gamma}{\partial z} - \frac{\partial}{\partial x}\left[\left(\frac{\partial P}{\partial x} - \rho_o g_x\right)\frac{h^3}{3\mu_o}\right] \\ - \left(\frac{h^3}{3\mu_o}\right)\left(\frac{\partial^2 P}{\partial z^2} - \frac{\partial \rho_o g_z}{\partial z}\right) - \left(\frac{\partial P}{\partial z} - \rho_o g_z\right)\frac{h^2}{\mu_o}\frac{\partial h}{\partial z} = 0 \end{aligned} \tag{4.18}$$

The following numerical quadrature should prove useful in deriving the wall boundary node equation:

$$\int_{t_1}^{t_2} h^2 \frac{\partial h}{\partial z} dt = \frac{3}{2} h_1 h_2 \left(\frac{\partial h_1}{\partial z} + \frac{\partial h_2}{\partial z}\right)(t_2 - t_1) \tag{4.19}$$

Since the wall boundary condition has not been tested in this present study, we defer in presenting the form of the wall node equation which includes the pressure gradient effects.

Other potentially useful boundary conditions include a plane of symmetry intersecting a solid wall, a solid wall intersecting another solid wall, and a general surface streamline. The general surface streamline boundary condition can be derived for the situation where the oil streamline is known and the boundary is chosen so as to align with the known surface streamline. The plane of symmetry boundary condition is a special case of the general surface streamline boundary condition. The general surface streamline boundary condition should prove most useful for a mapped grid and is based on equation A.3.

Finite-Volume Upwind-Implicit Direct Solver: Interior Node

An alternate approach to the finite-difference Box-Implicit numerical method is the Finite-Volume Upwind-Implicit numerical method. Here, we briefly develop only the interior node equation for a 1D thin oil film case, with $U_c > 0$. The extension to 2D and a change in sign of U_c is not considered here. Further, the pressure gradient, gravity, centrifugal and surface tension terms are not included, since these terms may be treated in a manner similar to that employed for the Box-Implicit numerical method.

Figure 6 shows a 1D interior node computational molecule for the Finite-Volume Upwind-Implicit method. For the Finite-Volume method, h_i represents the "average" oil film thickness within the node volume which lies between x_i and x_{i+1}. When needed, we may use the approximation that the height h_i is located at the midpoint of the node, $(x_i + x_{i+1})/2$. In contrast, for the finite-difference method, h_i represents the oil film thickness at x_i and the average oil film thickness between x_{i-1} and x_i is given by $(h_i + h_{i-1})/2$.

A mass balance during the time interval between t_1 and t_2 for the control volume defined between x_i and x_{i+1} is:

$$(\Delta m_{cv})_i + (\int_{t_1}^{t_2} F_{i+1/2} dt - \int_{t_1}^{t_2} F_{i-1/2} dt) = 0$$

where $\int_{t_1}^{t_2} F_i dt = (\rho_o \tau_x h_1 h_2 \Delta t / 2\mu_o)_i$. Observe that the mass flux, F_i, is evaluated at the cell volume midpoint, $x_{i+1/2} \equiv (x_i + x_{i+1})/2$. Thus, the value for $(\tau_x)_i$ is actually the value for the wall shear stress at $x_{i+1/2}$.

We do not directly know the mass flux at the control faces (i.e., $F_{i+1/2}$), but rather we know the state of the fluid at the midpoint of the control volume (i.e., h_i and F_i). The mass flux at the control volume face is obtained by a second-order upwind biased extrapolation.

$$F_{i+1/2} = (3F_i - F_{i-1})/2 \tag{4.20}$$

A first-order flux limit relation is substituted to eliminate overshoots and oscillations where $\partial F / \partial x$ changes sign:

$$F_{i+1/2} = F_i, \text{ if } (F_i - F_{i-1})(F_{i-1} - F_{i-2}) < 0 \tag{4.21}$$

For most nodes the flux limiter is not applied and the mass balance for node i becomes, with rearrangement:

$$(h_2 - h_1)_i \Delta x + \frac{\Delta t}{4}[3(\frac{\tau_x h_1 h_2}{\mu_o})_i - 4(\frac{\tau_x h_1 h_2}{\mu_o})_{i-1} + (\frac{\tau_x h_1 h_2}{\mu_o})_{i-2}] = 0 \tag{4.22}$$

Rearranging, we obtain the 1D Finite-Volume Upwind-Implicit interior node equation (without Flux Limiter):

$$(h_2)_i = [(h_1)_i + \frac{\Delta t}{\Delta x}(\frac{\tau_x h_1 h_2}{\mu_o})_{i-1} - \frac{\Delta t}{4\Delta x}(\frac{\tau_x h_1 h_2}{\mu_o})_{i-2}]/[1 + \frac{3\Delta t}{4\Delta x}(\frac{\tau_x h_1}{\mu_o})_i] \qquad (4.23)$$

For comparison purposes, the 1D Box-Implicit interior node equation (eq. 4.6) is:

$$(h_2)_i = [(h_1)_i + (h_1 - h_2)_{i-1} + \frac{\Delta t}{\Delta x}(\frac{\tau_x h_1 h_2}{2\mu_o})_{i-1}]/[1 + \frac{\Delta t}{\Delta x}(\frac{\tau_x h_1}{2\mu_o})_i]$$

Numerical boundary conditions are developed similar to the Box-Implicit method, but the boundaries occur at the node faces, rather than where the node value for h is known. For example, for a leading edge at $x = x_0$, $h_{i=0} \not\equiv 0$ since $(x_1 - x_0)h_{i=0}$ represents the oil volume contained in the control volume associated with the $i = 0$ node. Rather, the leading edge condition implies that $F_{-1/2} \equiv 0$ for the control volume face located at x_0.

Since, in the absence of surface tension, the partial differential equation is hyperbolic, the ith node depends on only those nodes upwind (e.g., $i - 1$, etc., for $U_c > 0$) and the nodes may be solved sequentially. Also, notice that the Finite-Volume Upwind-Implicit method is mass conservative due to the consistent mass flux treatment at each face. The method is second-order accurate in space, with a quasi-higher-order time variation treatment. Further, the node equation 4.23 is consistent with the 1D time self-similar solution for the case of constant τ_x.

A favorable comparison of results from the Finite-Volume Upwind-Implicit method with results from the finite-difference Box-Implicit method will be made in the application section (Section 5) for a 1D test problem.

4.2 INVERSE NUMERICAL SOLUTIONS

Numerical techniques for the inverse solution of the 2D thin oil film partial differential equation provide the basis for the experimental determination of the wall shear stress distribution generated on a 2D surface by a 3D flow. Because the inverse method described here is closely related to and derived from the Box-Implicit direct method described above, a brief derivation is provided of the interior node equation and boundary conditions. In the subsections below, we describe both a Two-Time-Level Box-Implicit inverse method and a One-Time-Level Box-Implicit method. The Two-Time-Level method is useful for experiments where sufficient optical access is available to view the test surface during the experiment, while the One-Time-Level method is suited to those experiments where an image of the oil film is acquired after the experimental wind tunnel run.

Two-Time-Level Box-Implicit Inverse Method

To apply the numerical technique described here, the oil film thickness at two distinct times, $h(x, z, t_1)$ and $h(x, z, t_2)$, over the entire test surface region of interest is assumed to be known from, for example, optical measurements[1-4,8,9-11]. Also required are measurements[9-11] of the surface streamline direction, $\gamma(x, z)$, over the same region. The aerodynamic flow over the surface is assumed to be steady between these two times. When pressure gradient effects are important, it is necessary to know the wall pressures during the same time interval, but the inclusion of pressure gradient, gravity or surface tension effects does not alter the solution strategy.

In the context of understanding the solution of the 2D thin oil film equation for the wall shear stress, $\vec{\tau}$, equation 2.2 may be rewritten as:

$$\frac{\partial}{\partial x}\frac{\tau_x h^2}{2\mu_o} + \frac{\partial}{\partial z}\frac{\tau_z h^2}{2\mu_o} + S = 0 \tag{4.24}$$

Where S is a source term absorbing all those terms of equation 2.2 which do not contain the wall shear stress, τ.

Next, apply a coordinate rotation as given in Appendix A (see eq. A.3) to equation 4.24 by the angle γ from the (x, z) coordinate system to the $(s, \tilde{z})$ coordinate system aligned locally with the wall shear stress:

$$\frac{\partial}{\partial s}\frac{\tau h^2}{2\mu_o} + \frac{\tau h^2}{2\mu_o}\frac{\partial \gamma}{\partial \tilde{z}} + \tilde{S} = 0 \tag{4.25}$$

By examining equation 4.25, notice that we now have a first-order differential equation for τ that can be solved along the s-direction which lies aligned with the characteristic direction, γ. The form of equation 4.25 emphasizes the hyperbolic nature of the thin oil film equation when solving for τ, and that the characteristic direction for the inverse solver is given locally by γ, regardless of the nature of the source terms (including possible pressure gradient, gravity or surface tension effects). In contrast, when equation 2.2 is solved in the direct mode for h, inclusion of the pressure gradient and gravity terms can significantly affect the characteristic direction (U_c, W_c). Further, if surface tension terms are included when solving in the direct mode for h, the nature of the equation changes from hyperbolic to elliptic. The consistent hyperbolic (upwind) nature of the thin oil film equation when solving for τ enables the inverse solver to incorporate the pressure gradient, gravity and surface tension effects in a more straightforward manner (without iteration) than the direct solver.

Although a possible solution strategy would be to solve equation 4.25 along identifiable surface streamlines, the approach here is to solve equation 2.2 on a 2D grid in a manner related to the direct solver described earlier. Such an approach is easier to implement for the general experimental case. A particular advantage to the chosen approach is that the

difficulty alluded to in Appendix A of finding the s-n coordinate system is thereby avoided. Knowledge of γ, the surface streamline direction, allows us to define the proper domain of influence, and, thus, which grid points are required to be included in the solution molecule.

The same solution molecule used to describe the interior node for the direct solver is also used to describe the inverse solver (see fig. 4). The domain of influence shown in figure 4 assumes $0 < \gamma < \pi/2$. A rectangular 2D grid is assumed, with even spacing of Δx and Δz. Such a 2D array of grid points might, for example, correspond to the 2D pixel arrangement for experimental data obtained from a series of digital camera images of a thin oil film on the test surface.

The control volume analysis which leads to the Box-Implicit direct solver interior node equation still applies for the Box-Implicit inverse solver. Thus, the interior node equation which forms the basis of the 2D inverse thin oil film solver is a straightforward rearrangement of the interior node equation for the Box-Implicit direct solver, equation 4.6:

$$\begin{aligned}(\tau)_{i,j} =&\{[(h_1-h_2)_{i,j}+(h_1-h_2)_{i-1,j-1}+(h_1-h_2)_{i-1,j}+(h_1-h_2)_{i,j-1}]/\Delta t\\ &+[(\tau_x h_1 h_2/\mu_o)_{i-1,j-1}+(\tau_x h_1 h_2/\mu_o)_{i-1,j}-(\tau_x h_1 h_2/\mu_o)_{i,j-1}]/\Delta x\\ &+[(\tau_z h_1 h_2/\mu_o)_{i-1,j-1}+(\tau_z h_1 h_2/\mu_o)_{i,j-1}-(\tau_z h_1 h_2/\mu_o)_{i-1,j}]/\Delta z\}\\ &/[(h_1 h_2/\mu_o)_{i,j}(\frac{\cos\gamma}{\Delta x}+\frac{\sin\gamma}{\Delta z})_{i,j}]\end{aligned} \tag{4.26}$$

Although the size of the time step between the two images, $(t_2 - t_1)$, may influence the accuracy of a solution, the stability of the inverse solver, which marches in space, is not dependent on the time step size.

A more complete form of equation 4.26 may be derived by rearrangement of equation 4.7 (rather than eq. 4.6) so as to include the pressure gradient, gravity and/or surface tension effects. The inverse solver, even with the inclusion of these terms, does not require either global or node iteration, unlike the direct solver.

Boundary conditions for the inverse solver may be derived from related boundary conditions for the direct solver, generally by rearrangement. For a leading edge, the boundary condition for the inverse solver is analogous to equation 4.11:

$$\begin{aligned}\tau_{1,j} =&[(h_1-h_2)_{1,j}+(h_1-h_2)_{1,j-1}+(h_1 h_2\Delta t/\mu_o)_{1,j-1}(\frac{2}{3}\frac{\tau_z}{\Delta z}-\frac{\tau_x}{\Delta x})_{1,j-1}]\\ &/[(h_1 h_2\Delta t/\mu_o)_{1,j}(\frac{\cos\gamma}{\Delta x}+\frac{2}{3}\frac{\sin\gamma}{\Delta z})_{1,j}],\ j=2,..,j\max\end{aligned} \tag{4.27}$$

For a plane of symmetry, the boundary condition for the inverse solver is analogous to equation 4.14:

$$\tau_{i,0} = [(h_1 - h_2)_{i,0} + (h_1 - h_2)_{i-1,0} + (\tau h_1 h_2 \Delta t/\mu_o)_{i-1,0}(\frac{1}{\Delta x} - \frac{1}{2}\frac{\partial \gamma}{\partial z})_{i-1,0}] \\ /[(h_1 h_2 \Delta t/\mu_o)_{i,0}(\frac{1}{\Delta x} + \frac{1}{2}\frac{\partial \gamma}{\partial z})_{i,0}] \tag{4.28}$$

The inverse solver then solves on a node-by-node basis, starting with the boundary nodes and then proceeding to each of the interior nodes as the information for each neighboring upwind node becomes complete. For example, provided $0 < \gamma < \pi/2$, the nodes would be swept according to the following simple row-column strategy:
a. For $i = 1$, and $j = 0$, advance the plane of symmetry/leading edge boundary node.
b. For $i = 1$, and $j = 1, j\text{max}$, advance each node in the leading edge boundary.
c. For $j = 0$, and $i = 2, i\text{max}$, advance each node in the plane of symmetry boundary.
d. For an outer loop of $i = 2, i\text{max}$, and an inner loop of $j = 1, j\text{max}$, advance each of the interior nodes.

The rectangular 2D grid array described above is a somewhat limiting feature of the present treatment of thin oil films. A more general grid mapping transformation of irregularly spaced nodes located at $(x_{i,j}, z_{i,j})$ to evenly spaced coordinate system $(\zeta_{i,j}, \eta_{i,j})$ may be accomplished, but is not treated here.

One-Time-Level Box-Implicit Inverse Method

Optical access to the test surface may be limited during an actual wind tunnel run. Thus, some researchers prefer to acquire a single image of the oil film taken immediately at the finish of the wind tunnel run. In this subsection, we derive an inversion method suitable for analyzing such a One-Time-Level 2D oil film thickness distribution.

The wind tunnel is assumed to have run sufficiently long and the oil film is thin enough that pressure gradient, gravity and surface tension effects are negligible. Further assume the oil film distribution has achieved time self-similarity, where $h(x, z, t) = H(x, z)/t$. Thus, we start our derivation with equation 3.3, rewritten here as:

$$\frac{\partial}{\partial x}(\frac{\tau_x H^2}{2\mu_o}) + \frac{\partial}{\partial z}(\frac{\tau_z H^2}{2\mu_o}) - H = 0$$

Wind tunnels seldom start immediately at the desired run conditions. Presumably, the oil film is applied before the wind tunnel starts. Some initial time must occur to establish the desired run condition, the tunnel then is held at the desired run conditions for a period of time, and then the tunnel takes a small amount of time to shut down. During the entire time of the oil flow, the wall shear stress varies, as does the dynamic head, q_∞. Following the suggestion of Monson, Mateer, and Menter[7,8], it seems best to consider that $C_f \equiv \tau/q_\infty$ is likely to vary less during the time of the oil flow than will τ.

We, therefore, rewrite the 2D self-similar equation above as:

$$\frac{\partial}{\partial x}(C_{fx}h^2) + \frac{\partial}{\partial z}(C_{fz}h^2) - 2h/\int_{t_s}^{t_f} \frac{q_\infty(t)}{\mu_o(t)}dt = 0 \tag{4.29}$$

where $C_f \equiv \tau/q_{nom}$, $C_{fx} \equiv C_f \cos\gamma$, $C_{fz} \equiv C_f \sin\gamma$, and q_{nom} is the nominal or desired wind tunnel dynamic head. The measured wind tunnel dynamic head during the wind tunnel run varies and is given by $q_\infty(t)$. Additionally, the oil viscosity is temperature sensitive and may vary during the wind tunnel run, which requires that the oil viscosity variation with wind tunnel time be determined, $\mu_o(t)$. This can be done by measuring the test surface temperature and then using a temperature calibration for the oil.

The derivation of equation 4.29 from equation 3.3 is not strictly rigorous in that we integrate equation 3.3 over the time interval from t_s to t_f, and approximate the integral:

$$\int_{t_s}^{t_f} q_\infty(t)H^2/\mu_o(t)dt \approx H^2 \int_{t_s}^{t_f} q_\infty(t)/\mu_o(t)dt$$

The difficulty with this is that the oil will not initially have been time self-similar, and $H = h/t$ will actually vary with time. For the purposes of this single time level scheme, however, we consider this error source acceptable. The success of the overall method will be considered in the applications section.

A One-Time-Level Box-Implicit numerical inverse equation form of equation 4.29 suitable for interior nodes may be derived in a manner similar to equation 4.26 which solves the interior node for the Two-Time-Level numerical inverse scheme. The One-Time-Level interior node equation is:

$$\begin{aligned}(C_f)_{i,j} =& \{[h_{i,j} + h_{i-1,j-1} + h_{i,j-1} + h_{i-1,j}]\beta \\ &+ [(C_f h^2 \cos\gamma)_{i-1,j-1} + (C_f h^2 \cos\gamma)_{i-1,j} - (C_f h^2 \cos\gamma)_{i,j-1}]/\Delta x \\ &+ [(C_f h^2 \sin\gamma)_{i-1,j-1} + (C_f h^2 \sin\gamma)_{i,j-1} - (C_f h^2 \sin\gamma)_{i-1,j}]/\Delta z\} \\ &/[h_{i,j}^2(\frac{\cos\gamma}{\Delta x} + \frac{\sin\gamma}{\Delta z})_{i,j}]\end{aligned} \tag{4.30}$$

where $\beta \equiv 1/\int_{t_s}^{t_f} q_\infty(t)/\mu_o(t)dt$. Further, because the oil film distribution for only one time level is used, the time level subscript on h is dropped.

Leading edge and plane of symmetry numerical boundary conditions for the One-Time-Level Box-Implicit method may be derived in a manner similar to that of equations 4.27 and 4.28.

5. APPLICATIONS

An understanding of the behavior of thin viscous oil films can be achieved through the study of selected 1D and 2D model problems. Selection of these model problems is made so as to emphasize those physical, mathematical and numerical features which might arise in considering the use of the methods described in this paper. The relative influence of wall shear stress, wall pressure, gravity, centrifugal and surface tension effects can be determined. Comparison between numerical solutions, both direct and inverse, for those 1D and 2D thin oil films for which closed form solutions can be found will reveal the suitability of the numerical methods for more general problems. The accuracy of approximate solution methods used by others in the analysis of experimental data can be assessed. Demonstration of the rigor, accuracy, and ease-of-use of the mathematical treatment of these thin oil films, as described here, tends to reinforce confidence in the continued development and expanding use of thin oil films in the important measurement of wall shear stress. The utility of the direct and inverse solvers for practical applications should become apparent from results of those cases presented.

Variable Wall Shear, 1D Case

The first problem considered is a simple 1D model problem where wall shear stress varies linearly. For this problem, we assume the pressure gradient is either zero or negligible. Gravity and surface tension effects are also ignored. The solution is known from the 1D analytical relations and we may evaluate the accuracy of both the Box-Implicit direct and inverse solvers for this case, as well as alternate solution methods which have been used in other studies for analyzing experimental data.

Assume the wall shear stress varies as $\tau(N/m^2) = a + bx = 20 + 100x$, where x is in meters, with the leading edge of the thin oil film at $x = 0$ and the film extending to $x = 0.1$ meter. Assume the oil film has a kinematic viscosity of $\nu_o = 100$ centiStokes, with a density of $\rho_o = 1000$ Kg/m^3. These properties are similar but not identical to commonly used silicone oil. For the numerical solutions, assume an initial oil film thickness at $t = 0$ of $h_0 = 10$ microns and a time step of $dt = 0.1$ second.

A closed form time self-similar solution can be obtained for this case using equation 3.7, the analytical relation for a 1D thin oil film:

$$H = ht = (\mu_o/\tau)^{1/2} \int_{x0}^{x} (\mu_o/\tau)^{1/2} dx = 2\frac{\mu_o}{b}(1 - \frac{1}{(1 + bx/a)^{1/2}}) \qquad (5.1)$$

Figure 7a shows the oil film thickness at several times (t = 0, 20, 40, 60, 80 and 100 seconds) from the analytical solution above, and from the 1D version of the Box-Implicit direct solver. An evenly spaced grid of 100 points is used for the numerical solver. The analytical solution assumes an infinite initial film thickness. Some of the observed

differences between the analytical and numerical solutions are due to this differing initial condition. However, very good agreement (< 1%) between the analytical and numerical solutions can be seen to occur for those regions and times where the oil film has reduced in thickness to 3/4 or less than the initial thickness. We consider that the decrease in differences between the numerical solution and the analytical solution appear to be more closely associated with the decrease in the oil film thickness relative to the initial thickness rather than with the increase in time. Clearly, however, the numerical solution approaches the analytical time self-similar solution as the oil film thins.

Another observation from figure 7a is that for "small" times a corner exists in the oil film thickness distribution (e.g., $x \approx 0.04$m for $t = 20$ seconds). For larger times, the corner has convected out of the solution domain. Note that by integration, for the $dh/dx = 0$ region with $\tau = a + bx$, of the 1D form of equation 3.1 for the time variation of h, we obtain:

$$h = h_0/(1 + h_0 bt/2\mu) \tag{5.2}$$

A piecewise analytical solution can thus be formed for this problem with the smaller h from equation 5.1 or 5.2 being selected. The observed corner occurs where equations 5.1 and 5.2 intersect, $x_c = (a/b)[(1 + h_0 bt/2\mu)^2 - 1]$.

For the Box-Implicit direct solver, an oscillation in the solution appears to originate from this corner. This oscillation is numerical rather than physical. To solve this numerical oscillation, a "Flux-Limit" concept is adapted to the Box-Implicit algorithm. For this Flux-Limit concept to be applied, a first-order (rather than second-order) form of the Box-Implicit algorithm is used for those nodes where the slope of the oil film thickness changes sign. The solution from the Box-Implicit Flux-Limit algorithm is shown in figure 7b. Examination of the solution in figure 7b at, for example, $t = 20$ seconds shows that the oil film slope changes sign at only two locations, meaning the first-order treatment at these two nodes is sufficient to eliminate the corner oscillation. Clearly, the corner oscillation is eliminated with excellent agreement otherwise.

Figure 7c shows the solution from the Finite-Volume Upwind-Implicit direct solver algorithm. Although the solution appears to be somewhat better behaved than the Box-Implicit direct solver, a corner oscillation still appears. A Flux-Limit form of the Finite-Volume Upwind-Implicit algorithm eliminates this oscillation as is evident in the solution given in figure 7d.

An adaptation of the MacCormack[22] explicit algorithm to the thin oil film problem leads to the solution given in figure 7e. The explicit algorithm is stable since the effective stability index (CFL$\equiv U_c \Delta t/\Delta x \approx \tau h \Delta t/2\mu_o \Delta x$) for this problem is less than 1. No corner oscillations occur, although slight differences (< 2%)in the oil film thickness distribution for $t = 20$ and $t = 40$ seconds compared to the other numerical solutions are observed.

A further test of the numerical methods is to consider the accuracy of the inverse solver. To accomplish this, we use the analytical oil film thickness for two times, $t = 80$

and $t = 100$ seconds, as the known input to the inverse or τ numerical solver. The τ vs x solution from the inverse solver can then be compared with the original known $\tau = 20 + 100x$ distribution. Figure 8a shows a τ vs x distribution from the Box-Implicit inverse solver. The comparison with the known result is excellent, within 1%. A further test is to use the oil film thickness distribution from the Box-Implicit direct solver as the input to the Box-Implicit inverse solver as shown in figure 8b. Clearly demonstrated is the accuracy of these methods for both direct and inverse solutions for this test case.

Shown in figure 8c is the τ vs x distributions derived by means of the One-Time-Level Box-Implicit inverse algorithm from the Box-Implicit Flux-Limit direct solver's oil film thickness at times $t = 40$ and $t = 100$ seconds. Agreement within 1% occurs except for where the corner region of the $t = 40$ second Box-Implicit oil film thickness distribution has not yet convected out of the region of interest. The One-Time-Level Box-Implicit inverse algorithm requires the input oil film distribution to have become fully time self-similar ($H(x) \equiv h(x,t)t$ =constant), which has not occurred as yet for the $t = 40$ second numerical oil film distributions. A reasonable estimate for the time at which an oil film becomes fully time self-similar is given by $t_s \approx L/U_c \approx L\mu/\tau h_0$. For this problem, $L = 0.1$ meter, $h_0 = 10$ microns and $t_s \approx 50$ seconds. When the input oil film thickness distribution has evolved to the point where it is time self-similar, the One-Time-Level Box-Implicit inverse algorithm yields quite accurate results.

An alternate method of solving for τ vs x that appears in the oil film literature is based on the ad hoc assumption that the local wall shear stress is inversely related to the local slope of the oil film height (only one time level is used):

$$\tau \approx (\frac{\mu_o}{t})/(\frac{dh}{dx}) \tag{5.3}$$

Figure 8d presents the result of application of this local slope method to determine the τ vs x distribution from the analytical oil film thickness at $t = 100$ seconds. Comparison with the known $\tau = 20 + 100x$ distribution reveals obviously large errors ($> 50\%$ of the rise in τ) which result from the use of equation 5.3. These errors can be shown to arise where $d\tau/dx \not\equiv 0$. In particular, by rearrangement of equation 3.5:

$$\tau = [(\frac{\mu_o}{t})/(\frac{dh}{dx})][1 - (\frac{ht}{2\mu_o})\frac{d\tau}{dx}] \tag{5.4}$$

The error in equation 5.3 is given by the $(ht/2\mu_o)d\tau/dx$ term. The increase in τ of $10N/\mathrm{m}^2$ over the region of the oil flow from $x = 0$ to $x = 0.1$m leads to an error of $6N/\mathrm{m}^2$ or 60% for this algorithm. It is strongly recommended that the relation of equation 5.3 not be used except for regions very close to the leading edge of the oil film (as was correctly done by Monson, Mateer, and Menter[7,8]). Where the oil film is time self-similar and a single image is available, the One-Time-Level Box-Implicit inverse algorithm described earlier is recommended instead due to its ease-of-use and high accuracy.

Constant Wall Shear, Increasing then Decreasing Film Thickness, 1D Case

A feature related to the nonlinearity of the thin oil film equation is explored with the next problem. The study of the behavior and solution of nonlinear partial differential equations (PDEs) invariably leads to Burgers' equation. A point to be made is that, where τ and μ_o are held constant, the simplest form of the 1D thin oil film equation is identical to the inviscid form of the Burgers equation. Much of what has been learned from the study of Burgers' equation about the behavior and solution of nonlinear PDEs directly applies to the present thin oil film work. In turn, we realize that the study of the thin oil film provides a quite practical and possibly interesting physical manifestation of Burgers' equation. A certain irony exists in the realization that each oil flow study performed by an experimentalist is also actually a Burgers' equation experiment.

One CFD problem area studied using Burgers' equation is the inviscid 1D (or normal) shock. The present problem examines this shock-like behavior that can arise from the nonlinear term, even for a thin oil film.

The 1D form of the thin oil film equation is given by:

$$\frac{\partial h}{\partial t} + \frac{\partial \tau h^2/2\mu_o}{\partial x} = 0$$

An advantage of the thin oil film form is that we may form model problems where τ varies and even changes sign, allowing us to examine a greater range of fluid physics. Such a model problem is examined in the next subsection. For the particular model problem under consideration, however, we assume that $\tau = 25$ N/m^2, $\rho = 1000$Kg/m^3, $\nu = 100$ centiStokes (e.g., $\nu = 100 \cdot 10^{-6}$ m^2/sec) and $\mu = \rho\nu = 0.1$Kg/m-sec and that these remain constant.

First note that oil thickness, h, is being convected in the mean at a velocity, $U_c = \tau h/2\mu$, which leads to the nonlinear h^2 term in the PDE. The characteristic wave velocity, found by expanding the $\partial/\partial x$ term, is given by $U_w = \tau h/\mu$, which is also equal to the oil velocity at the air/oil film interface at $y = h$.

Further assume for this current problem that the initial ($t_0 = 0$) oil film thickness increases linearly with x, followed by region of constant thickness, then decreases linearly with x followed by another region of constant thickness according to:

$$\begin{aligned}
h(t_0 = 0) &= 10^{-5}x/0.04, \text{ for } x < x_a = 0.04\text{m} \\
h(t_0 = 0) &= h_0 \equiv 10^{-5}\text{m}, \text{ for } x_a = 0.04\text{m} < x < x_b = 0.05\text{m} \\
h(t_0 = 0) &= 10^{-5}(3.5 - x/0.02), \text{ for } x_b = 0.05\text{m} < x < x_c = 0.068\text{m} \\
h(t_0 = 0) &= h_1 \equiv 10^{-6}\text{m}, \text{ for } x > x_c = 0.068\text{m}
\end{aligned}$$

Figure 9a shows this initial ($t_0 = 0$) oil film thickness distribution, as well as subsequent development of the oil film for times of t =4, 8, 12, 16 and 20 seconds. The corners

initially at $x_a = 0.04$m, $x_b = 0.05$m and $x_c = 0.068$m are also identified in figure 9a to aid in describing the subsequent oil film development.

By means of characteristic and mass-conservation based arguments, the development of the oil film thickness distribution with time can be established. Such piecewise analytical solutions of the oil film provide a basis for comparison with numerical solutions, as well as provide revealing insight into the shock-like behavior exhibited.

Consider the region between $x_0 = 0$ and x_a, where the oil film thickness increases linearly with x. Note that the convective velocity also increases linearly in x and the film tends to spread, leading to a decrease in the slope of the oil film thickness. Because the region between $x = 0$ and x_a is linear with constant τ and μ_o, we know the 1D time self-similar solution applies, where $\tau h(t - 16) = \mu_o x$. Rearranging slightly, we find the slope for this region is $\Delta h/\Delta x = \mu_o/\tau(t - 16)$. The corner at x_a, where the linear region intersects the $h = h_0$ plateau, thus moves to the right at a constant wave velocity such that:

$$x_a(t) - x_a(t_0) = \dot{h}_0/(\Delta h/\Delta x) = (\tau h_0/\mu_o)(t - t_0)$$

The wave velocity of the corner at x_a is $\tau h_0/\mu_o = 2.5$mm/sec. Similarly, the corner at x_b is an artifact that moves at the constant wave velocity, $\tau h_0/\mu_o = 2.5$mm/sec. Also, the corner at x_c moves at the constant wave velocity, $\tau h_1/\mu_o = 0.25$mm/sec.

The plateau between x_a and x_b will retain constant oil film thickness since $\partial h/\partial t \equiv -(\tau h/\mu)\partial h/\partial x \equiv 0$, with corners at $x_a(t)$ and $x_b(t)$ which appear to translate to the right at a constant wave velocity of $\tau h_0/\mu$.

In contrast, between x_b and x_c, the oil film thickness decreases linearly with x. Thus, the wave velocity, $\tau h/\mu_o$, also decreases in x. The corner at x_b tends to catch up with the slower moving corner at x_c and the oil film thickness slope becomes steeper, until a discrete jump of $h_0 - h_1$ occurs with $x_b(t) = x_c(t)$. The discrete jump forms when $x_b(t) = x_c(t) = 0.07$m at t=8 seconds.

Piecewise solutions for the oil film thickness at $t = 4$ and $t = 8$ seconds based on the above arguments are given in figure 9a.

For times past $t = 8$ seconds, the discrete jump moves with a wave velocity associated with the average height of the jump, $\tau(h_0 + h_1)/2\mu_o = 1.375$mm/sec. This wave velocity can be determined by considering a small control volume of length, Δx, with the jump just entering. The jump is from a plateau of constant thickness, h_0, to another plateau of constant thickness, h_1. Thus, the flow of oil into the control volume will occur at a constant volumetric rate, $\tau h_0^2/2\mu_o$. The flow of oil out of the control volume also occurs at a constant volumetric rate, $\tau h_1^2/2\mu_o$. The net rate of increase of oil volume in the control volume will be $\tau(h_0^2 - h_1^2)/2\mu_o$. However, the initial oil volume present as the jump just enters the control volume is $h_1\Delta x$. The oil volume present as the jump just exits the control volume is $h_0\Delta x$. The net change of the oil volume in the control volume as the jump travels the distance Δx is $(h_0 - h_1)\Delta x$. The amount of time, then, for the jump to

travel through the control volume is $\Delta t = ((h_0 - h_1)\Delta x)/(\tau(h_0^2 - h_1^2)/2\mu_o)$. Rearrangement gives the wave speed of the jump:

$$U_j = \Delta x/\Delta t = \tau(h_0 + h_1)/2\mu_o$$

The piecewise solution for the time $t = 12$ seconds, as shown in figure 9a, results from application of the above arguments.

When $t = 15\frac{3}{11}$ seconds, the corner at x_a will just catch up with the jump at $x_a = x_j = 78\frac{2}{11}$mm. Subsequently, the h_0 plateau will no longer exist, and the average height of the jump will decrease as the jump moves to the right, and the wave velocity of the jump will also decrease. However, a consideration of the known time variation of the slope of the linearly increasing region (x_0 to x_j), along with the known time variation of the total oil volume, $V = (0.431 - 0.0005t)10^{-6}\text{m}^2$, in the domain ($x = 0$ to $x = 0.1$mm) allows calculation of the jump movement and oil film thickness distribution past $t = 15\frac{3}{11}$ seconds. The oil film thickness distributions for $t = 16$ and 20 seconds are also shown in figure 9a.

Precise knowledge of the piecewise analytical solution for this "shock-like" 1D model problem allows for assessment of the accuracy of the Box-Implicit method and the Finite-Volume Upwind-Implicit method for direct numerical solvers. These numerical solutions are given in figures 9b, 9c, 9d and 9e.

With the exception of the region about the shock-like jump, the Box-Implicit and Finite-Volume Upwind-Implicit methods provide quite acceptable solutions. The jump region, however, leads to large oscillations in the numerical solutions particularly for the Box-Implicit method without the Flux-Limit treatment. For both the Box-Implicit and Finite-Volume Upwind Implicit methods, the Flux-Limit treatment improves the solution about the jump region, but with an apparent increase in jump wave velocity. This increase in jump wave velocity is likely because the rather simple Flux-Limit treatment is not mass-conservative as implemented.

Another criticism of the numerical solutions obtained is that the h_0 plateau is not preserved, becoming rounded at the x_a and x_b edges. Upwind methods are known to be dissipative and this appears to be the reason, with the Box-Implicit method being better behaved in this regard.

2D Surface Tension Bubble Problem

The next case considered is designed to demonstrate the inclusion of surface tension terms. The primary focus of the present paper is on the response of an oil film to a wall shear stress. However, in the vicinity of separation, the surface tension term can dominate. Thus, it is desirable to demonstrate that the surface tension terms are correctly implemented in the overall numerical procedure. To do this, we consider a problem where

the oil film is subjected to only the surface tension term, and, furthermore, the problem is designed so that features of the oil response are analytically known.

In constructing the present problem, we do not solve the surface tension problem in general, but only demonstrate inclusion of the surface tension terms and also prepare for the 3D separation problem of the next subsection. We consider here, then, the simpler case where the oil film thickness varies only in the x direction.

Where only surface tension effects occur, and then only in the x direction, equation 2.2 becomes:

$$\frac{\partial h}{\partial t} + \frac{\partial}{\partial x}\{\frac{h^3}{3\mu_o}[\frac{\partial}{\partial x}(\sigma h_{xx})]\} = 0 \tag{5.5}$$

Assume that oil is spread initially ($t = 0$) so as to assume the shape:

$$h(x, t = 0) = h_0[1 - (x/x_0)^4], \text{ for } -x_0 \leq x \leq x_0 \tag{5.6}$$

This initial bubble shape is not in equilibrium and the initial rate at which the bubble changes shape is known by simple substitution of equation 5.6 into equation 5.5:

$$\begin{aligned}(\frac{\partial h}{\partial t})_{t=0} &= -\frac{\partial}{\partial x}\{\frac{h^3}{3\mu_o}[\frac{\partial}{\partial x}(\sigma h_{xx})]\} \\ &= 8\frac{\sigma h_0^4}{\mu_o x_0^4}[1 - (x/x_0)^4]^2[1 - 13(x/x_0)^4]\end{aligned} \tag{5.7}$$

The bubble shape continues to change with time until steady state is reached. The steady state bubble shape will be given by:

$$h(x, t = \infty) = 1.2h_0[1 - (x/x_0)^2], \text{for} - x_0 \leq x < x_0 \tag{5.8}$$

Note the steady state bubble shape given by equation 5.8 satisfies equation 5.5 with $\partial h/\partial t = 0$, and also has the same oil volume as the initial bubble shape equation 5.6:

$$\int_{-x_0}^{x_0} h dx = 1.6h_0x_0$$

An accurate, mass-conservative numerical direct solution method given the initial bubble shape of equation 5.6 should lead to the steady state bubble shape of equation 5.8 and have an initial rate of change of oil film thickness given by equation 5.7.

As can be seen from equation 5.5, the surface tension term is highly nonlinear (h^3) involving a fourth-order derivative in space. To implement the surface tension term into the numerical solver, we choose here to use the linearized line-implicit method described below. Although the method is incorporated in the current example program for nodes

along the plane of symmetry as well as for purely interior nodes, we describe only the interior node treatment here.

First, integrate equation 5.5 with time between times t_1 and t_2:

$$h_2 - h_1 + \frac{\partial}{\partial x}[(\frac{\sigma}{3\mu_o}) \int_{t_1}^{t_2} h^3 h_{xxx} dt] = 0 \tag{5.9}$$

We linearize the $h^3 h_{xxx}$ term at t_2 as:

$$(h^3 h_{xxx})_2 \approx h_1^3 (h_2)_{xxx} + 3h_1^2 h_2 (h_1)_{xxx} - 3h_1^3 (h_1)_{xxx}$$

Substituting into equation 5.9:

$$h_2 - h_1 + \frac{\partial}{\partial x}[(\frac{\sigma \Delta t}{6\mu_o})(h_1^3 (h_2)_{xxx} + 3h_1^2 h_2 (h_1)_{xxx} - 2h_1^3 (h_1)_{xxx})] = 0 \tag{5.10}$$

Now evaluate equation 5.10 at the midpoint, $(i - 1/2)$:

$$\begin{aligned} h_{2,i} - h_{1,i} + h_{2,i-1} - h_{1,i-1} + (\frac{\sigma \Delta t}{3\mu_o \Delta x}) & \\ \{[h_1^3 (h_2)_{xxx} + 3h_1^2 h_2 (h_1)_{xxx} - 2h_1^3 (h_1)_{xxx}]_i & \\ - [h_1^3 (h_2)_{xxx} + 3h_1^2 h_2 (h_1)_{xxx} - 2h_1^3 (h_1)_{xxx}]_{i-1}\} = 0 & \end{aligned} \tag{5.11}$$

where $\Delta x = x_i - x_{i-1}$.

The derivative, h_{xxx}, may be found numerically by:

$$(h_{xxx})_i = \alpha_i h_{i+2} + \beta_i h_{i+1} + \epsilon_i h_i + \gamma_i h_{i-1} + \delta_i h_{i-2}$$

where the coefficients, (α, β, γ, δ and ϵ), are given in Appendix B.

Equation 5.10, with substitution and rearrangement, takes on the following matrix form:

$$A2_i h_{2,i-3} + A1_i h_{2,i-2} + A0_i h_{2,i-1} + B0_i h_{2,i} + C0_i h_{2,i+1} + C1_i h_{2,i+2} = D0_i \tag{5.12}$$

where

$$
\begin{aligned}
C2_i =& 0 \\
C1_i =& (\frac{\sigma \Delta t}{3\mu_o \Delta x})(h_{1,i}^3 \alpha_i) \\
C0_i =& (\frac{\sigma \Delta t}{3\mu_o \Delta x})(h_{1,i}^3 \beta_i - h_{1,i-1}^3 \alpha_{i-1}) \\
B0_i =& 1 + (\frac{\sigma \Delta t}{3\mu_o \Delta x})[h_{1,i}^3 \epsilon_i - h_{1,i-1}^3 \beta_{i-1} \\
& + 3h_{1,i}^2(\alpha_i h_{1,i+2} + \beta_i h_{1,i+1} + \epsilon_i h_{1,i} + \gamma_i h_{1,i-1} + \delta_i h_{1,i-2})] \\
A0_i =& 1 + (\frac{\sigma \Delta t}{3\mu_o \Delta x})[h_{1,i}^3 \gamma_i - h_{1,i-1}^3 \epsilon_{i-1} \\
& - 3h_{1,i-1}^2(\alpha_{i-1} h_{1,i+1} + \beta_{i-1} h_{1,i} + \epsilon_{i-1} h_{1,i-1} + \gamma_{i-1} h_{1,i-2} + \delta_{i-1} h_{1,i-3})] \\
A1_i =& (\frac{\sigma \Delta t}{3\mu_o \Delta x})(h_{1,i}^3 \delta_i - h_{1,i-1}^3 \gamma_{i-1}) \\
A2_i =& -(\frac{\sigma \Delta t}{3\mu_o \Delta x})(h_{1,i-1}^3 \delta_{i-1}) \\
D0_i =& h_{1,i} + h_{1,i-1} \\
& + 2h_{1,i}^3(\alpha_i h_{1,i+2} + \beta_i h_{1,i+1} + \epsilon_i h_{1,i} + \gamma_i h_{1,i-1} + \delta_i h_{1,i-2}) \\
& - 2h_{1,i-1}^3(\alpha_{i-1} h_{1,i+1} + \beta_{i-1} h_{1,i} + \epsilon_{i-1} h_{1,i-1} + \gamma_{i-1} h_{1,i-2} + \delta_{i-1} h_{1,i-3})
\end{aligned}
$$

The matrix equation 5.12 is then solved by means of a scalar septa-diagonal solver written for the present work. The scalar septa-diagonal solver is quite similar to commonly used scalar tridiagonal solvers available, but is seven elements wide rather than only three.

The initial oil film thickness distribution for the model surface tension problem, equation 5.6 (with 100 centiStoke oil of 1.0 specific gravity and $\sigma = 21.010^{-3}$N/m, $h_0 = 10.0$ microns and $x_0 = 0.1$ meter) is shown in figure 10. The known analytical steady state oil film thickness distribution, equation 5.8, is also compared in figure 10 with the present steady state numerical results using the method described above. The excellent agreement of the numerical and analytical steady state oil film thickness distribution is clearly indicated.

Figure 11 shows the initial rate of change in the oil film thickness, $(\partial h/\partial t)_{t=0}$, for the model surface tension problem. Again the excellent agreement of the numerical results and the known analytical form (eq. 5.7) of this feature is clearly indicated. Suggested by this level of agreement for these features between the numerical result and the known analytical forms is that the surface tension terms are correctly implemented into the present oil film solver using the methods described in this subsection.

Saddle on Plane of Symmetry, 2D Case

As a final example problem, the important practical case of a saddle located on a plane of symmetry is next examined. Such a flow occurs, for example, in the region ahead of a cylinder (or airfoil) mounted normal to a wall (or fuselage). Both a saddle of separation and a saddle of attachment are considered. These saddle cases are calculated by the 3D direct solver numerical methods described previously and are compared to the known closed form solution, also described previously. The additional effects of wall pressure gradients and surface tension for these saddle cases are also examined. This model problem is an example of a highly 3D separated flow, and the ability of the numerical methods described to accurately calculate this category of flows is a prime focus of the present study.

For both saddle cases, we assume the saddle (where both τ_x and τ_z equal zero) is located at $x = 0$ and $z = 0$. The oil is applied initially ($t = 0$) as a thin film of $h_0 = 10$ micron thickness with a leading edge located at $x = -0.01$ meter. The oil properties were chosen to be nearly (but not identical to) those of silicone oil with a constant kinematic viscosity of $\nu_o = 100$ centiStokes, a density of $\rho_o = 1000$ Kg/m^3, and a surface tension of $\sigma = 21 \cdot 10^{-3}$N/m.

The wall shear stress is assumed to vary according to:

$$\tau_x = ax, \text{ and } \tau_z = bz$$

For the saddle of separation case, $a = -2000$N/m^3 and $b = 1500$N/m^3.
For the saddle of attachment case, $a = -2000$N/m^3 and $b = 2500$N/m^3.

In the absence of surface tension and pressure gradient effects, a time self-similar analytical solution is given by equation 3.21, repeated here:

$$h = Ht = (\frac{2\mu_o t}{a+b})(1 - (\frac{x}{x_0})^{\frac{(a+b)}{-2a}}), \text{ for } 0 < x < x_0 \tag{5.13}$$

Further, the shape of the surface streamlines (passing through the arbitrary point (x_s, z_s)) are given from the analytical solution by equation 3.19 repeated here:

$$\frac{z}{z_s} = (\frac{x}{x_s})^{b/a} = (\frac{x_s}{x})^{b/-a} \tag{5.14}$$

Figures 3a and 3b show the shape of the surface streamlines for the two saddle cases presently considered.

Direct Solver, With and Without Surface Tension Terms

Numerical solutions for the oil film thickness distribution were obtained using the Box-Implicit method for the two saddle cases, both with and without surface tension. Figure 12 shows the numerical solutions at a time of $t = 100$ seconds, both with and without surface

tension. Also shown in figure 12 is the comparable analytical solution (eq. 5.13) for each case. Figure 13 is similar to figure 12, but shows the region near the saddle point in more detail. For this problem, the oil film thickness varies only with x and not z, even though the shear field varies in (x,z). However, the numerical solution procedures are indeed fully 3D with $h(x,z)$. Only the plane of symmetry solution is shown, but the $z \neq 0$ numerical solutions prove to be identical as would be expected for this particular test problem.

The excellent agreement in figures 12 and 13 between the analytical solution and the numerical solution (without surface tension) gives a clear indication of the suitability of the Box-Implicit numerical methods we have implemented in the present direct solver. Only for the grid point located at $x = 0$ does a considerable difference between the analytical and numerical thickness solutions exist. The analytical solutions for both a saddle of separation and a saddle of attachment are cusped at $x = 0$. Furthermore, for a saddle of separation, the cusp at $x = 0$ leads to an infinite oil film thickness, $h(x,0) \rightarrow \infty$ as $x \rightarrow 0$. The numerical solutions have some difficulty in resolving this cusp for the last grid point at $x = 0$. A further observation is that as the numerical grid becomes finer (not shown), the cusp in the numerical solutions at $x = 0$ becomes higher appearing to approach the analytical result.

This sharp cusp, however, will not occur in a real oil film due to surface tension. Therefore, the inability of the numerics to resolve the sharp infinite cusp at $x = 0$ is of little practical significance. Also shown in figure 13 are the numerical solutions for $t = 100$ seconds where surface tension is included using the line-implicit numerical procedures described and tested in the previous (surface-tension-only) problem. As can be seen in figure 13, the surface tension removes the sharp cusp which otherwise appears in the analytical and numerical solutions. Also, grid refinement (not shown) of the numerical solutions with surface tension no longer noticeably affects the oil film solutions obtained in the region of $x = 0$.

Surface tension appears to more greatly affect the saddle of separation solutions than the saddle of attachment solutions, due to the more pronounced cusp occurring for the saddle of separation. From an order-of-magnitude analysis, the extent of domain affected by surface tension can be approximated by:

$$L_\sigma = \left(\frac{\sigma h^2}{|a|}\right)^{1/4} \tag{5.15}$$

For the present saddle of separation test case, $L_\sigma \approx 110$ microns, while for the present saddle of attachment test case, $L_\sigma \approx 80$ microns. Based on figure 13, the observed domain actually affected by surface tension appears to be in the region of $\Delta x \approx 2L_\sigma$.

The above calculations do not include pressure gradient effects. The pressure gradient terms has an all but negligible influence on the thin oil film solutions presented. According to equation 3.18, the pressure gradient associated with a saddle characterized by $\tau_x = ax$ and $\tau_z = bz$, will have a magnitude of $P_x = -(3a+b)/\tan\theta$, where $\theta \approx 30\,\text{deg}$ is the angle of

departure from the surface of the streamline originating from the saddle into the flowfield. An order-of-magnitude analysis, shows that the oil film peak will be displaced upstream of the saddle by $L_p \approx (3 + b/z)h_0$. For figure 13, the oil film peak associated with the saddle of separation would be displaced about $L_p \approx 4h_0 \approx 20$ microns. This displacement caused by the pressure gradient would be about 1 grid point upstream. For the saddle of attachment shown in figure 13, the oil film peak would be displaced upstream even less, by $L_p \approx 10$ microns, or 1/2 grid point. In the absence of pressure gradient terms, the saddle problem is symmetric in x as well as in z about the saddle. The surface tension terms are easily incorporated for the symmetric problem. However, the pressure gradient terms lead to a nonsymmetric (in x) saddle problem. Because the effect of pressure gradient on the oil film is so small for these thin oil films, the pressure gradient terms were not included in the calculations for the oil film at this time.

In the remaining portion of this saddle flow subsection, we use the above direct solutions in lieu of experimental data to explore several techniques for analysis of experimental oil film data. The context of the present study suggests three approaches. The first and simplest experimental thin oil film analysis in the vicinity of a saddle is to examine the surface streamlines for a rough estimate of b/a, thereby determining whether the saddle is a saddle of separation or a saddle of attachment. A second analysis is to examine the oil film thickness, h vs x/x_0, along the centerline, $z = 0$, for estimates of the ratio of the shear gradients, b/a, and, again, whether the saddle is a saddle of separation or a saddle of attachment. However, the third and most thorough experimental thin oil film analysis of a saddle is to measure the thin oil film distribution $h(x, z)$, at one or more times, along with a surface streamline measurement, $\gamma(x, z)$, and then use an inverse solver, such as described earlier in this paper, to deduce the complete wall shear field, $(\tau_x(x, z), \tau_z(x, z))$, in the vicinity of the saddle.

Placement of a pattern of oil dots or other conventional surface oil flow visualization techniques in the vicinity of a saddle point is straightforward and will result in an image similar to figure 3a or 3b. From figure 3a or 3b, for each selected surface streamline, s, we may identify an arbitrary point (x_s, z_s) through which that streamline passes. Other arbitrary points (x_i, z_i) which lay on the same streamline may then be tabulated. In the vicinity of the saddle, the streamline coordinates will behave according to equation 3.19, rewritten here in logarithmic form as:

$$\log(\frac{z}{z_s}) = (b/a) \log(\frac{x}{x_s}) \tag{5.16}$$

A log-log plot of (z/z_s) vs (x/x_s) for the saddle cases solved above is shown in figure 14. Note that all the streamlines for each saddle case fall on one line associated with the b/a ratio for that case. The several saddle cases are clearly distinguishable in figure 14, providing estimates of b/a and identifying which case is a saddle of separation or attachment. On a plot such as figure 14, each quadrant is associated with either saddles of

separation or with saddles of attachment but not both. The simplicity of this streamline analysis approach is compelling. Anticipated experimental complications not evident in this brief example include the fact that in general the sepratrix emanating from the saddle will typically be curved rather than straight.

Figure 15 explores the utility of a plot of h vs $\log_{10}(x/x_0)$, as mentioned in the section on analytical solutions (Section 3). In figure 15, x is the distance from the saddle along the plane of symmetry, x_0 is the distance to the leading edge of the applied oil, and h is the oil film thickness.

The ability to determine experimentally whether a given saddle is a saddle of separation or a saddle of attachment may prove desirable. We also may wish to estimate the ratio of the shear stress gradients, b/a. Figure 15 demonstrates how this might be done. Consider, in particular, the line shown in figure 15, which represents the special case where $a + b = 0$. This is a saddle which is intermediate between a saddle of separation and a saddle of attachment. For the case where $a + b = 0$, a plot of h vs $\log_{10}(x/x_0)$ will be a straight line, as indicated by the analytical solution given by equation 3.23 repeated here:

$$ht = H = (-\mu_o/a)\ln(x_0/x), \text{ for } x < x_0,\ a < 0, \text{ and } a + b = 0 \qquad (5.17)$$

For a saddle of separation, $a+b < 0$, a plot of h vs $\log_{10}(x/x_0)$ will curve upward from the straight line as shown in figure 15, even with the effect of surface tension included.

For a saddle of attachment, $a + b > 0$, a plot of h vs $\log_{10}(x/x_0)$ will curve downward from the straight line as shown in figure 15, again even with the effect of surface tension included. Clearly from figure 15, to use a log plot to unambiguously distinguish between a saddle of separation and a saddle of attachment, oil film thickness data must be obtained quite close to the saddle ($x < 0.03x_0$).

Inverse Solver, With and Without Surface Tension Terms

An important aim of the present work was the development and validation of a 2D thin oil solver suitable for determining the 2D wall shear stress field on the surface bounding a complex 3D flow. To test, in this subsection, the inverse solver methods described earlier in this paper, we use the oil film thickness distributions obtained above by our direct solver for the 3D saddle of separation as the input to the inverse solver. A first oil film height distribution input case is considered where surface tension effects are not included in the direct solver, and then a second oil film height distribution input case where surface tension effects are included in the direct solver. Both the Two-Time-Level (eq. 4.26) and the One-Time-Level (eq. 4.30) versions of inverse solver algorithm are considered. Surface tension terms may also be explicitly added to the inverse Two-Time-Level solver algorithm and are also considered.

Figure 16a and 16b show the $\tau_x(N/m^2) = -2000x(m)$ and the $\tau_z(N/m^2) = 1500z(m)$ distributions, respectively, for the saddle of separation problem being considered. The

oil film distribution for this case was obtained using the direct solver without the surface tension terms (also see fig. 12) and was then used as the input to both the One-Time-Level and the Two-Time-Level (without surface tension) inverse solvers. For the Two-Time-Level solver, oil film distributions at $t = 75$ and $t = 100$ seconds were used, while for the One-Time-Level inverse solver, only the oil film distribution at $t = 100$ seconds was used. The wall shear stress distributions obtained by the inverse solvers are also shown in figures 16a and 16b. Note that uneven spacing in z was used to demonstrate the ability of both the direct and inverse solvers to deal with uneven grid spacing and also so as to better resolve the immediate vicinity of the saddle. Figure 16c shows the τ_x vs x results in the vicinity of the saddle to a finer scale than that of figure 16a. From the earlier discussion of the direct solver, we know the oil film distribution in the absence of surface tension agrees quite well with the analytical solution for this case. Figures 16a-16c clearly indicate that the inverse solver, both the One-Time-Level and the Two-Time-Level algorithms, also performs nearly ideally, in the absence of surface tension, in calculation of the 2D wall shear stress field about a saddle of separation.

Surface tension effects do occur about a saddle of separation in an actual experimental setting. Thus, to examine the ability of the present inverse solver to deal with surface tension effects, we also consider the case where the input oil film thickness distribution was produced using the direct solver which included surface tension effects (see also the discussion of fig. 13). The ability of the direct solver to correctly incorporate surface tension effects was previously validated in the discussion of the surface tension bubble problem earlier in this section.

Figures 17a and 17b are wall shear stress results, τ_x vs x and τ_z vs x, respectively, for the inverse solvers without surface tension terms in the inverse algorithm. Unlike the results in figures 16a-16c, however, the input oil film distribution for figures 17a and 17b does include surface tension effects. Some error in the wall shear stress τ_x appears in the immediate vicinity of the saddle of separation as a result of introducing surface tension effects into the oil film thickness distribution; however, errors in τ_z close to the saddle become quite large. The surface-tension-induced errors are limited to a region of $\Delta x \approx 2L_\sigma$ about the saddle. In spite of the errors we observe, both the One-Time-Level and the Two-Time-Level inverse algorithms provide nearly identical results.

Next, we add surface tension terms to the inverse Two-Time-Level solver to determine if these surface-tension-induced errors can be removed. Since the One-Time-Level inverse solver algorithm relies exclusively on the time self-similar relation $h \approx H/t$, which is not valid for the surface tension term, the One-Time-Level inverse algorithm cannot be easily corrected for surface tension.

Figure 18a and 18b are the wall shear stress results, τ_x vs x and τ_z vs x, respectively, for the Two-Time-Level inverse solver with surface tension terms added. Note that the surface-tension-induced errors close to the saddle of separation are still present but are smaller than those of figures 17a and 17b. To improve the accuracy for large time steps, an

assumption that $h \approx 1/t$ was incorporated into the derivation of both the direct solver and the inverse solver algorithms. Where the wall shear stress terms dominate, this assumption aids accuracy considerably. However, where surface tension terms become dominant, large time steps are not as accurately accomplished with this assumption. The direct solver results are obtained with a time step of $\Delta t = 0.1$ second. The inverse solver algorithm is designed for use with experimental data having large time steps between images and is tested here with a time step of $\Delta t = 25$ seconds.

We have in this subsection demonstrated that the direct solver provides an excellent representation of the oil film thickness distribution about a saddle of separation or a saddle of attachment even to the extent of including surface tension effects in the vicinity of the saddle. Surface tension is found to influence only a quite limited region in the immediate vicinity of the saddle ($\Delta x = 2L_\sigma \approx 200$ microns). The One-Time-Level and Two-Time-Level inverse solver algorithms have also been demonstrated to provide accurate wall shear stress distributions for the saddle of separation case, except for this limited surface-tension-dominated region.

6. CONCLUDING REMARKS

The flow of a thin film of oil placed on a surface and then subjected to the 2D wall shear stress generated by a 3D aerodynamic flow is extensively considered. The governing partial differential equation is derived to include the effect of a wall shear stress and wall pressure gradient on the thin film of oil. Surface tension and gravity terms are included. We refer to the resultant partial differential equation as the "Thin Oil Film Equation." The "Squire form" and the "Tanner form" of the thin oil film equation are shown, in Appendix A, to be equivalent through a metric transformation. Numerous analytical time self-similar solutions for the thin oil film equation are described. Of particular interest is the flow of a thin oil film in the vicinity of 3D aerodynamic surface streamline singularities such as the saddle of separation and the saddle of attachment.

Another result of this study is that both direct and inverse numerical solution techniques are developed. In addition to the wall shear stress terms, these direct and inverse solution techniques may additionally include the effects of the wall pressure gradient, gravity and surface tension terms. A Two-Time-Level inverse solver is described which includes these effects. A One-Time-Level version of the inverse solver is for use in the absence of the wall pressure gradient and surface tension terms. When the oil film thickness variations are provided from experimental images of the oil film, the inverse methods provide a rigorous mathematical basis for an improved form of the oil film based wall-shear-stress instrument.

The numerical solvers are applied to several model problems having known analytical solutions so as to evaluate the fundamental accuracy of these numerical methods. Both the direct and inverse numerical solvers are shown to be stable, accurate and computationally efficient. One alternate τ vs x solution method based on the local slope of the film thickness sometimes suggested elsewhere for oil film based wall-shear-stress instrumentation is shown to have fundamental accuracy problems leading to, in one example considered, errors of 50% or more. A model surface tension problem with an analytical solution is also derived to demonstrate the ability of the present solvers to correctly implement the surface tension terms, which can become important near separation.

An extensive application of the direct and inverse numerical solvers to the case where oil film flows on the surface in the vicinity of a saddle of separation provides a clear demonstration of the success and utility of these numerical methods. The saddle of attachment case is also successfully treated.

Techniques for the rigorous analysis of the behavior of thin oil films on test surfaces bounding complex 3D aerodynamic flows have been demonstrated. Instrumentation for the measurement of the 2D wall shear stress which use these numerical techniques should be accurate and suitable for use in complex 3D aerodynamic flows.

REFERENCES

1. Tanner, L. H.; and Blows, L. G.: A Study of the Motion of Oil Films on Surfaces in Air Flow, with Application to the Measurement of Skin Friction. J. Physics E: Scientific Instruments, vol. 9, no. 3, 1976, pp. 194-202.
2. Tanner, L. H.: A Skin Friction Meter, Using the Viscosity Balance Principle, Suitable for Use with Flat or Curved Metal Surfaces. J. Physics E: Scientific Instruments, vol. 10, no. 3, 1977, pp. 278-284.
3. Tanner, L. H.; and Kulkarni, V. G.: The Viscosity Balance Method of Skin Friction Measurement: Further Developments including Applications to Three-Dimensional Flow. J. Physics E: Scientific Instruments, vol. 9, no. 12, 1976, pp. 1114-1121.
4. Tanner, L. H.: Surface Flow Visualization and Measurement by Oil Film Interferometry. Proc. 2nd Intl. Symp. on Flow Visualization, Sept. 1980, Bochum W. Germany, Ed. Merzkirch, Hemisphere Publishing Co., NY, 1980, pp. 613-617.
5. Monson, D. J.: A Nonintrusive Laser Interferometer Method for Measurement of Skin Friction. Exp. Fluids, vol. 1, no. 1, 1983, pp. 15-22.
6. Monson, D. J.: A Laser Interferometer for Measuring Skin Friction in Three Dimensional Flows. AIAA J., vol. 22, April 1984, pp. 557-559.
7. Monson, D. J.; Mateer, G. G.; and Menter, F. R.: Boundary-Layer Transition and Global Skin Friction Measurement with an Oil-Fringe Imaging Technique. SAE Paper 932550, Aerotech 93, Costa Mesa, CA, Sept. 1993.
8. Mateer, G. G.; Monson, D. J.; and Menter, F. R.: Skin-Friction Measurements and Calculations on a Lifting Airfoil. AIAA J., vol. 34, no. 2, Feb. 1996, pp 231-236.
9. Naughton, Jonathan W.; and Brown, James L.: Surface Interferometric Skin-Friction Measurement Technique. AIAA Paper 96-2183, 19th AIAA Advanced Measurement and Ground Testing Conference, New Orleans, LA, June 1996.
10. Naughton, Jonathan W.; and Brown, James L.: Uncertainty Analysis for Oil-Film Interferometry Skin-Friction Measurement Techniques. ASME Paper FEDSM 97-3475, 1997 ASME Fluids Engineering Division Summer Meeting, FEDSM97, June 22-26, 1997.
11. Naughton, Jonathan W.; and Brown, James L.: Skin Friction Distribution Near a Cylinder Mounted on a Flat Plate. AIAA Paper 97-1783, 28th AIAA Fluid Dynamics Conference, Snowmass Village, CO, June 1997.
12. Maltby, R. L., ed.: Flow Visualization in Wind Tunnels Using Indicators. AGARDograph 70, April 1962.
13. Tobak, Murray; and Peake, David J.: Topology of 3D Separated Flows. Annual Review of Fluid Mechanics, vol. 14, 1982, pp. 61-85.
14. Chapman, G. T.; and Yates, L. T.: Topology of Flow Separation on Three Dimensional Bodies. Applied Mechanics Reviews, vol. 44, no. 7, July 1991, pp 329-345.
15. Squire, L. C.: The Motion of a Thin Oil Sheet Under the Boundary Layer on a Body. J. Fluid Mech., vol. 11, part 2, Sept. 1961, pp. 161-179; also see Flow Visualization

in Wind Tunnels Using Indicators. Compiled by R. L. Maltby, AGARDograph 70, April 1962, pp. 7-23.
16. Burgers, J. M.: A Mathematical Model Illustrating the Theory of Turbulence. In Advances in Applied Mechanics, R. von Mises and Th. von Karman, eds., vol. 1, 1948, pp. 171-199.
17. Homann, F.: Der Einfluss grosser Zähigkeit bei der Strömung um den Zylinder und um die Kugel. Z. Angew. Math. Mech., Vol. 16 (1936), pp. 153 and Forsch. Gebiete Ingenieurow., Vol. 7 (1936): English translation, The Effect of High Viscosity on the Flow around a Cylinder and around a Sphere. NACA TM-1334, Washington, D.C. (1952).
18. White, F. M.: Viscous Fluid Flow. McGraw-Hill, New York, 1974.
19. Churchill, S. W.: Viscous Flows: The Practical Use of Theory. Butterworths, Boston, 1988.
20. Perry, A. E.; and Fairlie, B. D.: Critical Points in Flow Patterns. Advances in Geophysics, vol. 18B, 1974, pp. 229-315.
21. Hung, C.-M.; Sung, C.-H.; and Chen, C.-L.: Computation of Saddle Point of Attachment. AIAA J., vol. 30, no. 6, June 1992, pp. 1561-1569.
22. MacCormack, R. W.: The Effect of Viscosity in Hypervelocity Impact Cratering. AIAA Paper 69-354, 1969.

APPENDIX A
The Equivalence of the Tanner Form and the Squire Form of the Thin Oil Film Equation

In this appendix, we show that the 2D thin oil film equation of the form as given by Squire (see eq. 2.2) and of the form as given by Tanner (eq. A.6 derived below) are equivalent and may be derived from each other by means of a metric transformation. Understanding of the details of this transformation is useful in the construction of boundary conditions. The Tanner form of the thin oil film equation can be useful in formulation of certain types of boundary conditions, whereas the Squire form of the thin oil film equation is more compatible with current computational fluid dynamics numerical procedures.

Consider that the test surface covered by an oil film may be described by a cartesian x-z coordinate system or by an s-n coordinate system attached to the surface streamlines as depicted in figure A1. Thus, n is constant for a given surface streamline, and s is the distance along the surface streamline. The local transformation between these two coordinate systems is accomplished by first a rotation ($(x, z) \Rightarrow (\tilde{x}, \tilde{z})$) by the local shear stress angle, γ, followed by a stretching $dn = \alpha d\tilde{z}$ to account for the divergence (or convergence) of the surface streamlines. Note the stretching function, α, varies with position on the test surface.

Clearly,

$$ds = \frac{\partial s}{\partial x}dx + \frac{\partial s}{\partial z}dz = \cos\gamma dx + \sin\gamma dz$$
$$dn = \frac{\partial n}{\partial x}dx + \frac{\partial n}{\partial z}dz = -\alpha\sin\gamma dx + \alpha\cos\gamma dz$$

Inversion of the transformation matrix above gives:

$$dx = \frac{\partial x}{\partial s}ds + \frac{\partial x}{\partial n}dn = \cos\gamma ds - (\sin\gamma/\alpha)dn$$
$$dz = \frac{\partial z}{\partial s}ds + \frac{\partial z}{\partial n}dn = \sin\gamma ds + (\cos\gamma/\alpha)dn$$

Further, transformation of partial derivatives between these two coordinate systems may be locally accomplished by:

$$\frac{\partial}{\partial x} = \frac{\partial s}{\partial x}\frac{\partial}{\partial s} + \frac{\partial n}{\partial x}\frac{\partial}{\partial n}$$
$$\frac{\partial}{\partial z} = \frac{\partial s}{\partial z}\frac{\partial}{\partial s} + \frac{\partial n}{\partial z}\frac{\partial}{\partial n}$$

and

$$\frac{\partial}{\partial s} = \frac{\partial x}{\partial s}\frac{\partial}{\partial x} + \frac{\partial z}{\partial s}\frac{\partial}{\partial z}$$
$$\frac{\partial}{\partial n} = \frac{\partial x}{\partial n}\frac{\partial}{\partial x} + \frac{\partial z}{\partial n}\frac{\partial}{\partial z}$$

In the x-z coordinate system, consider the thin oil film equation of the form given by Squire (restricted to wall shear stress effects):

$$\frac{\partial h}{\partial t} + \frac{\partial}{\partial x}\left(\frac{\tau_x h^2}{2\mu_o}\right) + \frac{\partial}{\partial z}\left(\frac{\tau_z h^2}{2\mu_o}\right) = 0 \qquad (A.1)$$

To transform to the s-n coordinate system for the form given by Tanner, we first expand:

$$\frac{\partial}{\partial x}\left(\frac{\tau_x h^2}{2\mu_o}\right) + \frac{\partial}{\partial z}\left(\frac{\tau_z h^2}{2\mu_o}\right) = \tau\cos\gamma\frac{\partial h^2/2\mu_o}{\partial x} + \tau\sin\gamma\frac{\partial h^2/2\mu_o}{\partial z} + (h^2/2\mu_o)\left(\frac{\partial \tau\cos\gamma}{\partial x} + \frac{\partial \tau\sin\gamma}{\partial z}\right)$$

Next, apply the coordinate transformation:

$$\begin{aligned}\frac{\partial}{\partial x}\left(\frac{\tau_x h^2}{2\mu_o}\right) + \frac{\partial}{\partial z}\left(\frac{\tau_z h^2}{2\mu_o}\right) =& \tau\cos\gamma\left(\cos\gamma\frac{\partial h^2/2\mu_o}{\partial s} - \alpha\sin\gamma\frac{\partial h^2/2\mu_o}{\partial n}\right)\\ &+ \tau\sin\gamma\left(\sin\gamma\frac{\partial h^2/2\mu_o}{\partial s} + \alpha\cos\gamma\frac{\partial h^2/2\mu_o}{\partial n}\right)\\ &+ (h^2/2\mu_o)\left(\cos\gamma\frac{\partial \tau\cos\gamma}{\partial s} - \alpha\sin\gamma\frac{\partial \tau\cos\gamma}{\partial n}\right.\\ &\left.+ \sin\gamma\frac{\partial \tau\sin\gamma}{\partial s} + \alpha\cos\gamma\frac{\partial \tau\sin\gamma}{\partial n}\right)\end{aligned}$$

Now, contract the left hand side (mostly, $\cos^2 + \sin^2 = 1$), and rearrange giving:

$$\frac{\partial}{\partial x}\left(\frac{\tau_x h^2}{2\mu_o}\right) + \frac{\partial}{\partial z}\left(\frac{\tau_z h^2}{2\mu_o}\right) = \frac{\partial}{\partial s}\left(\frac{\tau h^2}{2\mu_o}\right) + (\tau h^2/2\mu_o)\alpha\frac{\partial \gamma}{\partial n}$$

which then leads to the s-n form for the 2D thin oil film equation:

$$\frac{\partial h}{\partial t} + \frac{\partial \tau h^2/2\mu_o}{\partial s} + (\tau h^2/2\mu_o)\alpha\frac{\partial \gamma}{\partial n} = 0 \qquad (A.2)$$

Note that in analyzing surface streamline images, α would seldom actually be established since the stretching, α, distorts angles, and the rotated coordinate, $\tilde{z}$, would be used locally rather than n. Thus, the substitution into the above equation of $\partial\gamma/\partial\tilde{z} = \alpha\partial\gamma/\partial n$ would be appropriate, particularly in the formulation of numerical boundary conditions:

$$\frac{\partial h}{\partial t} + \frac{\partial \tau h^2/2\mu_o}{\partial s} + (\tau h^2/2\mu_o)\frac{\partial \gamma}{\partial \tilde{z}} = 0 \qquad (A.3)$$

To proceed toward Tanner's form of the 2D thin oil film equation, consider figure A2 which seeks to relate the streamline divergence term used by Tanner (note Tanner uses the symbol n rather than η) to the shear stress angle γ used in this paper. In figure A2, two surface streamlines are initially separated by a small distance, $\eta_n = \alpha(s,n)\eta$. Note, η_n is given in term of the stretched coordinate, n, whereas η is given in terms of the local unstretched coordinate, $\tilde{z}$. Thus, the angle formed between the two streamlines is given by $\Delta\gamma = (\partial\gamma/\partial\tilde{z})\eta$. A small distance, Δs, along the streamlines the separation will increase by $\Delta\eta = (\partial\gamma/\partial\tilde{z})\eta\Delta s$. In the limit of small η and Δs, we obtain the relationship:

$$(\frac{1}{\eta})\frac{\partial \eta}{\partial s} = \frac{\partial \gamma}{\partial \tilde{z}} = \alpha\frac{\partial \gamma}{\partial n} \qquad (A.4)$$

Substituting this relation into equation A.2 we obtain:

$$\frac{\partial h}{\partial t} + \frac{\partial \tau h^2/2\mu_o}{\partial s} + (\tau h^2/2\mu_o)(\frac{1}{\eta})\frac{\partial \eta}{\partial s} = 0 \qquad (A.5)$$

Rearranging, we obtain Tanner's form for the 2D thin oil film equation:

$$\frac{\partial h}{\partial t} + (\frac{1}{\eta})\frac{\partial \eta\tau h^2/2\mu_o}{\partial s} = 0 \qquad (A.6)$$

Note, η can be obtained by integrating equation A.4 along a surface streamline (the choice for η_0 at s_0 can be arbitrarily small):

$$\eta = \eta_0 e^{(\int_{s0}^{s} \partial\gamma/\partial\tilde{z}ds)} \qquad (A.7)$$

Thus, the two streamlines initially some small distance apart, η_0, at s_0 will be separated by η at s. But, in terms of the n coordinate, the separation, η_n, is fixed:

$$\eta_n = \alpha(s,n)\eta(s,n) = \text{constant}$$

which leads to:

$$\alpha = \alpha_0 e^{-(\int_{s0}^{s} \partial\gamma/\partial\tilde{z}ds)} \qquad (A.8)$$

Equation A.8 does give us the means to analyze a surface streamline image, with known $\gamma(x,z)$, for the stretching function, $\alpha(x,z)$, and known rotation function, $\gamma(x,z)$, required to establish the s-n coordinate system if so desired.

The demonstration presented here that Tanner's form and Squire's form of the 2D thin oil film differ only in the coordinate system reveals the details of the required coordinate

system transformation. These details should prove useful in correctly formulating general boundary conditions.

APPENDIX B
Numerical Forms for $\partial^3 h/\partial x^3$

A centered numerical approximation to the partial derivative, $\partial^3 h/\partial x^3$, may be found on an unevenly spaced grid $(x_{i-2},x_{i-1},x_i,x_{i+1},x_{i+2})$ by:

$$(\partial^3 h/\partial x^3)_i = \alpha_i h_{i+2} + \beta_i h_{i+1} + \epsilon_i h_i + \gamma_i h_{i-1} + \delta_i h_{i-2}$$

$$\alpha_i = \frac{-6(x_{i+1} + x_{i-1} + x_{i-2} - 3x_i)}{(x_{i+2} - x_i)(x_{i+2} - x_{i+1})(x_{i+2} - x_{i-1})(x_{i+2} - x_{i-2})}$$

$$\beta_i = \frac{6(x_{i+2} + x_{i-1} + x_{i-2} - 3x_i)}{(x_{i+1} - x_i)(x_{i+2} - x_{i+1})(x_{i+1} - x_{i-1})(x_{i+1} - x_{i-2})}$$

$$\gamma_i = \frac{6(x_{i+2} + x_{i+1} + x_{i-2} - 3x_i)}{(x_{i-1} - x_i)(x_{i+2} - x_{i-1})(x_{i-1} - x_{i+1})(x_{i-1} - x_{i-2})}$$

$$\delta_i = \frac{6(x_{i+2} + x_{i+1} + x_{i-1} - 3x_i)}{(x_{i-2} - x_i)(x_{i+2} - x_{i-2})(x_{i-2} - x_{i+1})(x_{i-2} - x_{i-1})}$$

$$\epsilon_i = -(\alpha_i + \beta_i + \gamma_i + \delta_i)$$

A biased numerical approximation to the partial derivative $\partial^3 h/\partial x^3$, may be found on an unevenly spaced grid $(x_{i-1},x_i,x_{i+1},x_{i+2},x_{i+3})$ by:

$$(\partial^3 h/\partial x^3)_i = \alpha_i h_{i+3} + \beta_i h_{i+2} + \gamma_i h_{i+1} + \epsilon_i h_i + \delta_i h_{i-1}$$

$$\alpha_i = \frac{-6(x_{i+2} + x_{i+1} + x_{i-1} - 3x_i)}{(x_{i+3} - x_i)(x_{i+3} - x_{i+2})(x_{i+3} - x_{i+1})(x_{i+3} - x_{i-1})}$$

$$\beta_i = \frac{6(x_{i+3} + x_{i+1} + x_{i-1} - 3x_i)}{(x_{i+2} - x_i)(x_{i+3} - x_{i+2})(x_{i+2} - x_{i+1})(x_{i+2} - x_{i-1})}$$

$$\gamma_i = \frac{6(x_{i+3} + x_{i+2} + x_{i-1} - 3x_i)}{(x_{i+1} - x_i)(x_{i+3} - x_{i+1})(x_{i+1} - x_{i+2})(x_{i+1} - x_{i-1})}$$

$$\delta_i = \frac{6(x_{i+3} + x_{i+2} + x_{i+1} - 3x_i)}{(x_{i-1} - x_i)(x_{i+3} - x_{i-1})(x_{i-1} - x_{i+2})(x_{i-1} - x_{i+1})}$$

$$\epsilon_i = -(\alpha_i + \beta_i + \gamma_i + \delta_i)$$

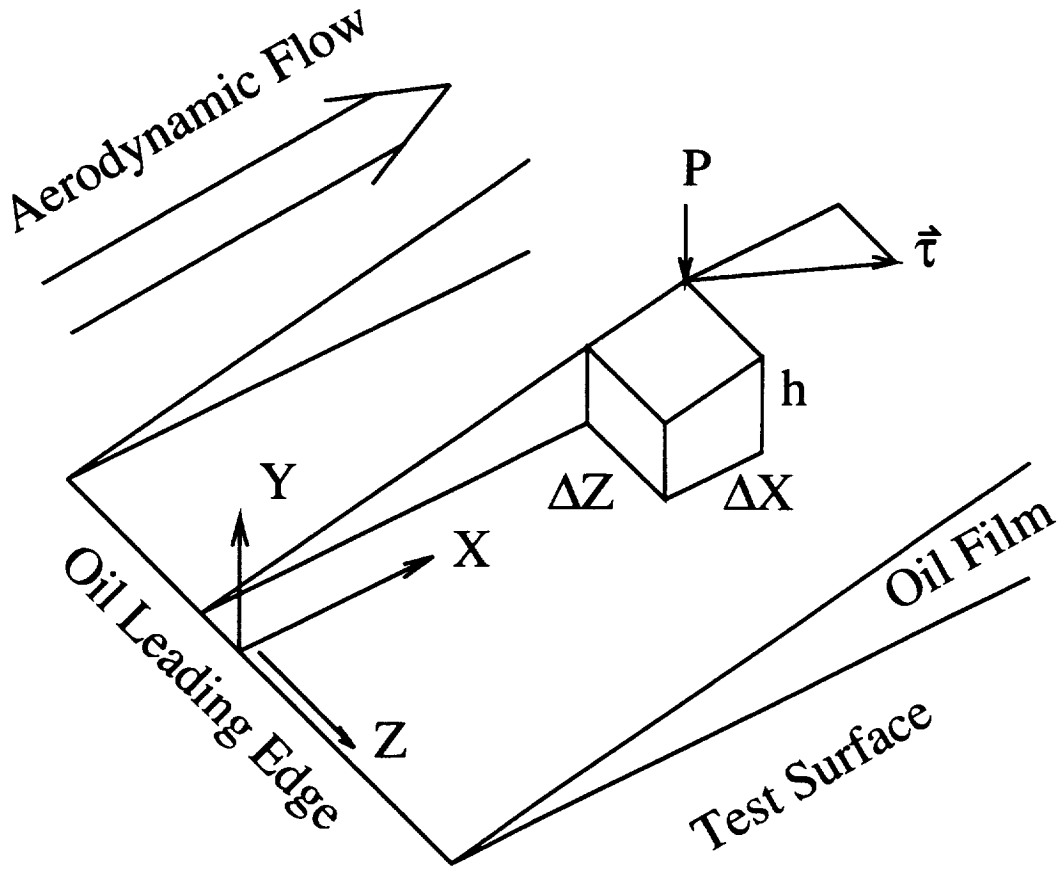

Figure 1. The thin oil film on a test surface.

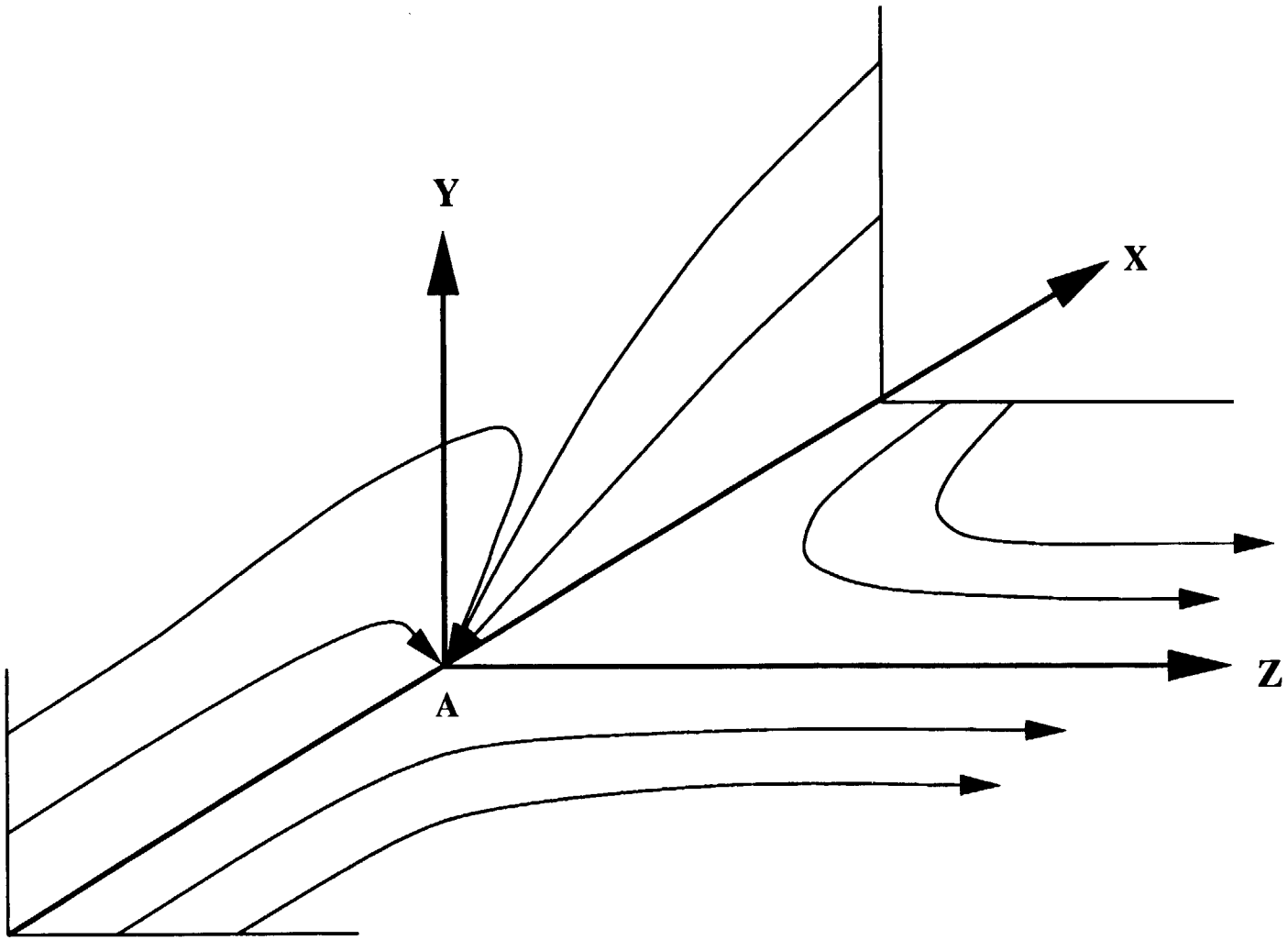

Figure 2a. Saddle of attachment surface and plane of symmetry flowfield streamlines.

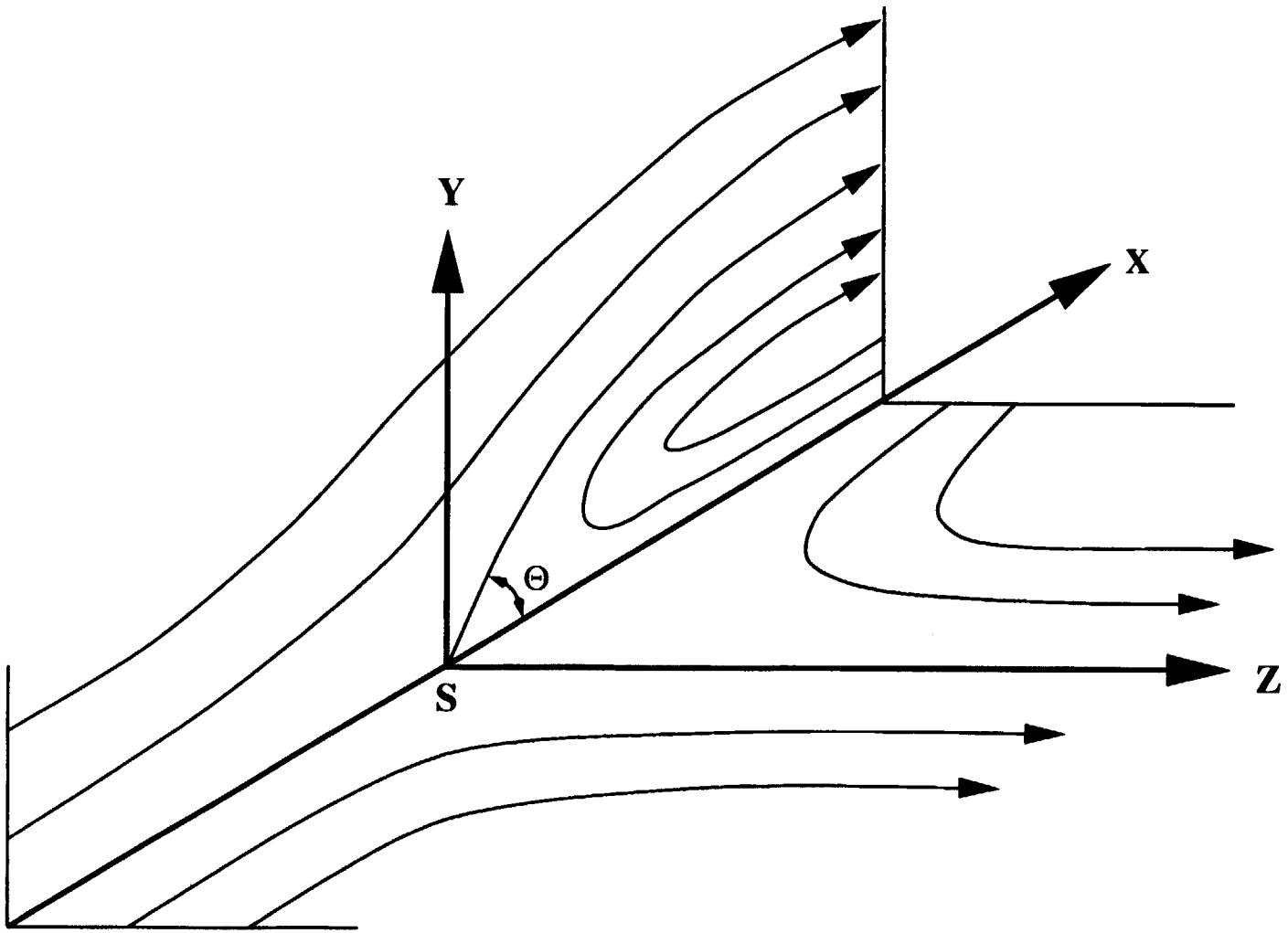

Figure 2b. Saddle of separation surface and plane of symmetry flowfield streamlines.

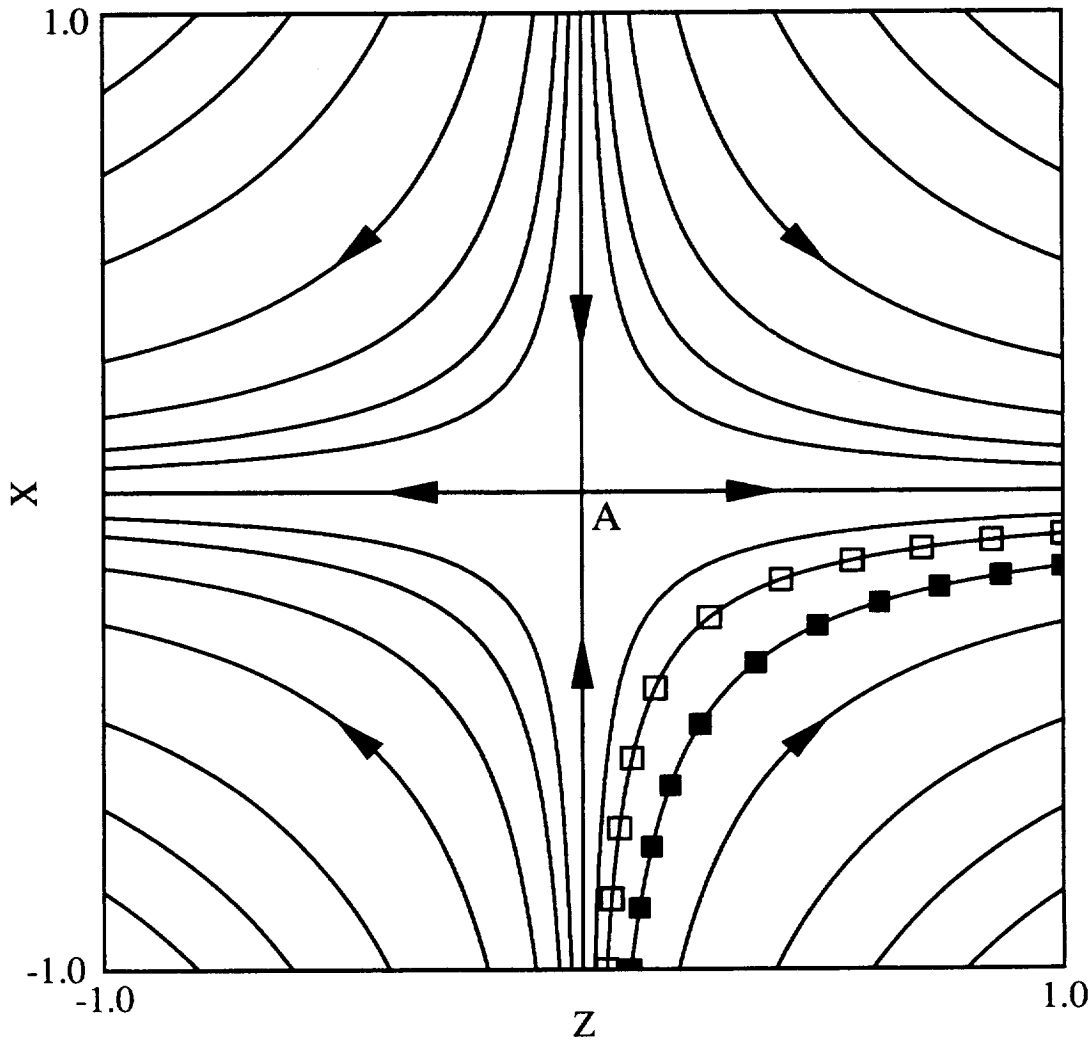

Figure 3a. Saddle of attachment surface streamlines.

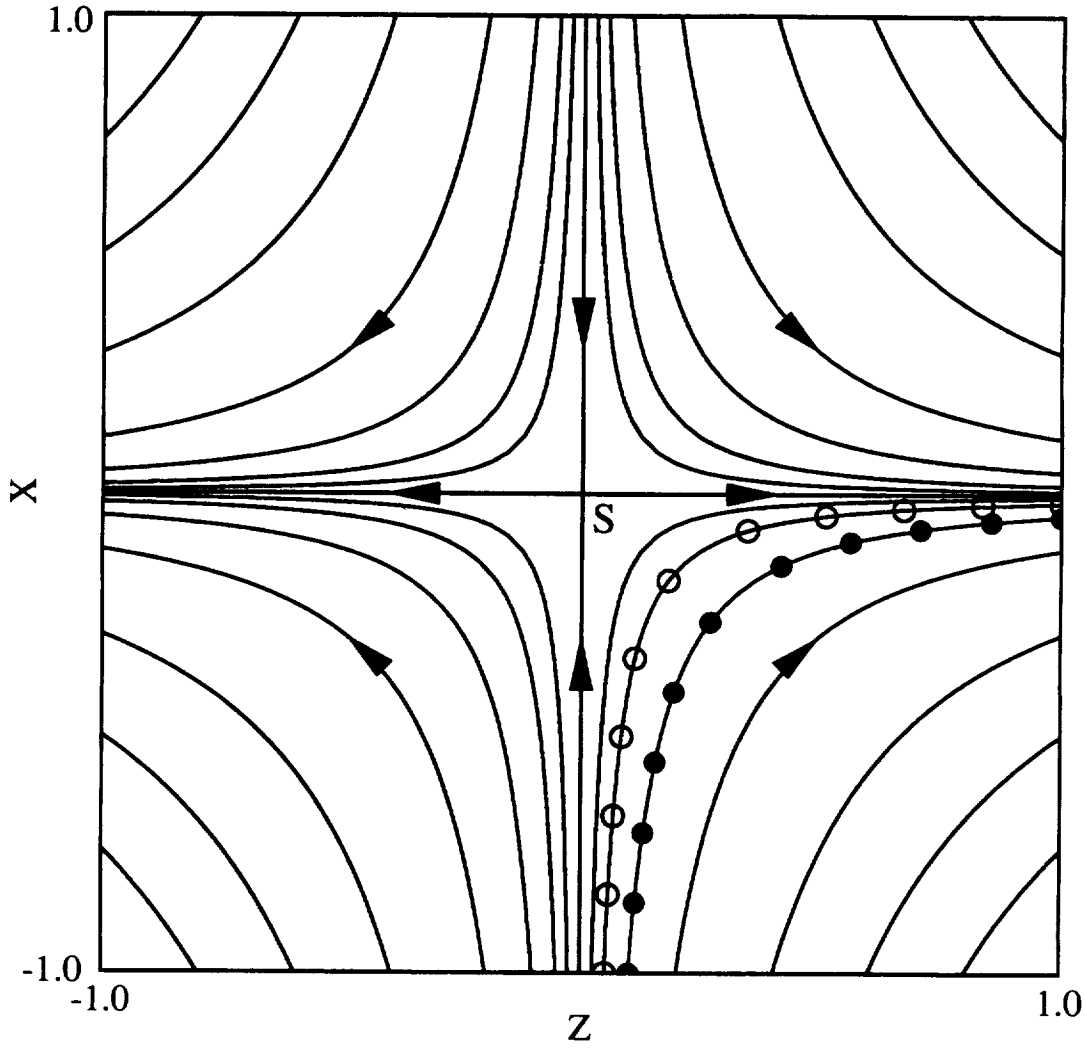

Figure 3b. Saddle of separation surface streamlines.

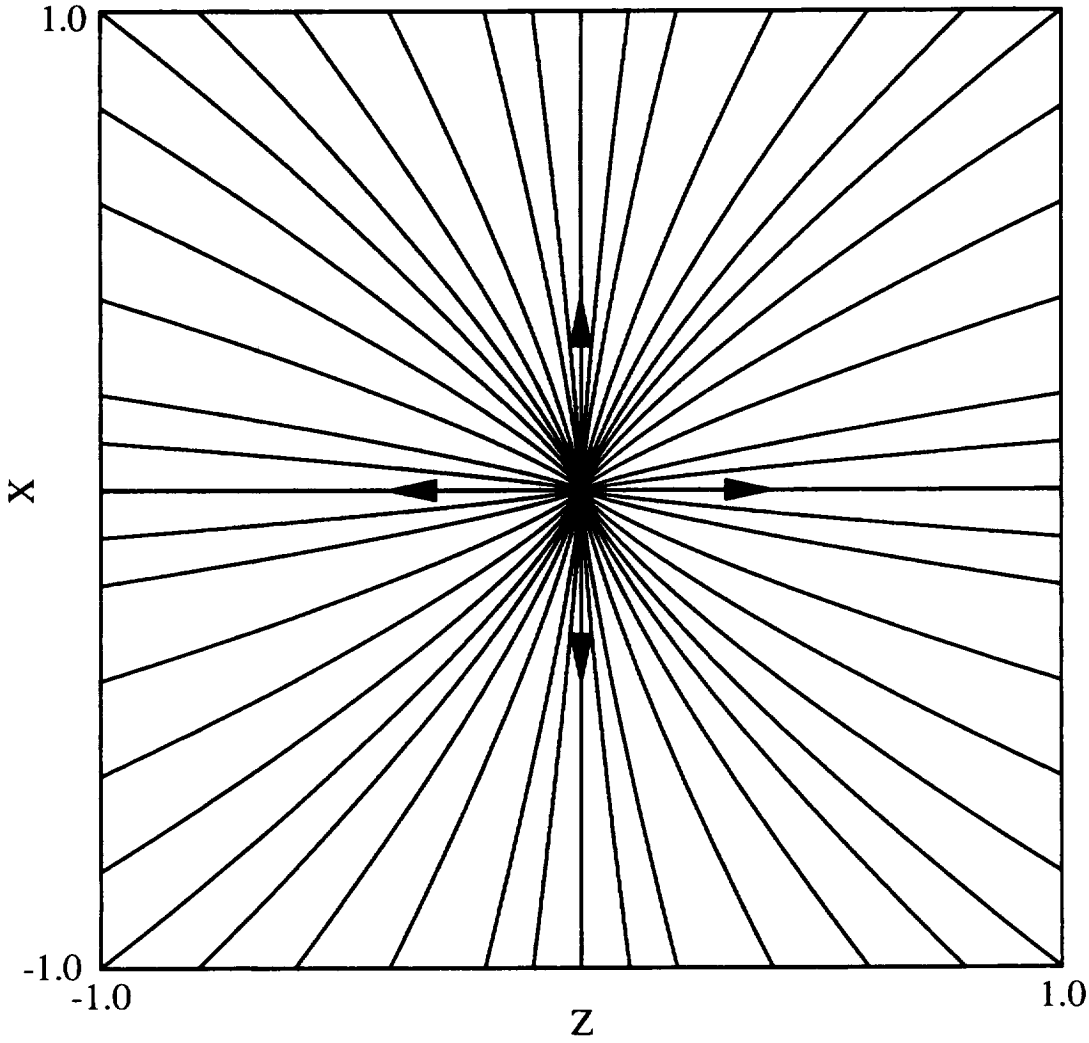

Figure 3c. Node of attachment surface streamlines.

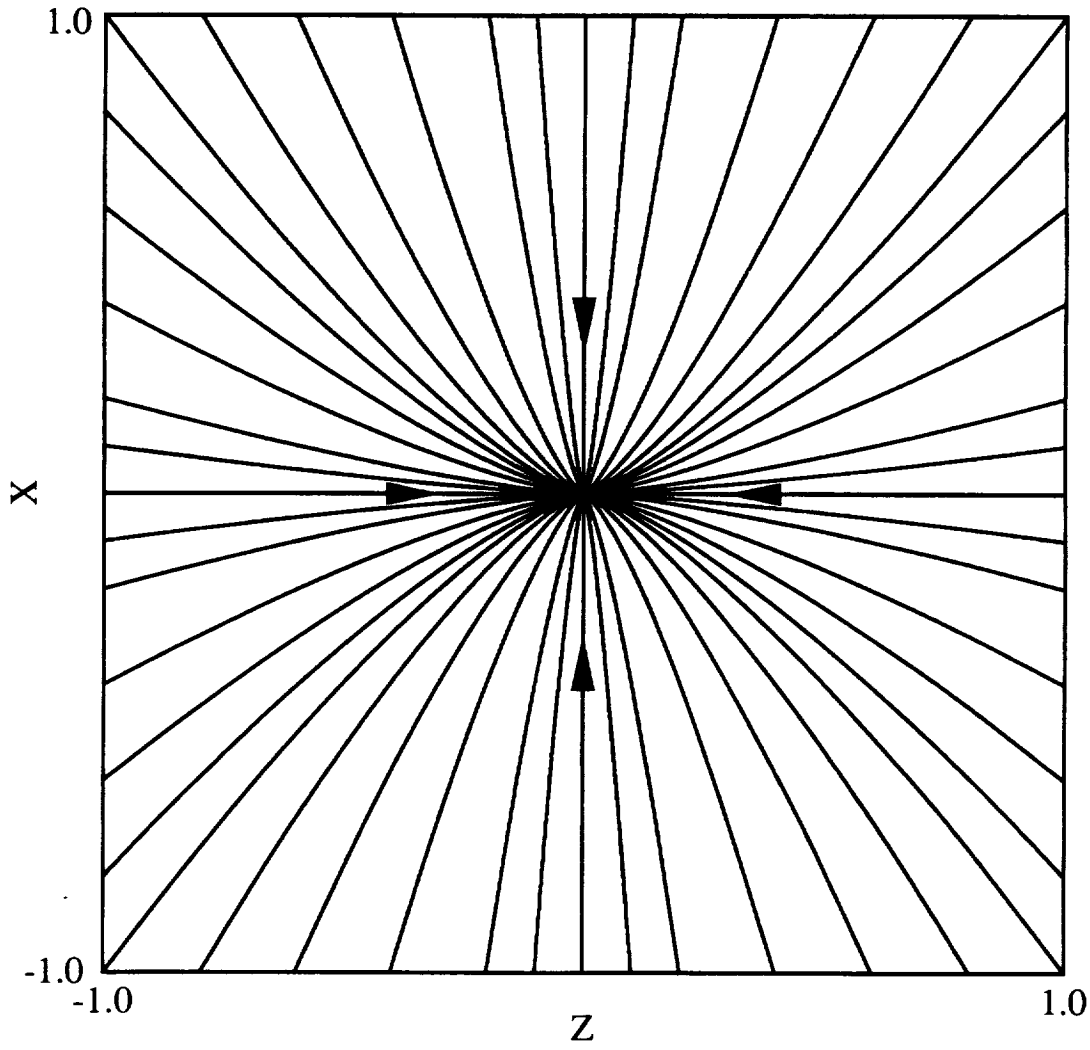

Figure 3d. Node of separation surface streamlines.

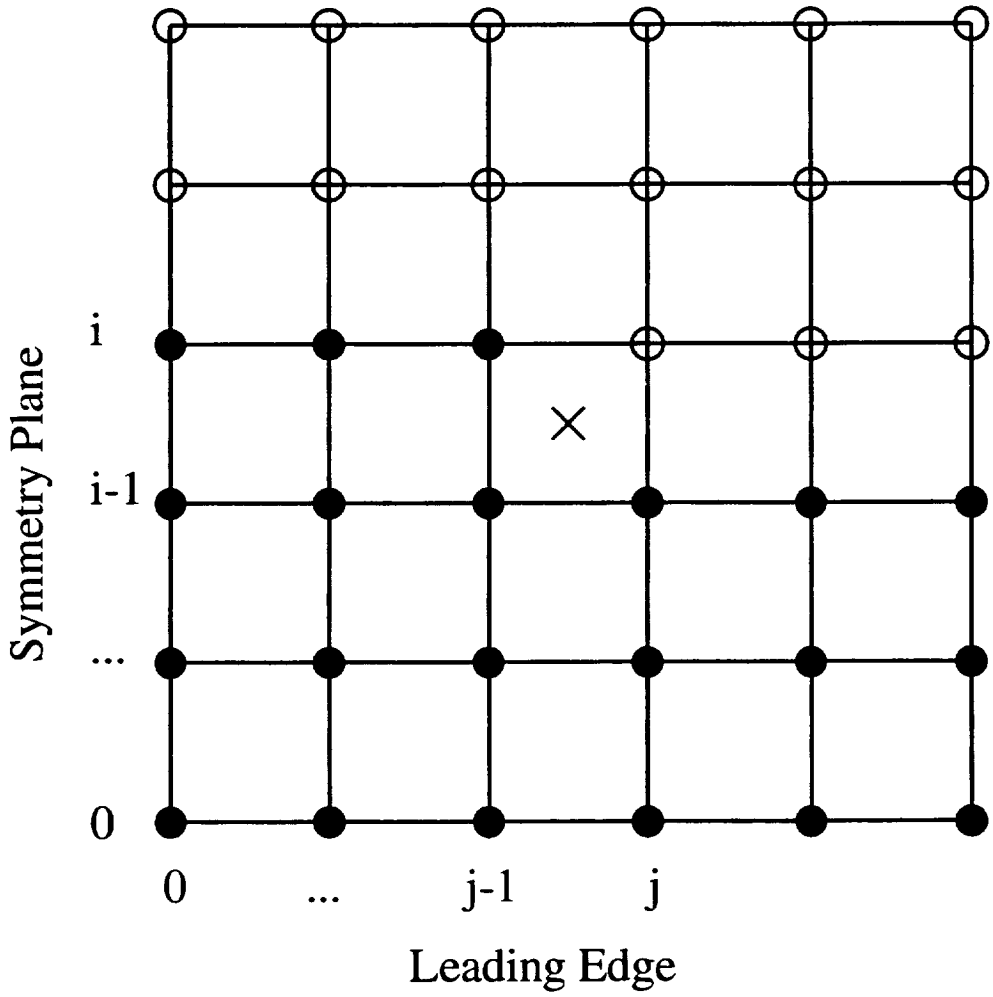

Figure 4. Box-Implicit solution molecule.

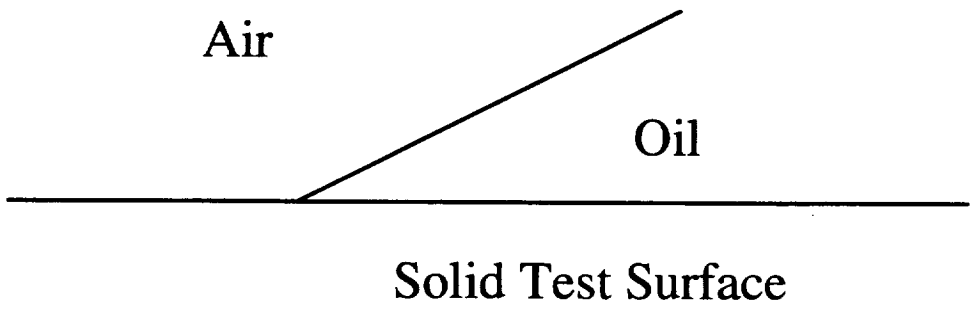

Figure 5. Thin oil film leading edge.

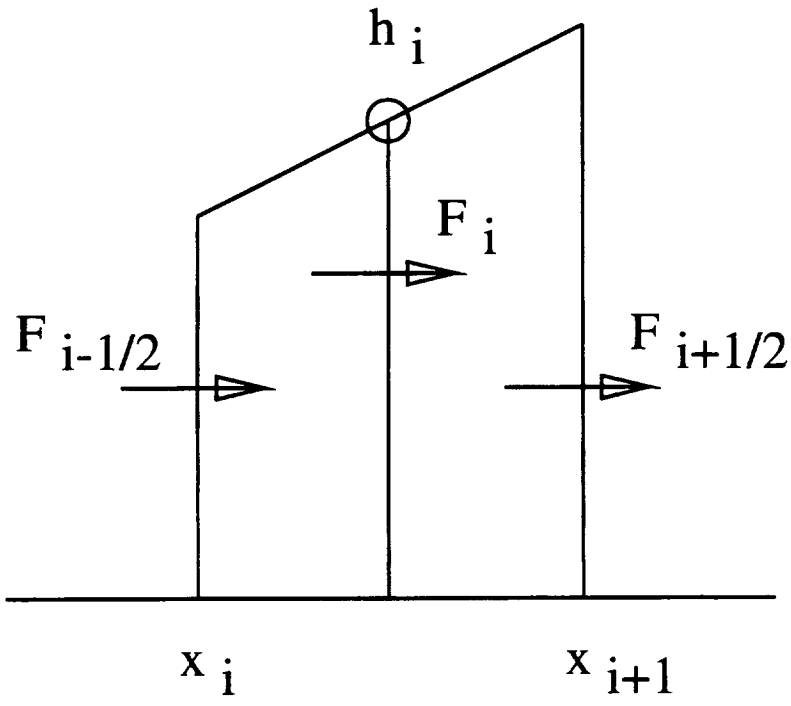

Figure 6. Control volume for Finite-Volume algorithm.

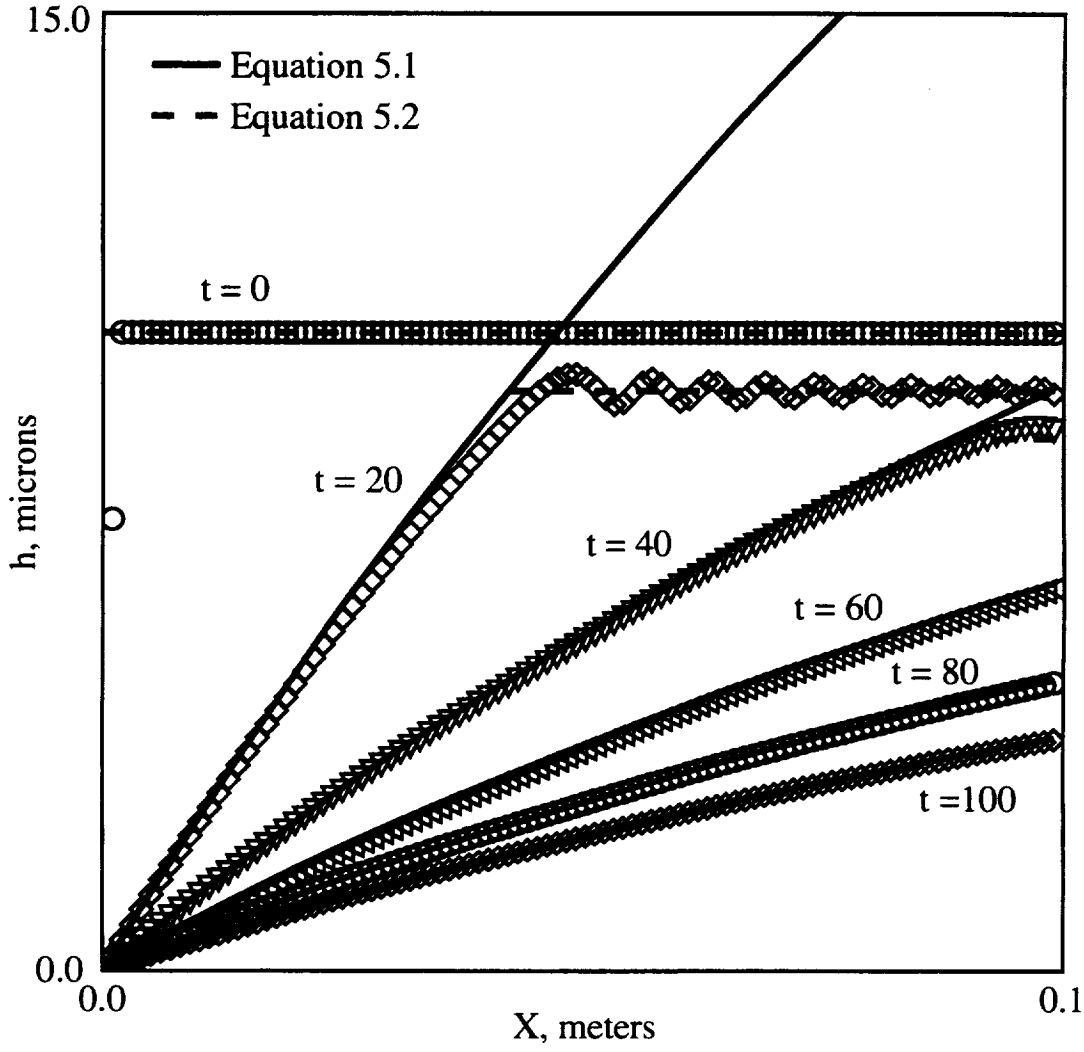

Figure 7a. Oil film thickness from Box-Implicit direct solver (symbols) compared to analytical solution (lines) for linear wall shear stress (= 20 + 100 x) case.

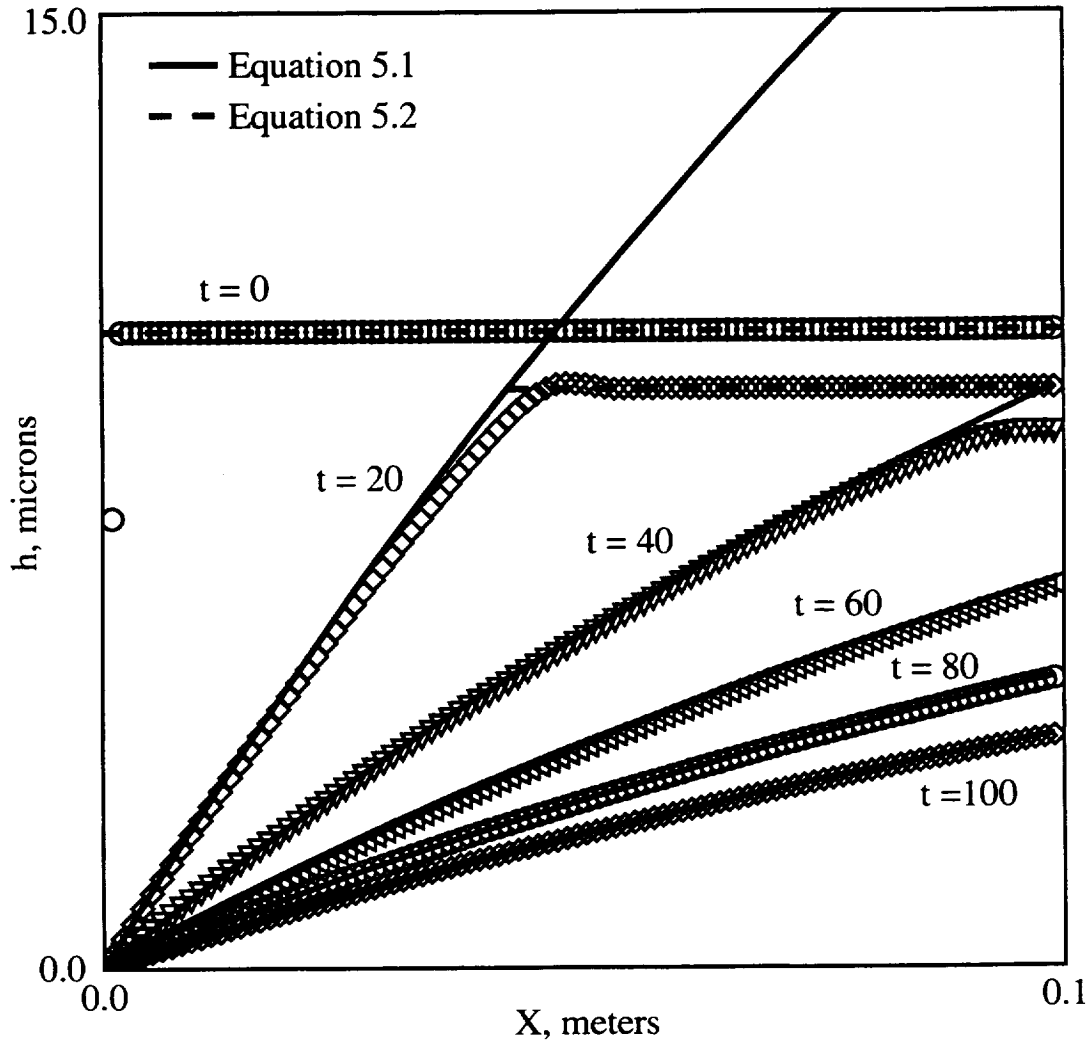

Figure 7b. Oil film thickness from Box-Implicit Flux-Limit direct solver (symbols) compared to analytical solution (lines) for linear wall shear stress (= 20 + 100 x) case.

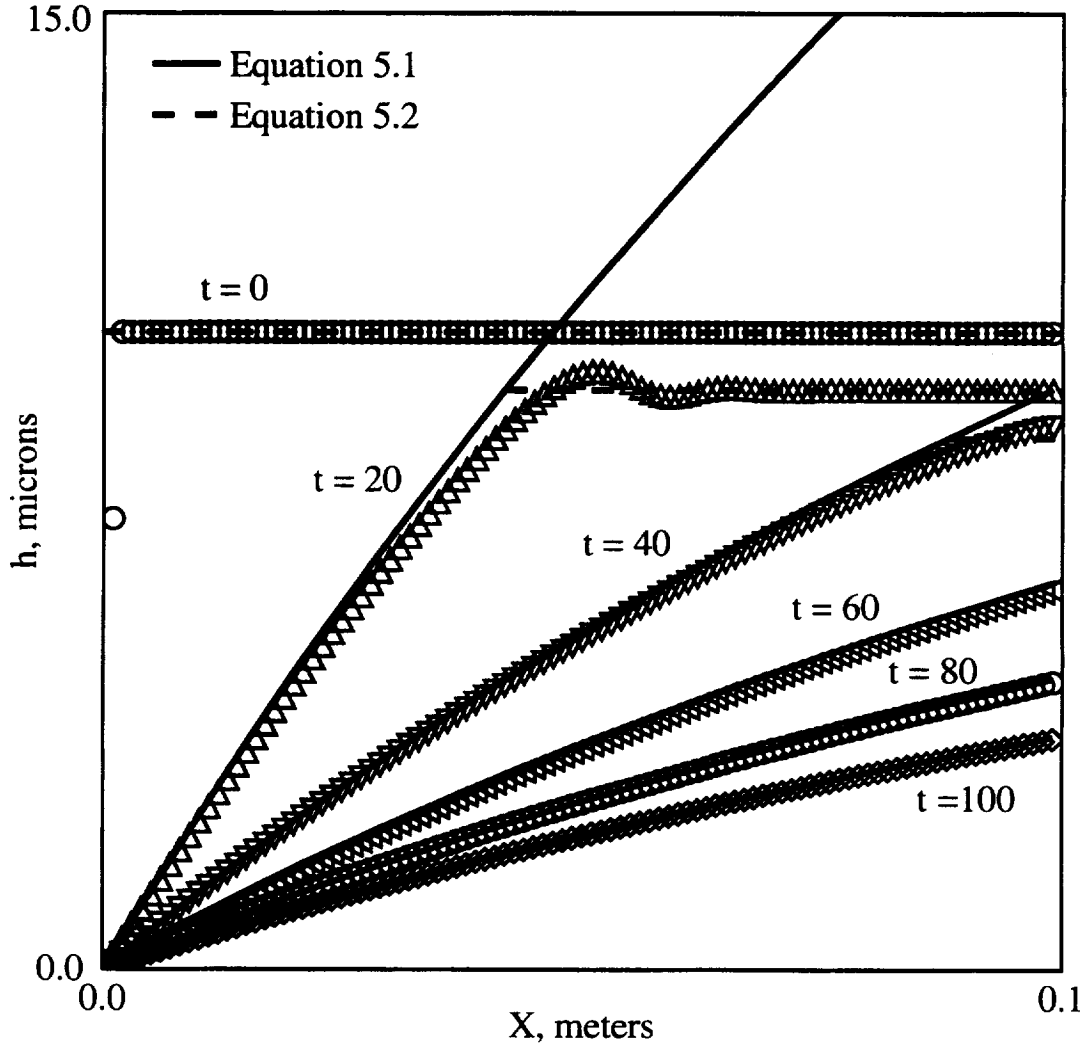

Figure 7c. Oil film thickness from Finite-Volume Upwind-Implicit direct solver (symbols) compared to analytical solution (lines) for linear wall shear stress (= 20 + 100 x) case.

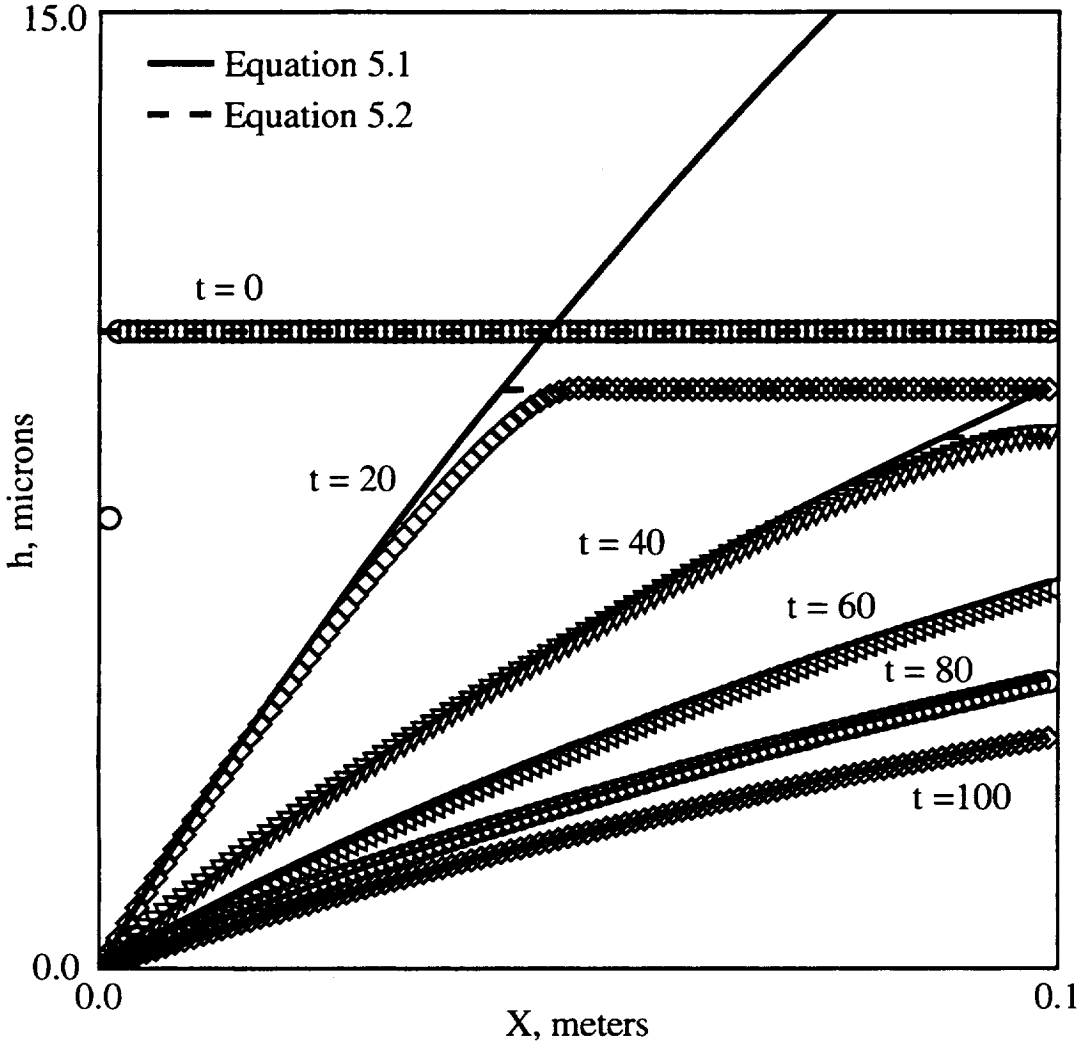

Figure 7d. Oil film thickness from Finite-Volume Upwind-Implicit Flux-Limit direct solver (symbols) compared to analytical solution (lines) for linear wall shear stress (= 20 + 100 x) case.

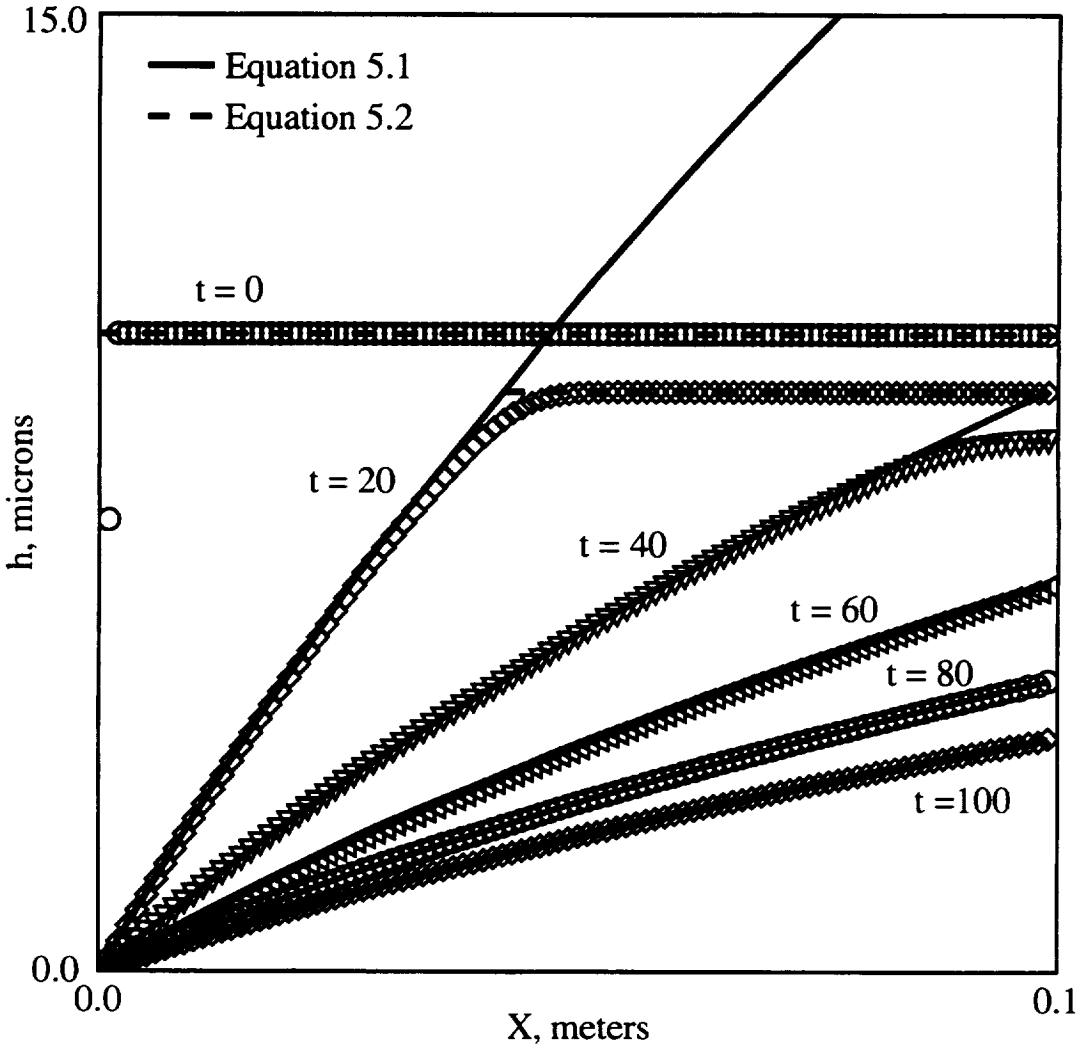

Figure 7e. Oil film thickness from McCormack direct solver (symbols) compared to analytical solution (lines) for linear wall shear stress (= 20 + 100 x) case.

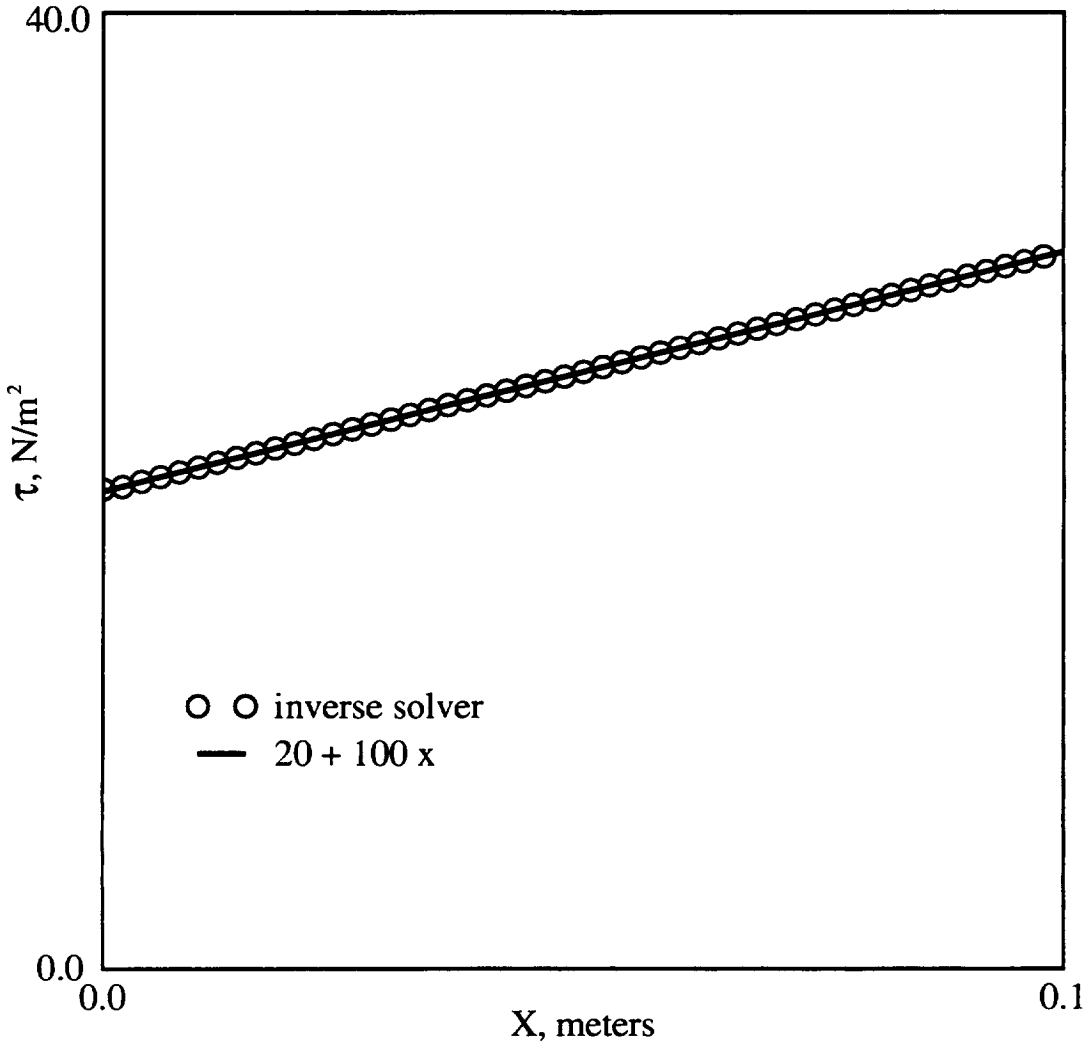

Figure 8a. Wall shear stress from Box-Implicit inverse solver. Analytical oil film thickness at t=80 and 100 seconds used as input to inverse solver.

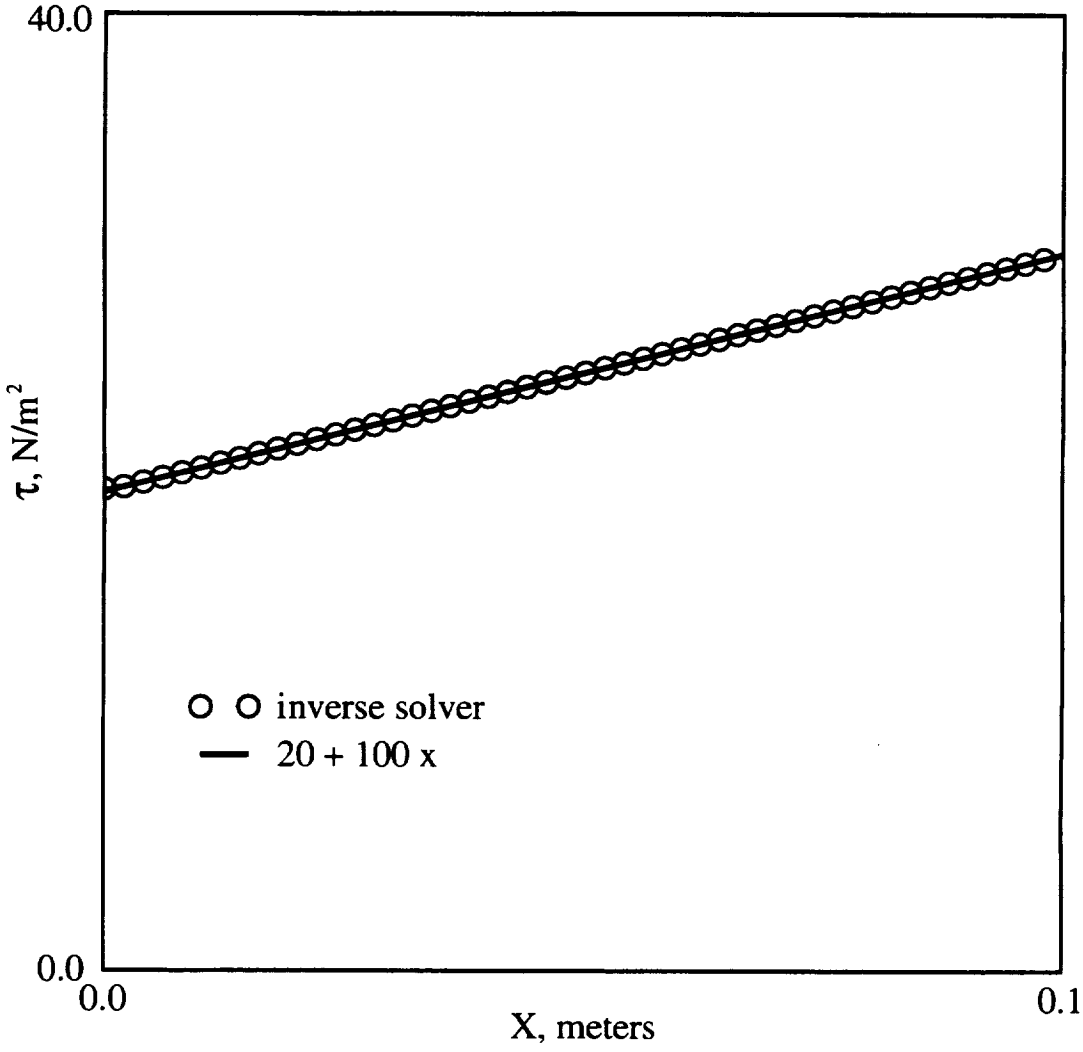

Figure 8b. Wall shear stress from Box-Implicit inverse solver.
Oil film thickness at t=80 and 100 seconds from
Box-Implicit direct solver used as input to inverse solver.

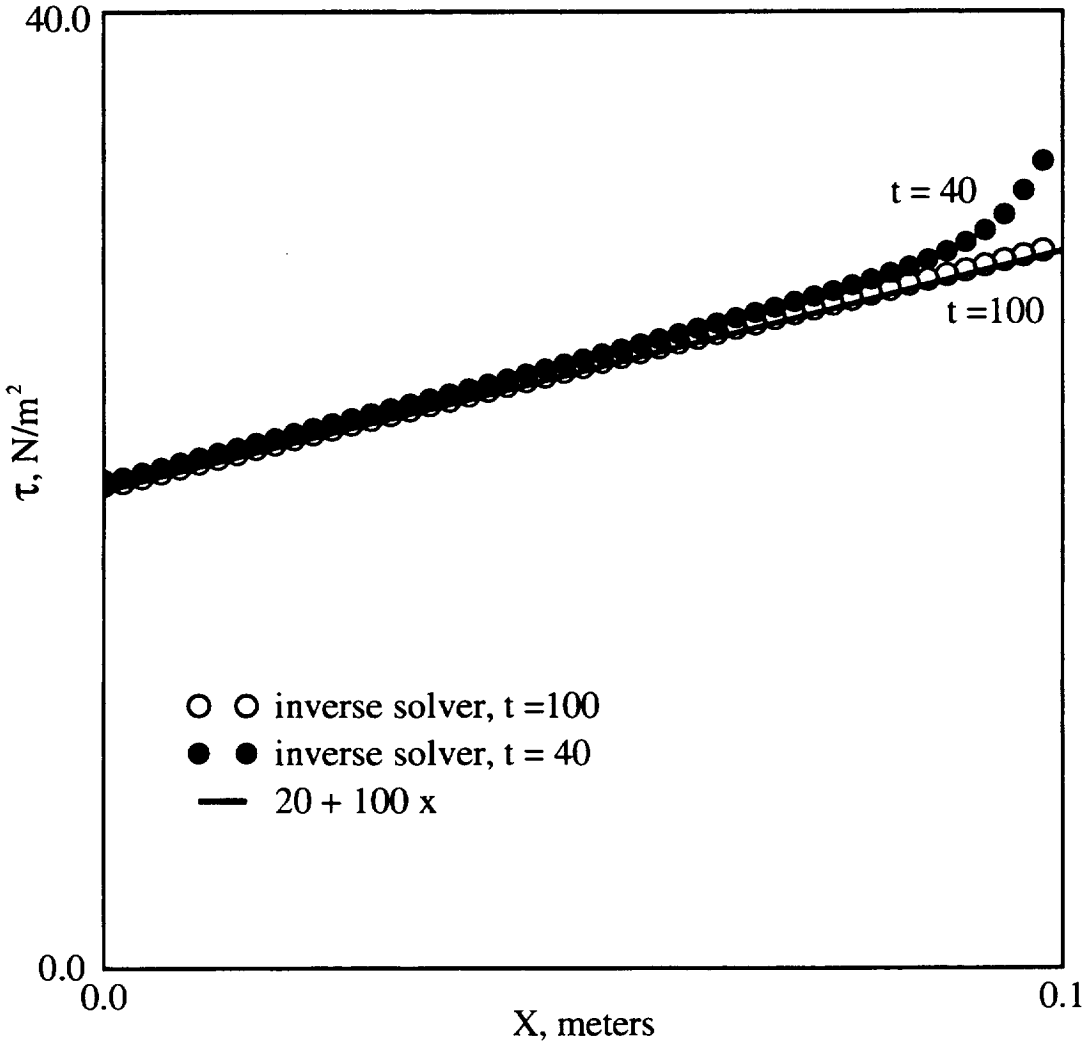

Figure 8c. Wall shear stress from One-Time-Level Box-Implicit inverse solver. Box-Implicit direct solver oil film thickness at t=40 and 100 seconds as inverse solver input.

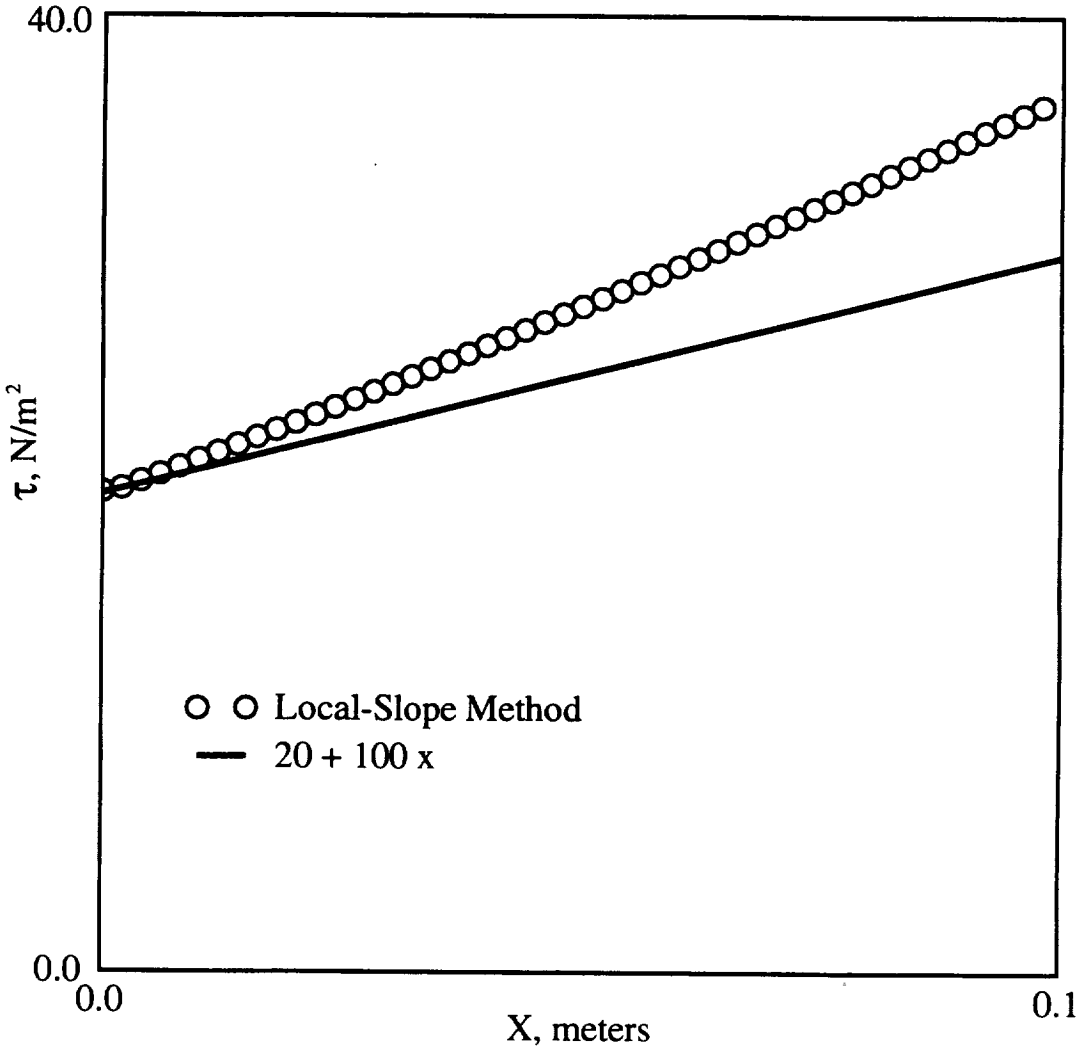

Figure 8d. Wall shear stress from local-slope method. Analytical oil film thickness at t=100 seconds used as input to local-slope method.

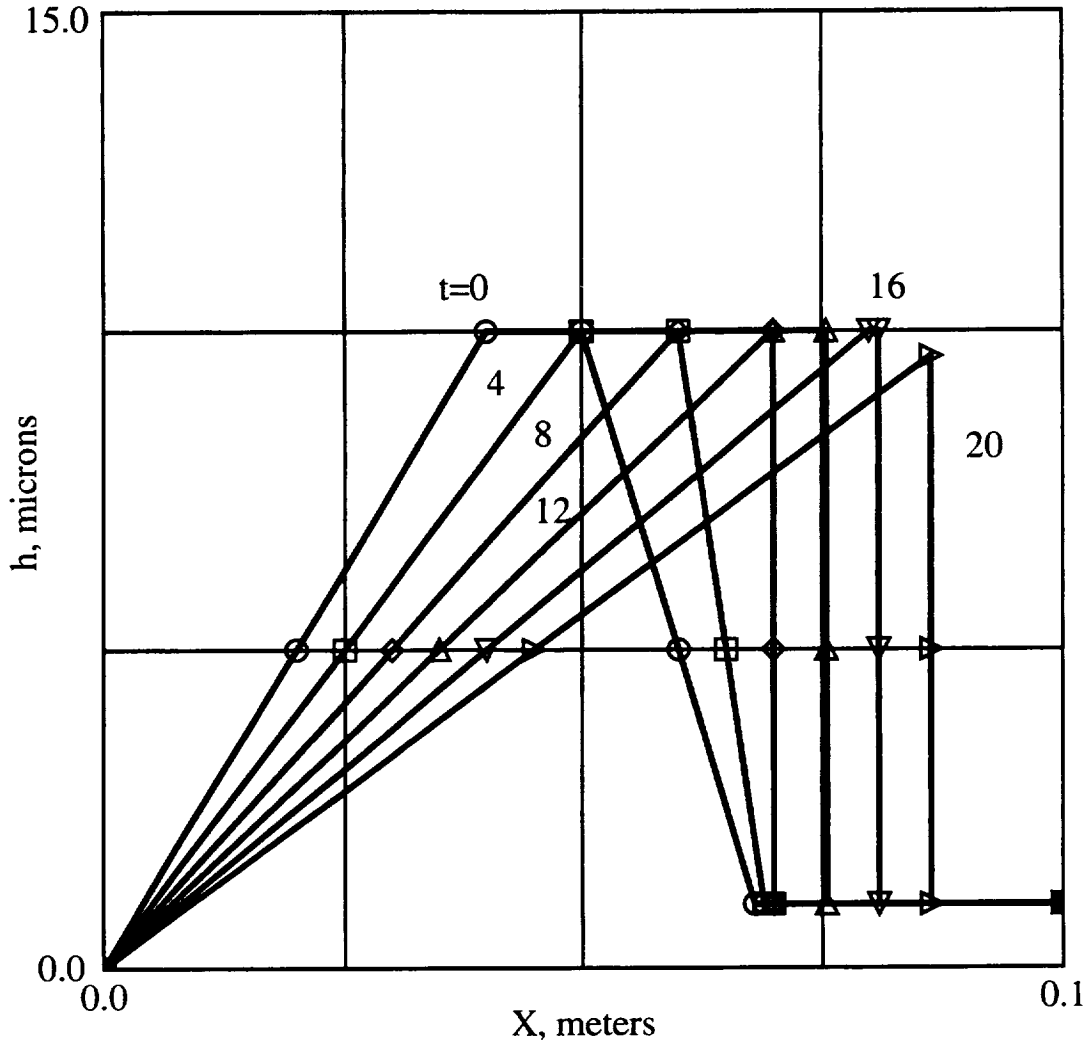

Figure 9a. Analytical oil film thickness at discrete times (t= 0, 4, 8, 12, 16 and 20 seconds) for constant wall shear stress, non-monotonic initial thickness problem.

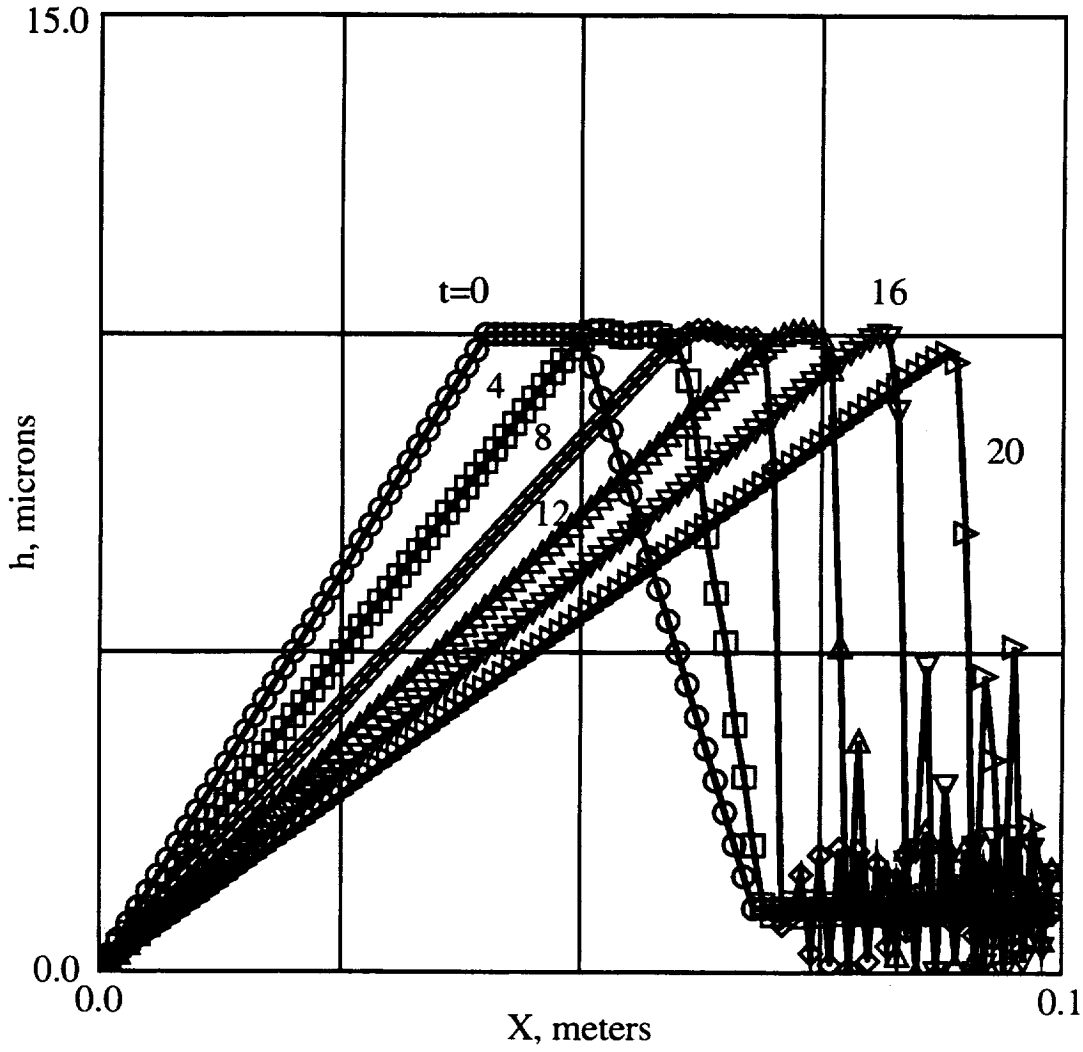

Figure 9b. Box-Implicit direct solver oil film thickness at discrete times for constant wall shear stress, non-monotonic initial thickness problem.

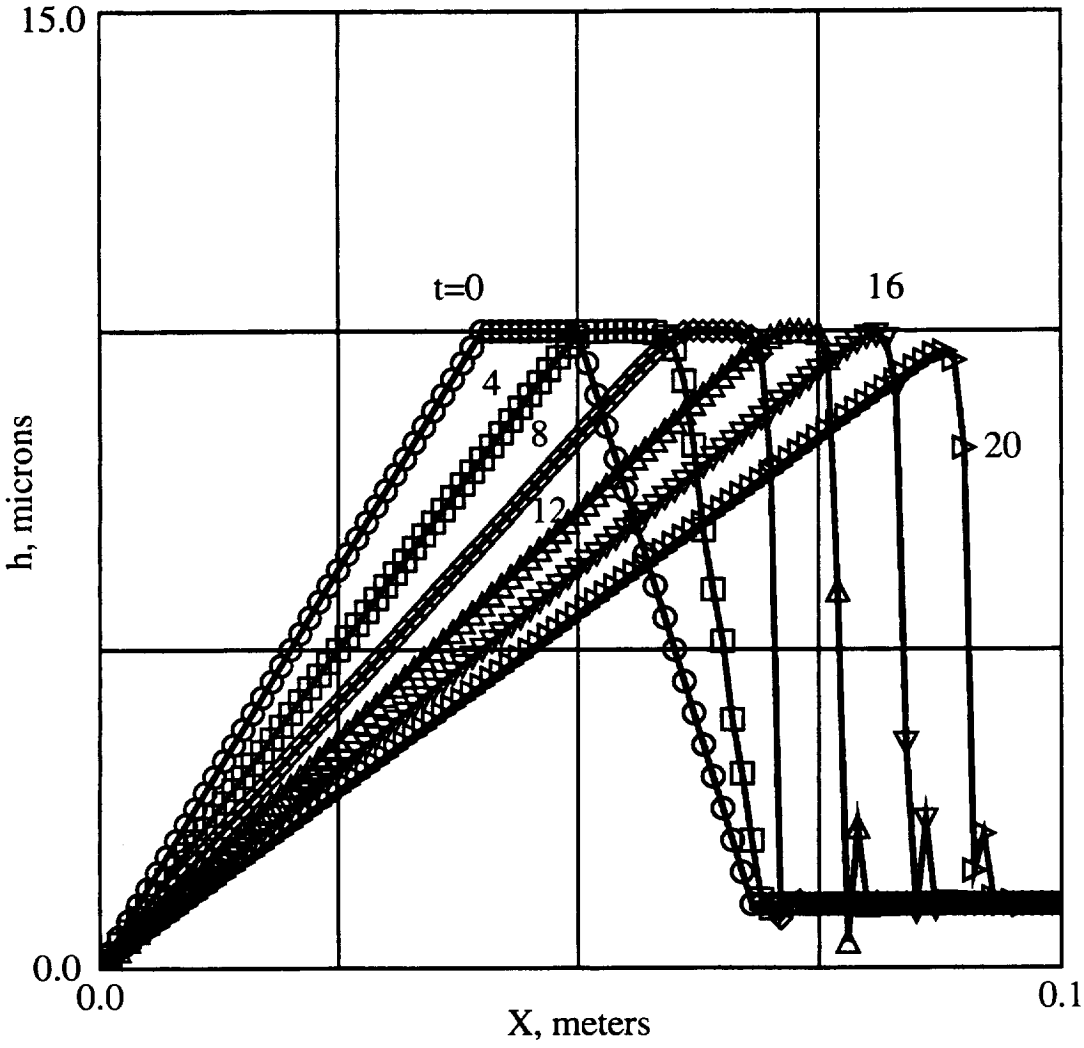

Figure 9c. Box-Implicit, Flux-Limit direct solver oil film thickness at discrete times for constant wall shear stress, non-monotonic initial thickness problem.

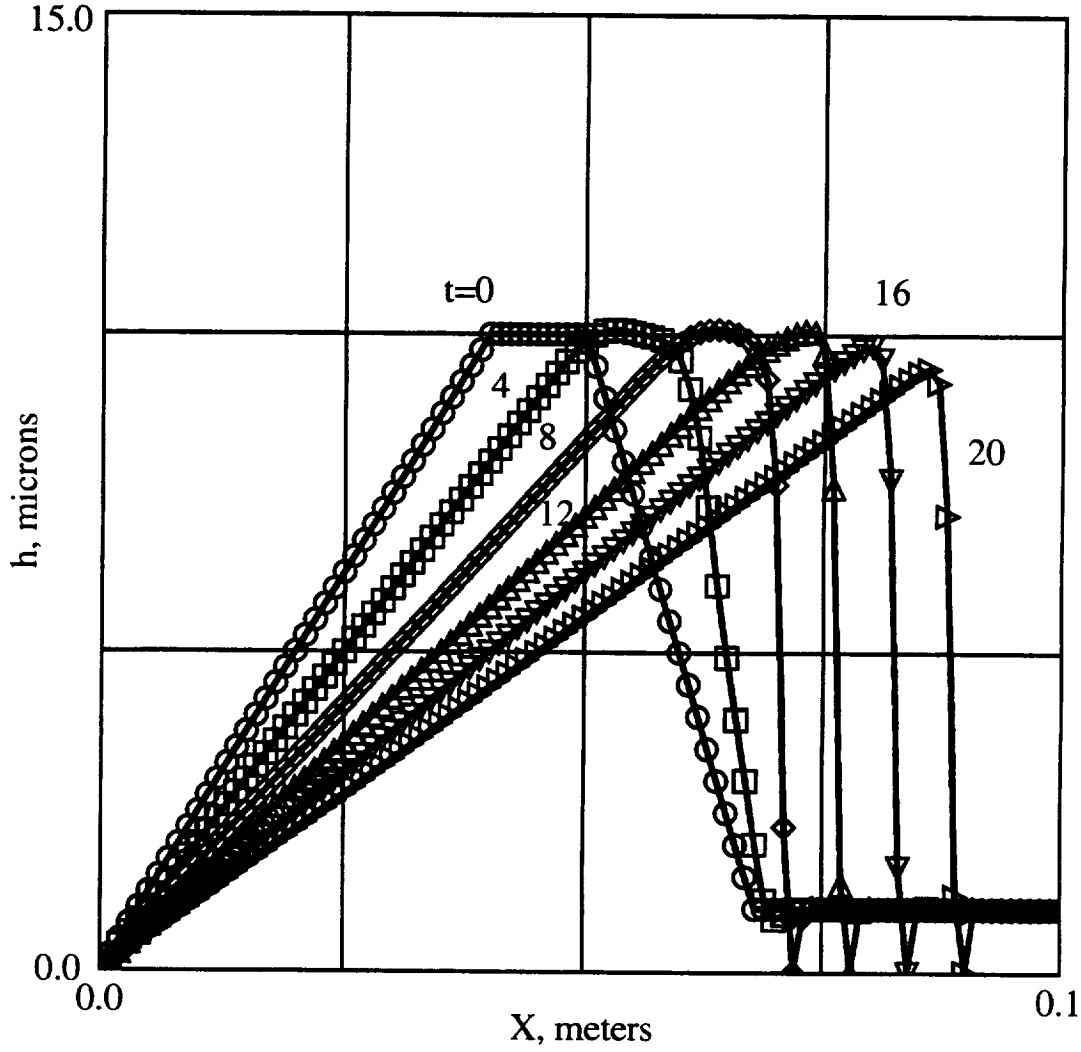

Figure 9d. Finite-Volume Upwind-Implicit direct solver oil film thickness at discrete times for constant wall shear stress, non-monotonic initial thickness problem.

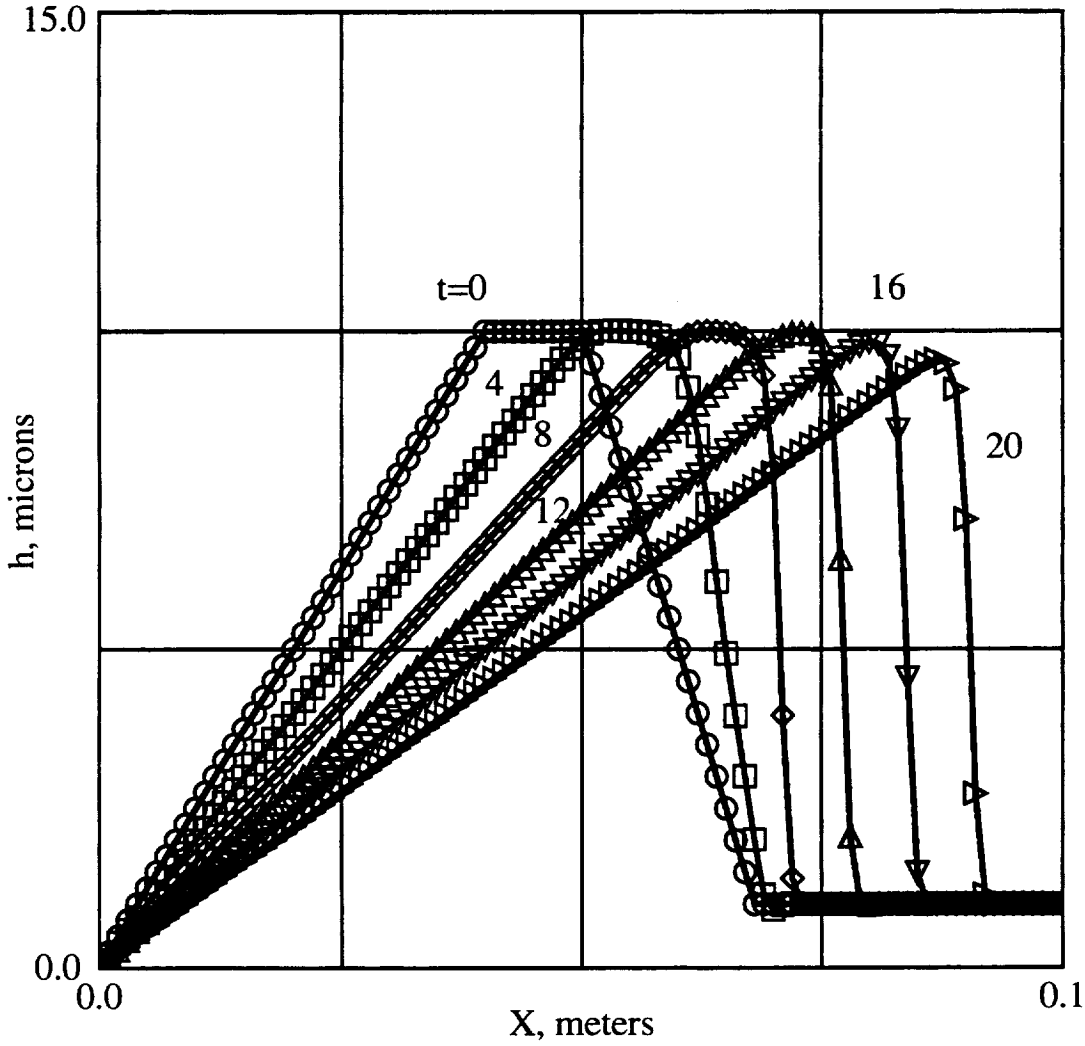

Figure 9e. Finite-Volume Upwind-Implicit, Flux-Limit direct solver oil film thickness at discrete times for constant wall shear stress, non-monotonic initial thickness problem.

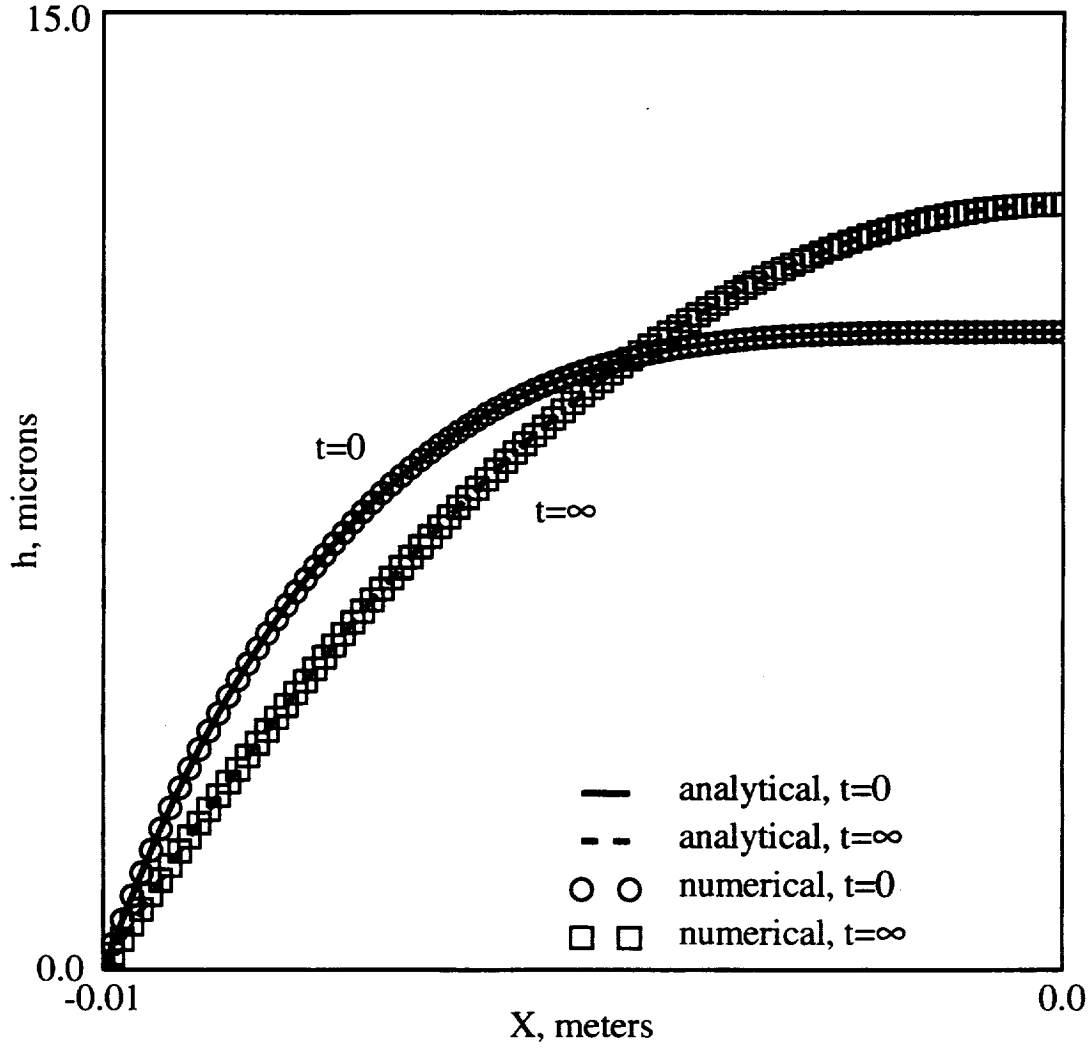

Figure 10. Initial and final oil film thickness, surface tension problem.

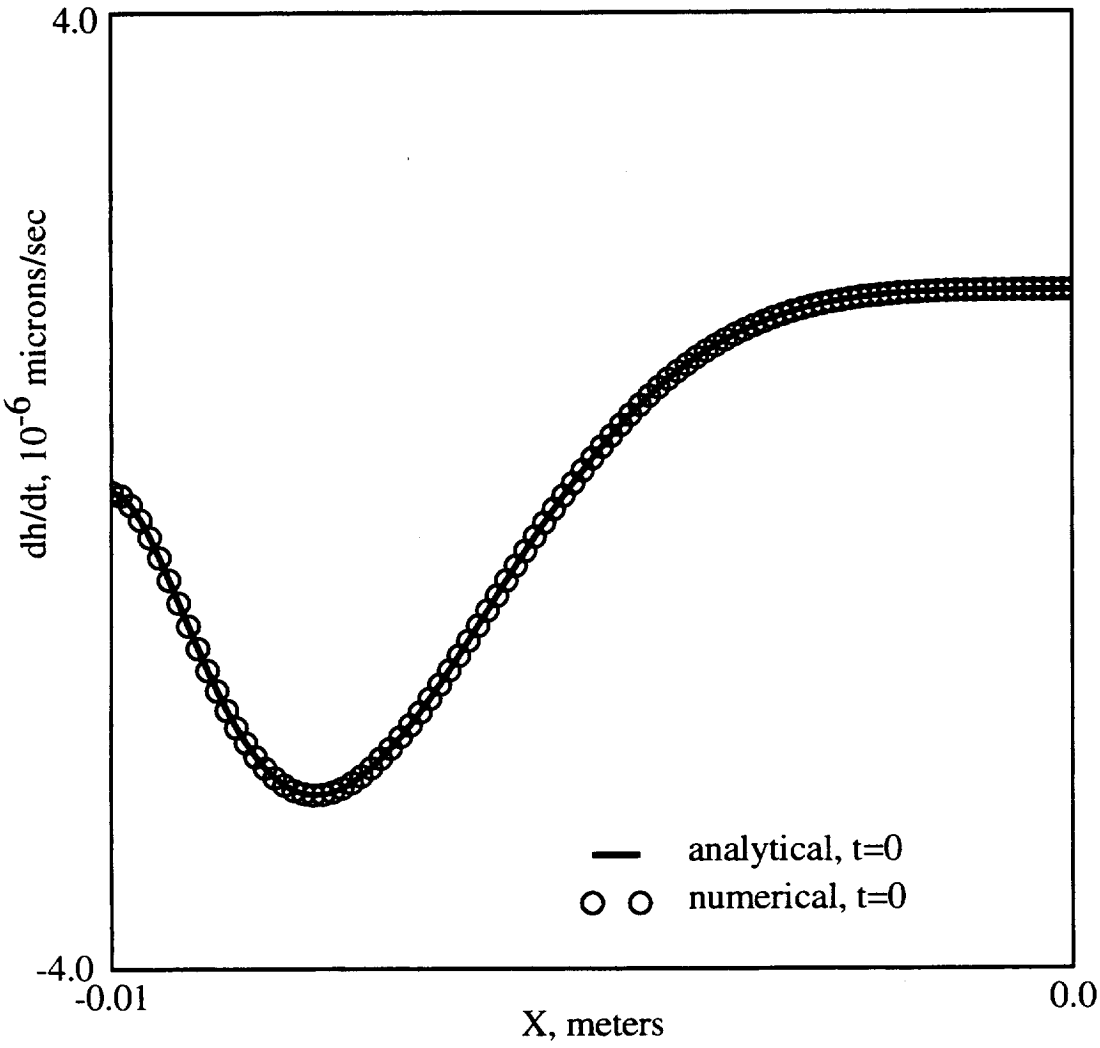

Figure 11. Initial oil film thickness rate, surface tension problem.

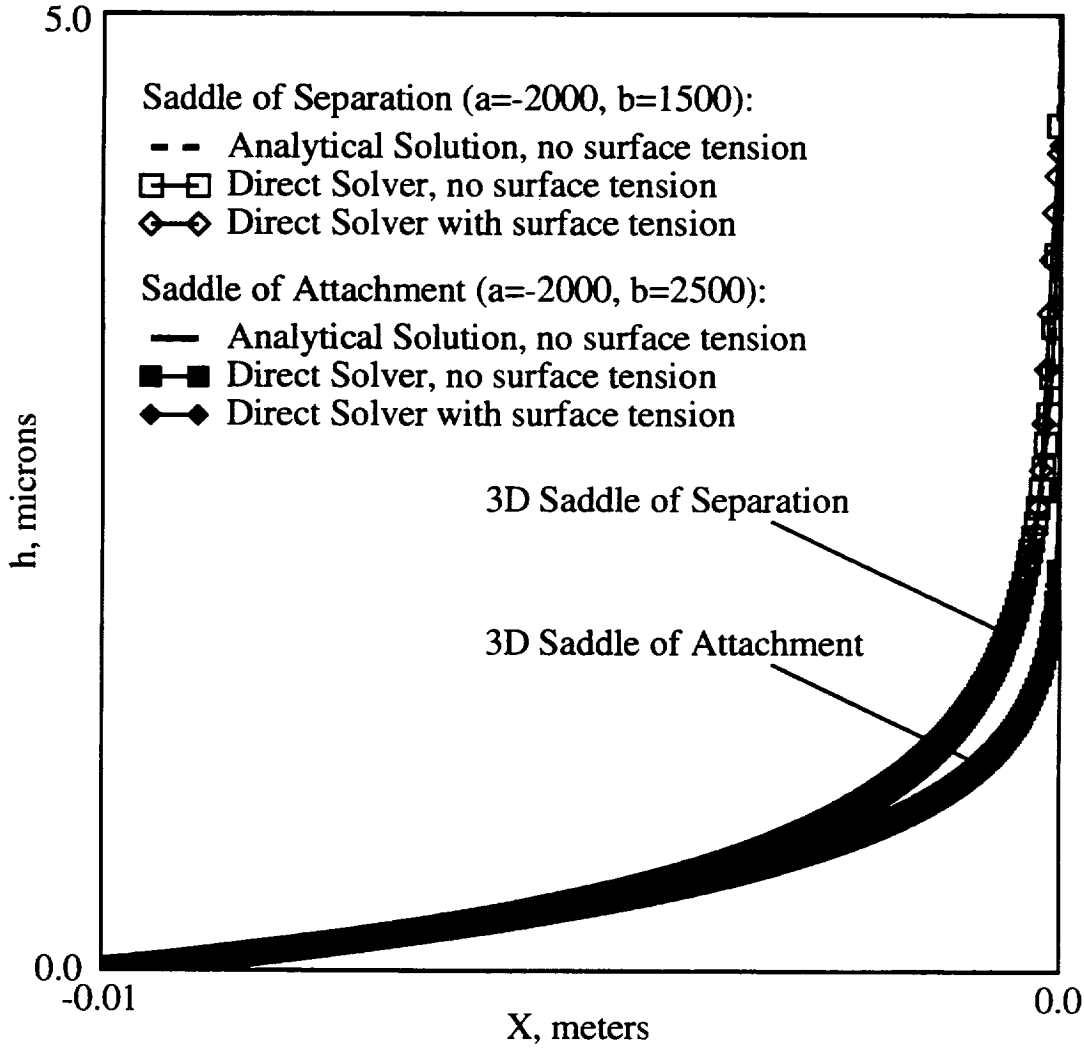

Figure 12. Oil film thickness for saddle problem, Box-Implicit method, t=100 seconds.

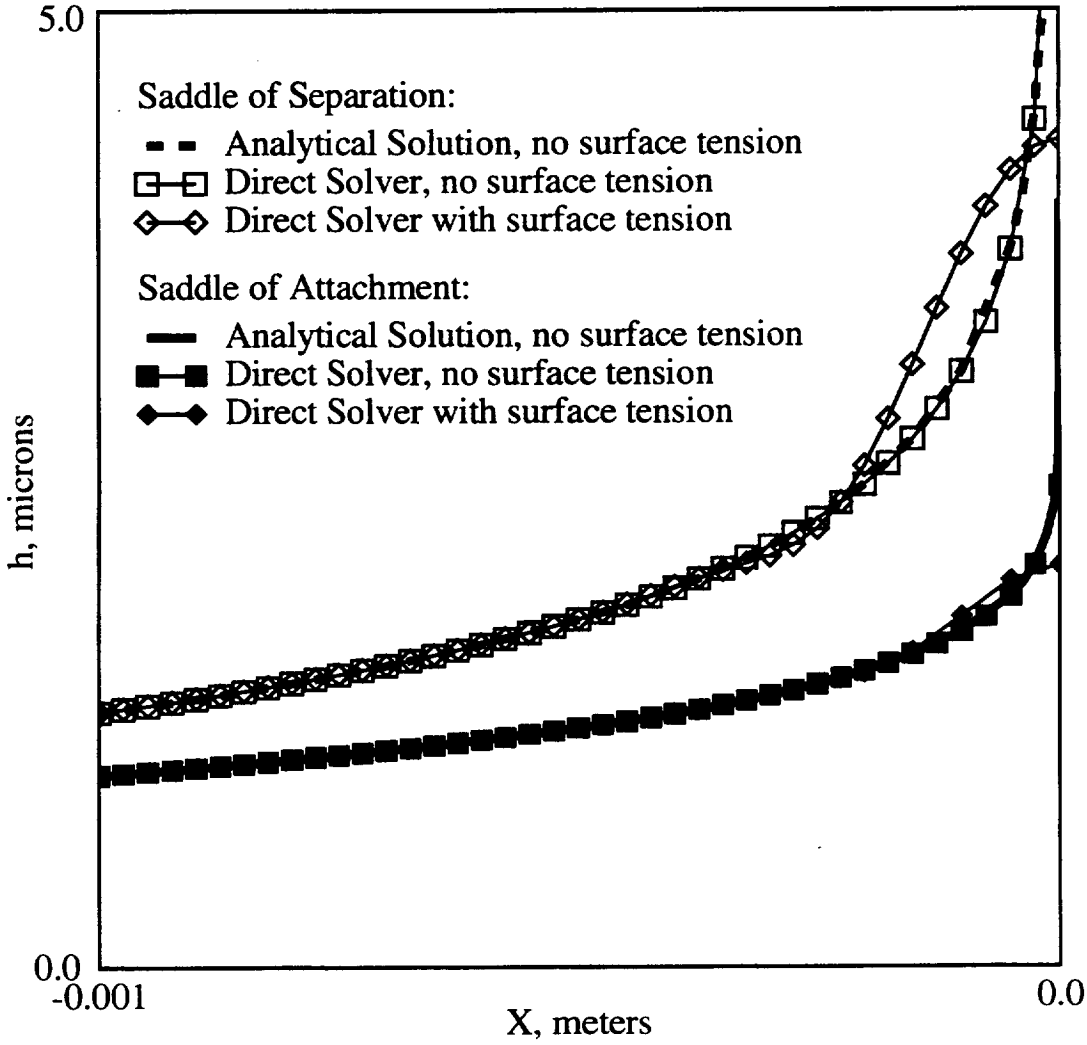

Figure 13. Oil film thickness for detailed region near saddle point of saddle problem, Box-Implicit method, t=100 seconds.

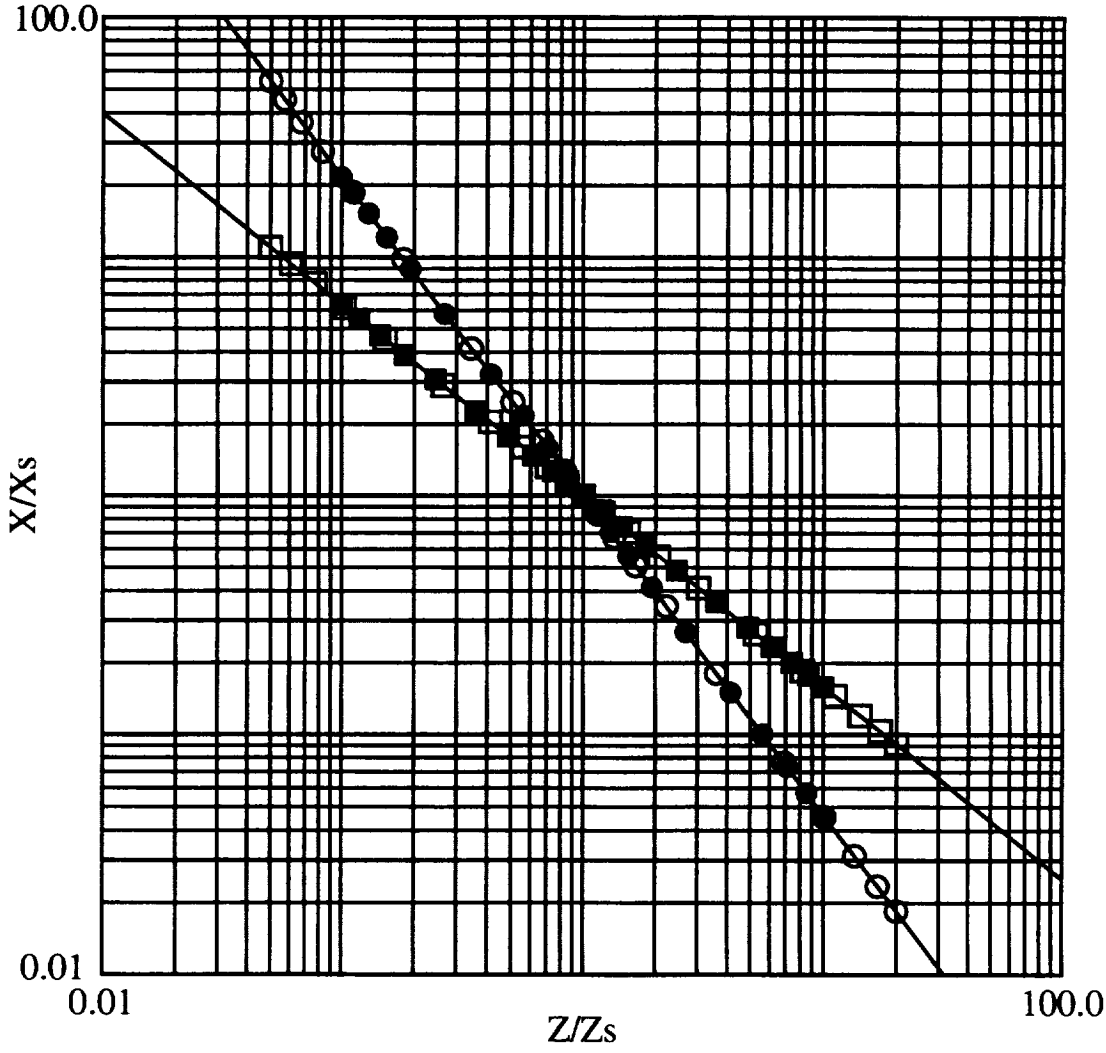

Figure 14. Log quadrant analysis of saddle streamlines.
Square symbols form figure 3a, a saddle of attachment.
Circle symbols form figure 3b, a saddle of separation.

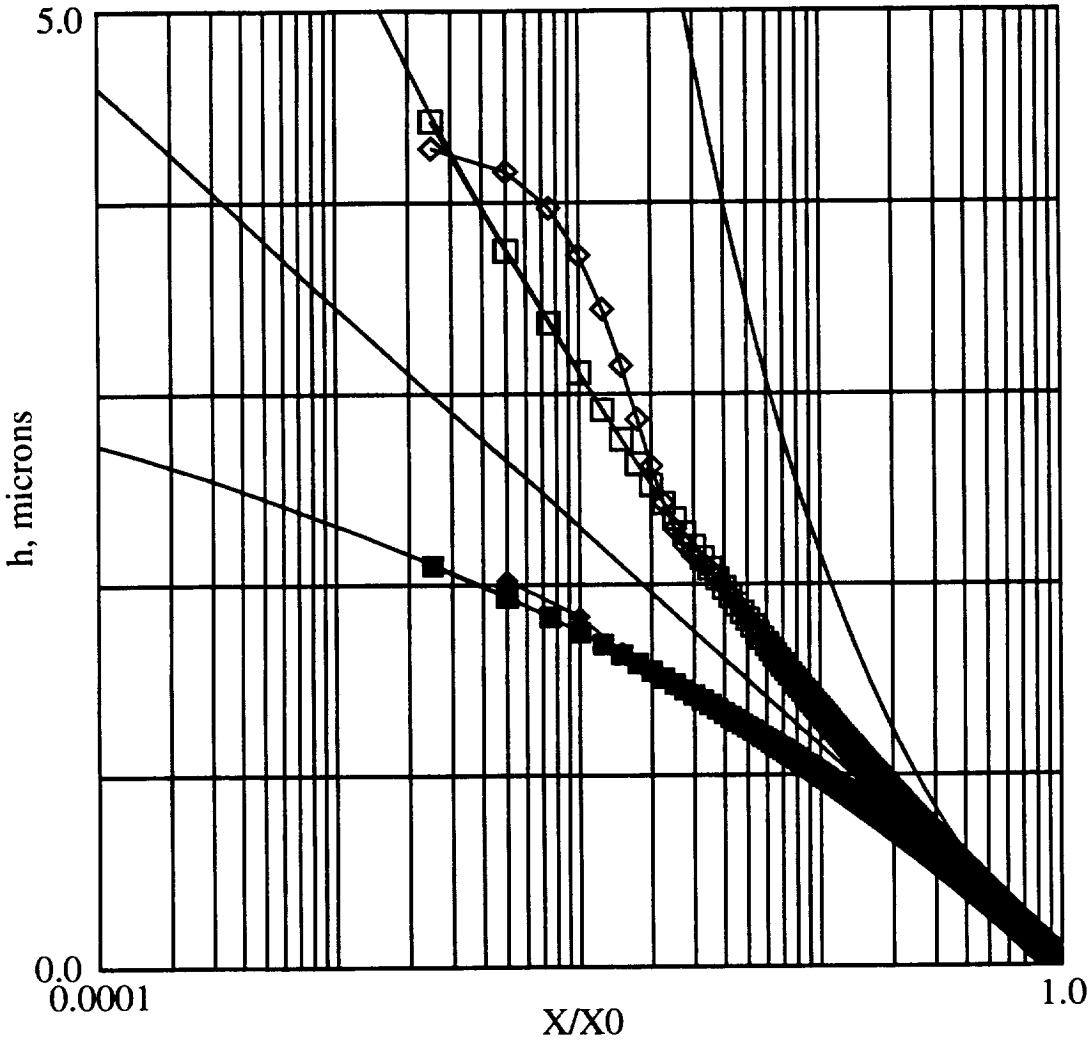

Figure 15. Centerline log analysis for saddle oil film thickness.
- □ Saddle of separation without surface tension terms.
- ◇ Saddle of separation with surface tension terms.
- ■ Saddle of attachment without surface tension terms.
- ◆ Saddle of attachment with surface tension terms.

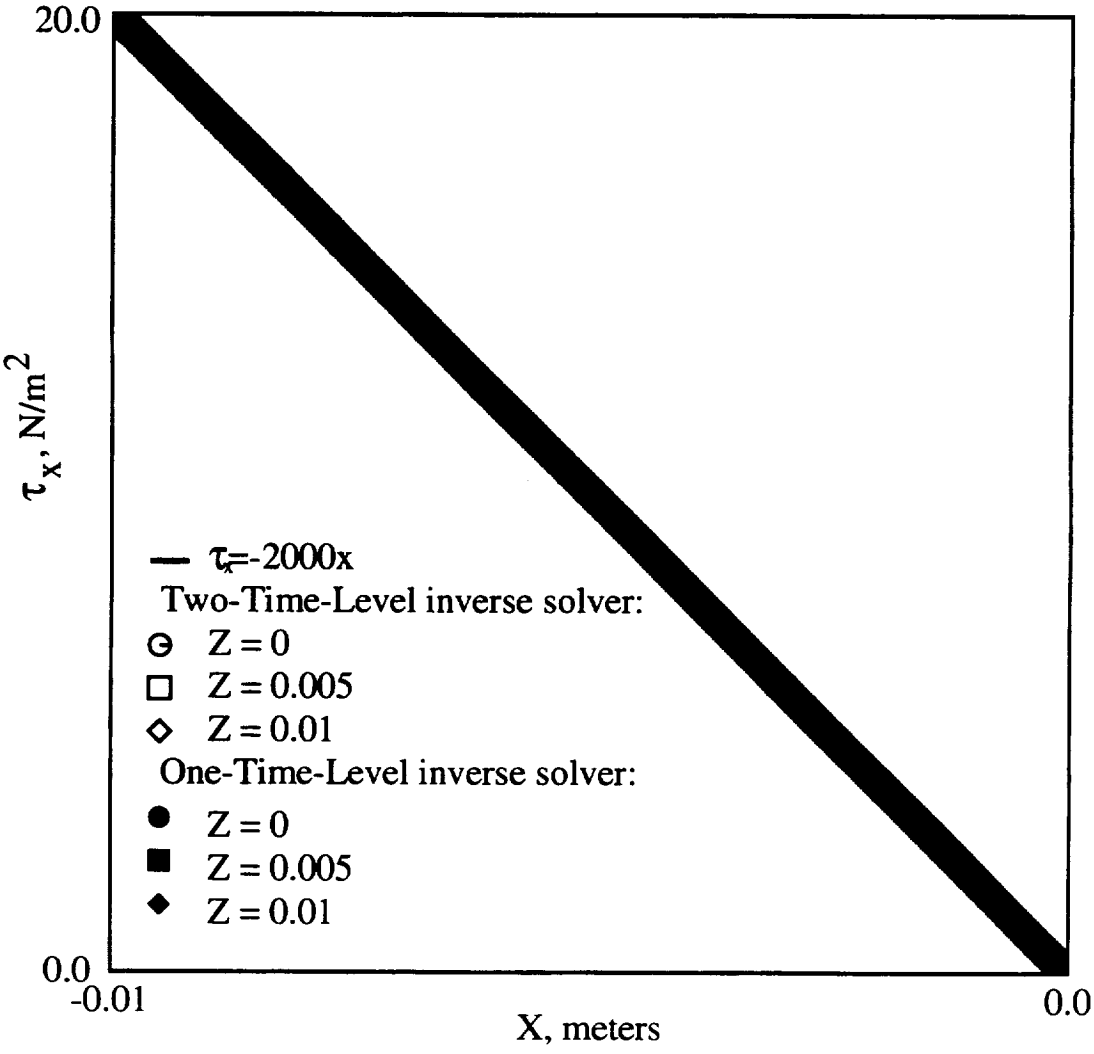

Figure 16a. Oil film wall shear stress for saddle problem using Two- and One-Time-Level inverse solvers, no surface tension.

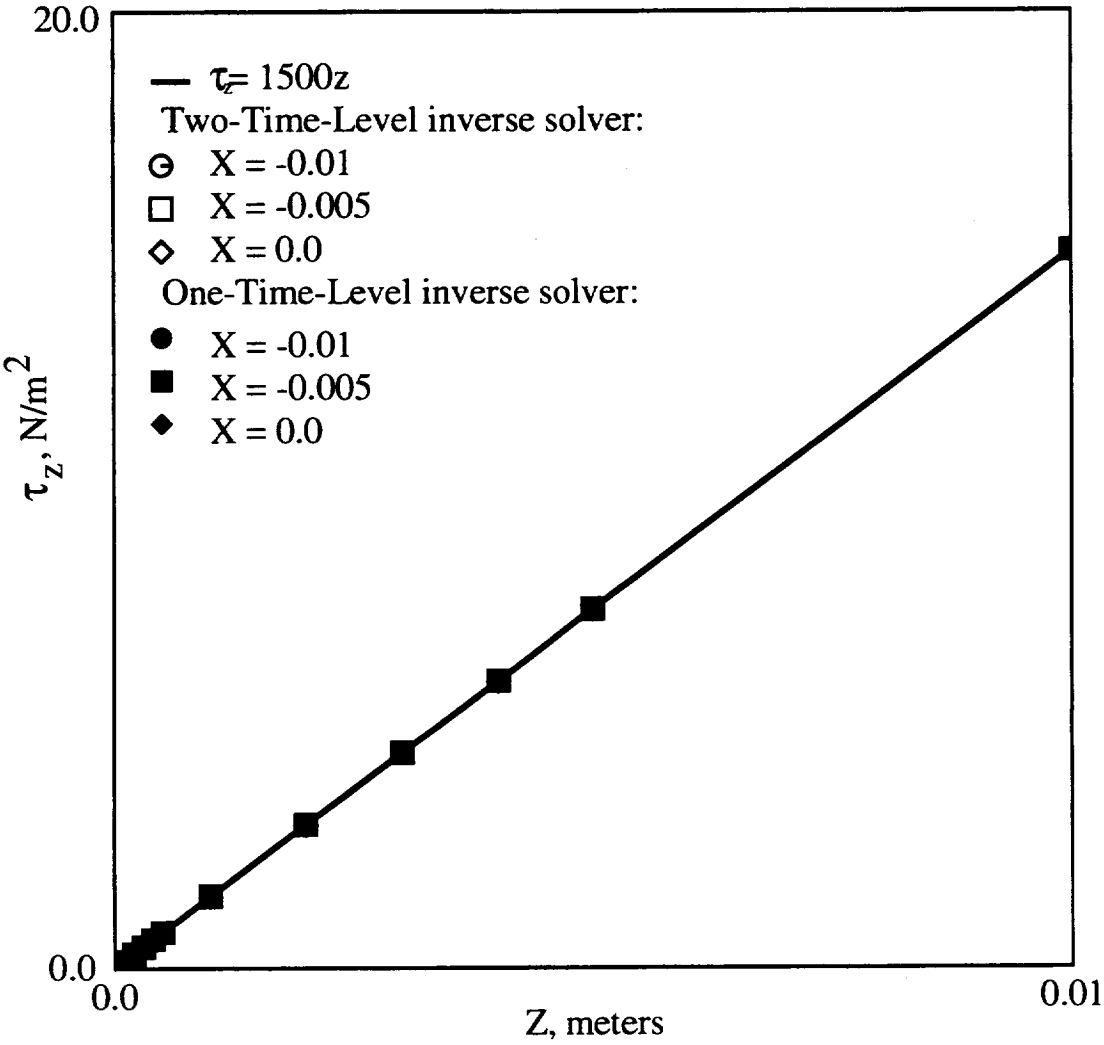

Figure 16b. Oil film wall shear stress for saddle problem using Two-Time-Level inverse solver, no surface tension.

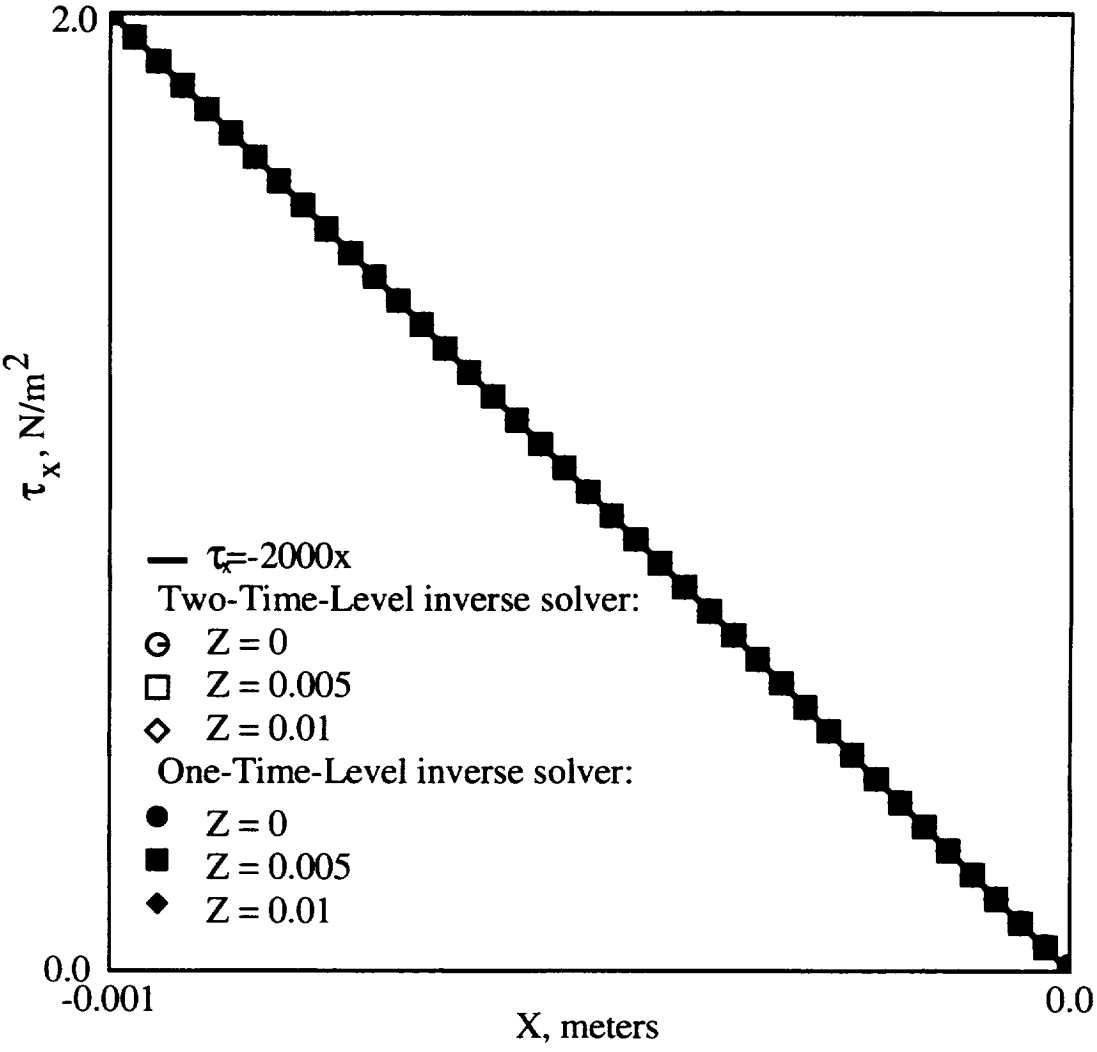

Figure 16c. Oil film wall shear stress for detailed region near saddle point using Two- and One-Time-Level inverse solvers, no surface tension.

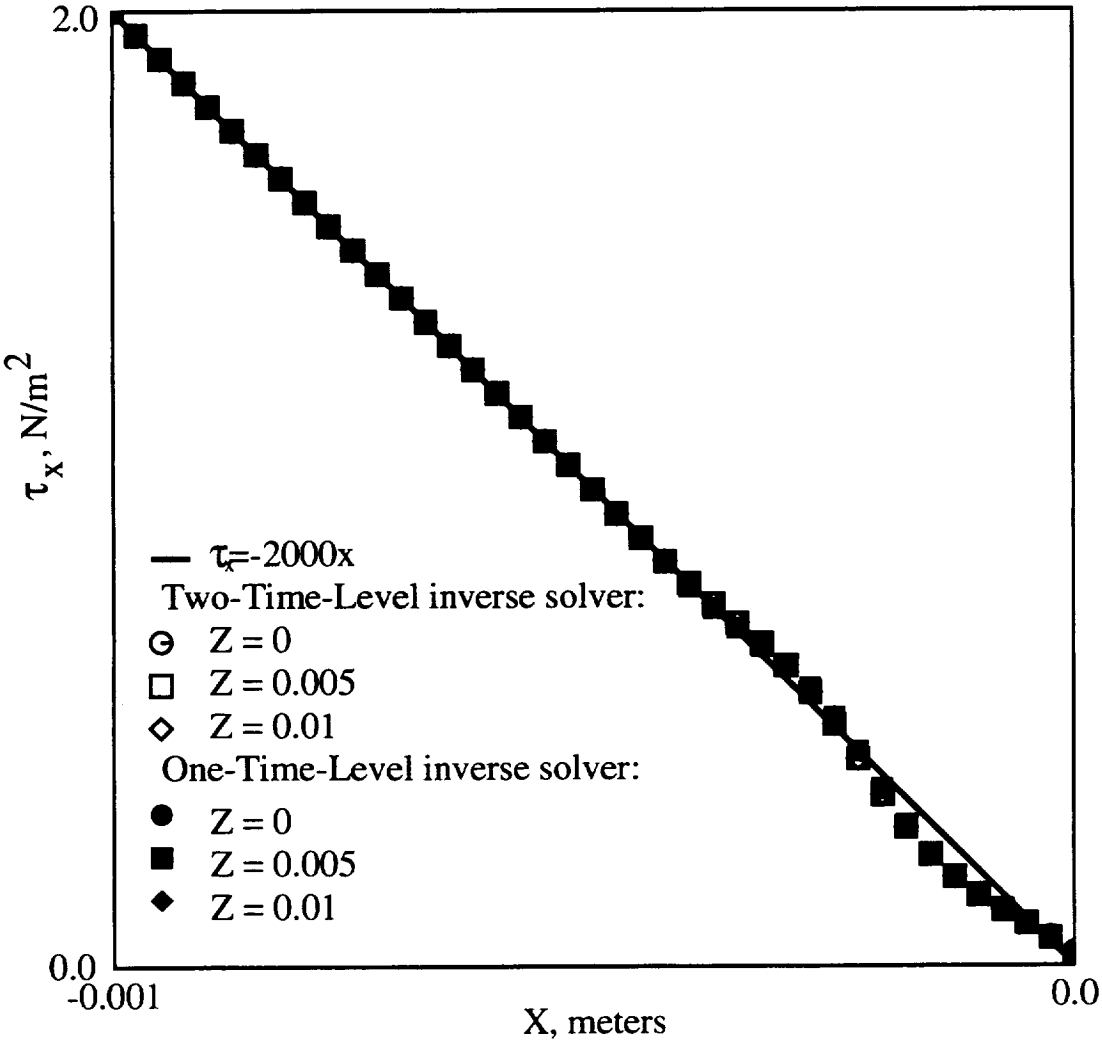

Figure 17a. Wall shear stress for saddle problem with surface tension effects using Two- and One-Time-Level inverse solver without surface tension terms.

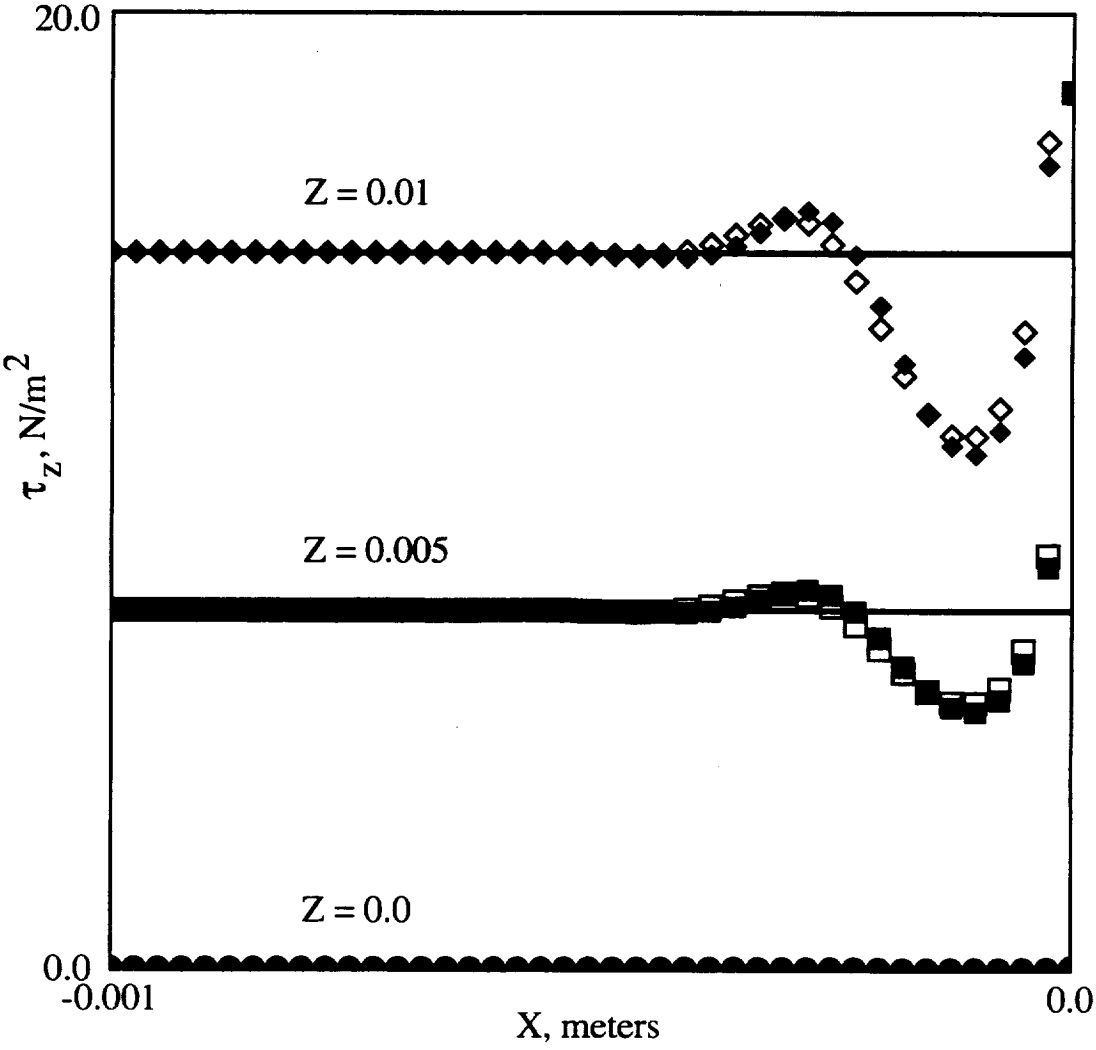

Figure 17b. Wall shear stress for saddle problem with surface tension effects using Two- and One-Time-Level inverse solver without surface tension terms.
Open symbols are Two-Time-Level inverse solver results.
Filled symbols are One-Time-Level inverse solver results.

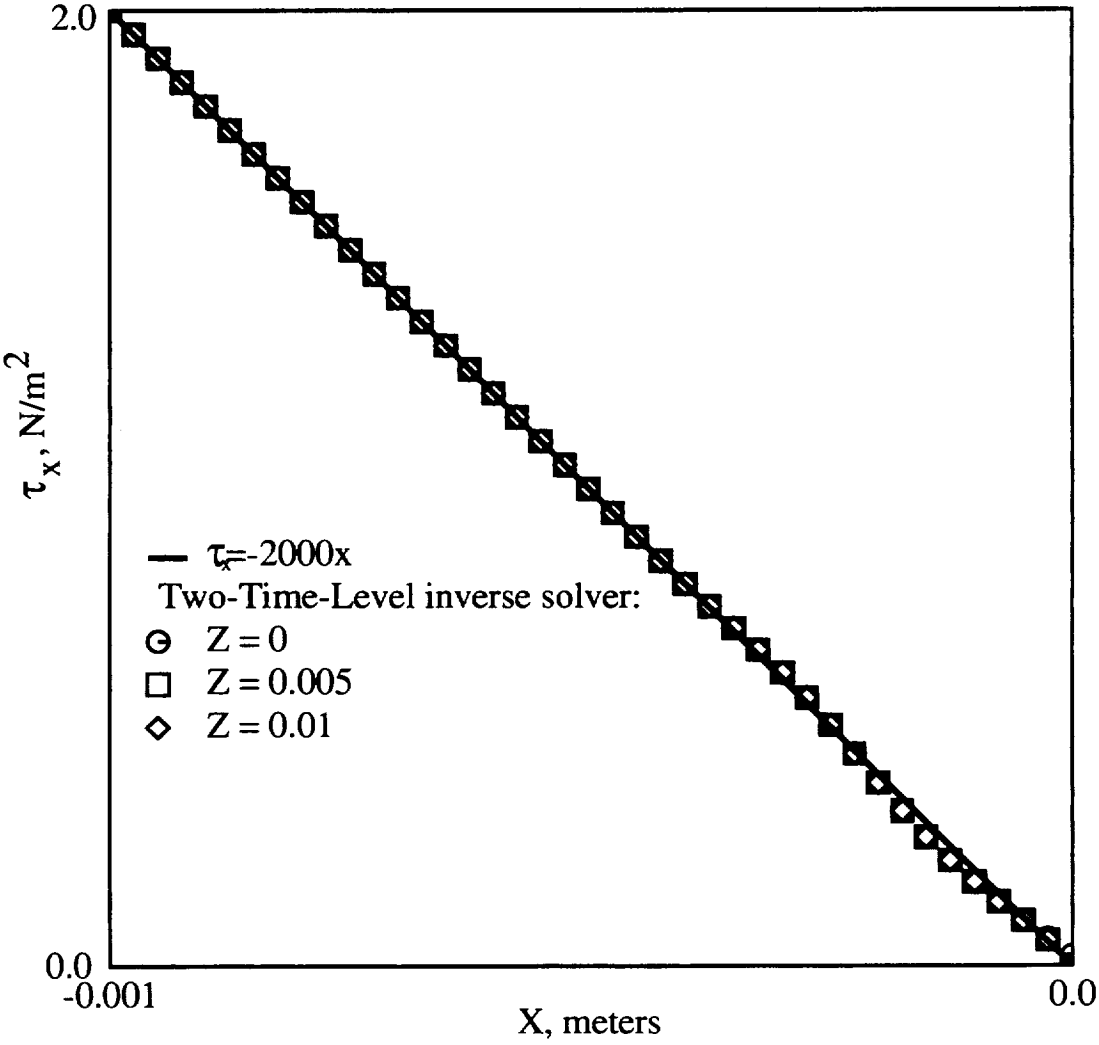

Figure 18a. Wall shear stress for saddle problem with surface tension effects using Two-Time-Level inverse solver with surface tension terms.

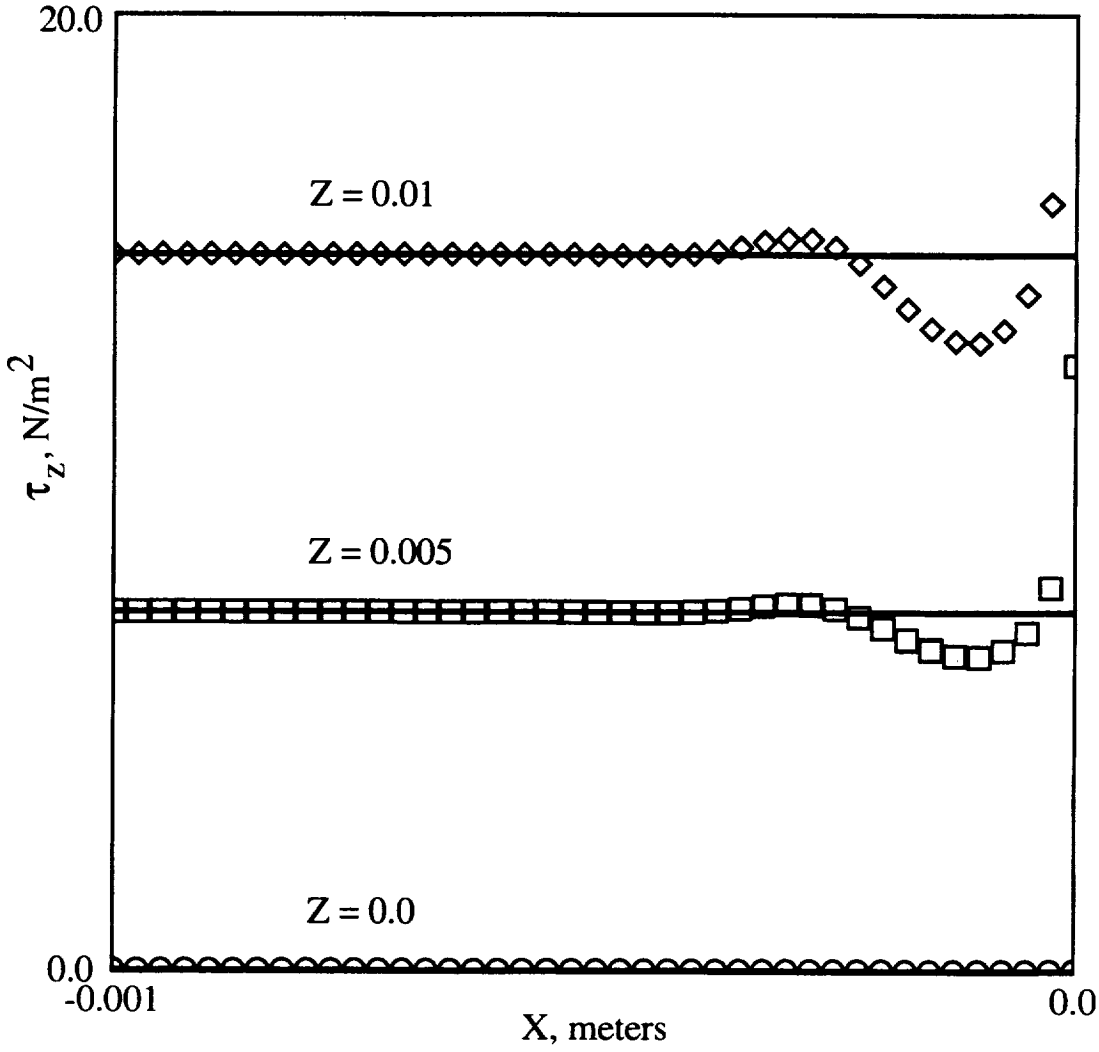

Figure 18b. Wall shear stress for saddle problem with surface tension effects using Two-Time-Level inverse solver with surface tension terms.

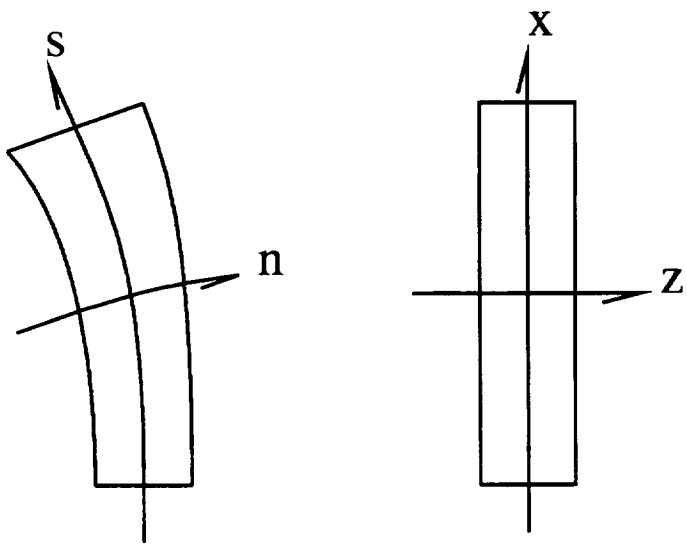

Figure A1. Streamline coordinate system.

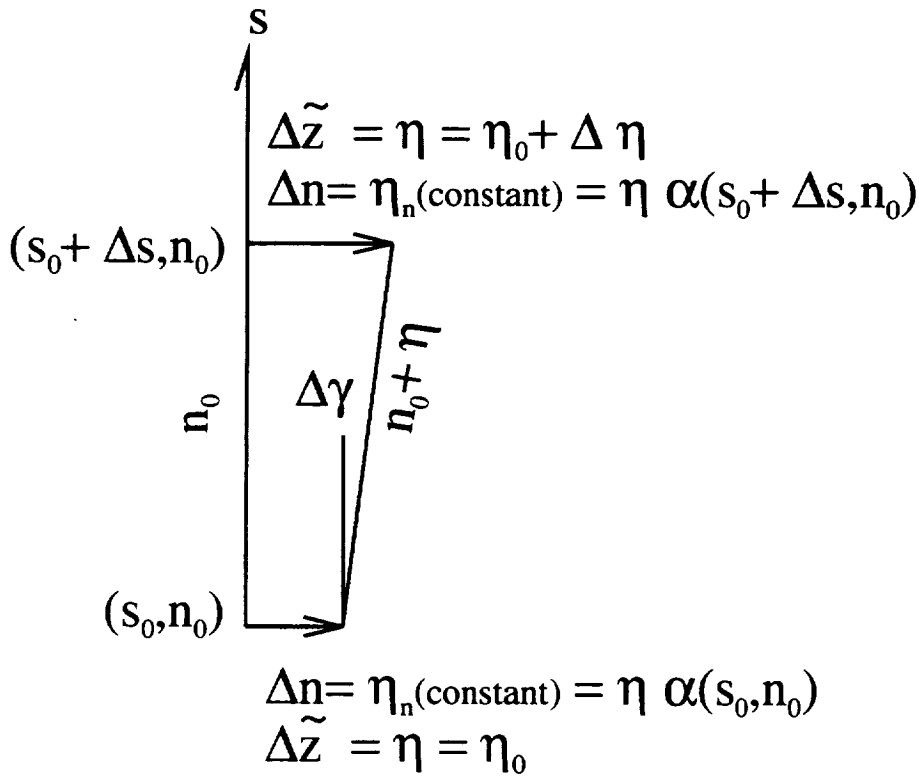

Figure A2. Streamline divergence.

REPORT DOCUMENTATION PAGE

Form Approved
OMB No. 0704-0188

1. AGENCY USE ONLY *(Leave blank)*	2. REPORT DATE	3. REPORT TYPE AND DATES COVERED
	March 1999	Technical Memorandum

4. TITLE AND SUBTITLE

The Thin Oil Film Equation

5. FUNDING NUMBERS

519-20-22

6. AUTHOR(S)

James L. Brown and Jonathan W. Naughton

7. PERFORMING ORGANIZATION NAME(S) AND ADDRESS(ES)

Ames Research Center
Moffett Field, CA 94035-1000

8. PERFORMING ORGANIZATION REPORT NUMBER

A-99V0007

9. SPONSORING/MONITORING AGENCY NAME(S) AND ADDRESS(ES)

National Aeronautics and Space Administration
Washington, DC 20546-0001

10. SPONSORING/MONITORING AGENCY REPORT NUMBER

NASA/TM–1999-208767

11. SUPPLEMENTARY NOTES

Point of Contact: James L. Brown, Ames Research Center, MS 229-1, Moffett Field, CA 94035-1000
(650) 604-6229

12a. DISTRIBUTION/AVAILABILITY STATEMENT

Unclassified — Unlimited
Subject Category 34 Distribution: Standard
Availability: NASA CASI (301) 621-0390

12b. DISTRIBUTION CODE

13. ABSTRACT ***(Maximum 200 words)***

A thin film of oil on a surface responds primarily to the wall shear stress generated on that surface by a three-dimensional flow. The oil film is also subject to wall pressure gradients, surface tension effects and gravity. The partial differential equation governing the oil film flow is shown to be related to Burgers' equation. Analytical and numerical methods for solving the thin oil film equation are presented. A direct numerical solver is developed where the wall shear stress variation on the surface is known and which solves for the oil film thickness spatial and time variation on the surface. An inverse numerical solver is also developed where the oil film thickness spatial variation over the surface at two discrete times is known and which solves for the wall shear stress variation over the test surface. A One-Time-Level inverse solver is also demonstrated. The inverse numerical solver provides a mathematically rigorous basis for an improved form of a wall shear stress instrument suitable for application to complex three-dimensional flows. To demonstrate the complexity of flows for which these oil film methods are now suitable, extensive examination is accomplished for these analytical and numerical methods as applied to a thin oil film in the vicinity of a three-dimensional saddle of separation.

14. SUBJECT TERMS

Thin oil film, Burgers' equation, Wall shear stress, Skin friction, Saddle of Separation

15. NUMBER OF PAGES

98

16. PRICE CODE

A05

17. SECURITY CLASSIFICATION OF REPORT	18. SECURITY CLASSIFICATION OF THIS PAGE	19. SECURITY CLASSIFICATION OF ABSTRACT	20. LIMITATION OF ABSTRACT
Unclassified	Unclassified		